Glaciers are huge and slow moving rivers of ice which exist in various parts of the world: Alaska, the Rockies, the Alps, Spitzbergen, China, for example. They drain areas in which snow accumulates, much as rivers drain catchment areas where rain falls. Glaciers also flow in the same basic way that rivers do. Although glacier ice is solid, it can deform by the slow creep of dislocations within the lattice of ice crystals which form the fabric of the ice. Thus, glacier ice effectively behaves like a viscous material, with, however, a very large viscosity: a typical value of ice viscosity is 6 bar year (in the metre-bar-year system of units!). Since 1 bar $= 10^5$ Pa, 1 year $\approx 3 \times 10^7$ s, this is a viscosity of some 2×10^{13} Pa s, about 10^{16} times that of water. As a consequence of their enormous viscosity, glaciers move slowly — a typical velocity would be in the range 10–100 m y^{-1} (metres per year), certainly measurable but hardly dramatic. More awesome are the dimensions of glaciers. Depths of hundreds of metres are typical, widths of kilometres, lengths of tens of kilometres. Thus glaciers can have an important effect on the human environment in their vicinity. They are also indirect monitors of climate; for example, many lithographs of Swiss glaciers show that they have been receding since the nineteenth century, a phenomenon thought to be due to the termination of the 'Little Ice Age' which lasted from about 1500 to about 1900.

Where glaciers are the glacial equivalent of rivers, i.e. channelled flow, *ice sheets* are the equivalent of droplets, but altogether on a grander scale.[1] When an entire continent, or at least a substantial portion thereof, has a polar climate, then snow accumulates on the uplands, is compressed to form ice, and flows out to cover the continent, much as a drop of fluid on a table will spread under the action of gravity. However, whereas droplets can reach a steady state through the contractile effect of surface tension, this is not relevant to large ice sheets. In them, equilibrium can be maintained through a balance between accumulation in the centre and *ablation* at the margins. This can occur either through melting of the ice in the warmer climate at the ice margin, or through calving of icebergs. (Indeed, the same balance of accumulation at higher elevations with ablation at lower elevations is responsible for the normal quasi-steady profile of valley glaciers.)

[1] Ice *caps* are smaller scale sheet flows, such as the Vatnajökull ice cap in Iceland, whose horizontal dimension is about 100 km.

There are two major ice sheets on the Earth, namely those in Antarctica and Greenland (the Arctic is an ocean, and its ice is sea ice, rarely more than three metres thick). They are on the order of thousands of kilometres in extent, and kilometres deep (up to four for Antarctica). They are thus, in fact, *shallow* flows, a fact which greatly facilitates the solution of mathematical models for their flow. Possibly more famous are the ice sheets which covered much of North America (the Laurentide ice sheet) and northern Europe (the Fennoscandian ice sheet) during the last ice age. Throughout the Pleistocene era (that is, the last two million years), there have been a succession of ice ages, each lasting a typical period of around 90,000 years, during which global ice sheet volume gradually increases, interspersed with shorter (10,000 year) *interglacials*, when the ice sheets rapidly retreat. The last ice age finished some ten thousand years ago, so that it would be no surprise if another were to start now. Perhaps the Little Ice Age was indeed the start of ice sheet build-up, only to be interrupted by the Industrial Revolution and the resultant global warming: nobody knows.

Further back in Earth's geologic history, there is evidence for dramatic, large scale glaciation in the Carboniferous (c. 300 My (million years) ago), Ordovician (c. 500 My ago), Neoproterozoic (c. 600–800 My ago) and Huronian (c. 2,500 My ago) periods. In the Neoproterozoic glaciation, it seems that the whole landmass of the Earth may have been glaciated, leading to the concept of 'snowball Earth'. It was following the shrinkage of the global ice sheet that the explosion of life on Earth started.[2]

Drainage and sliding

While the motion of ice sheets and glaciers can be understood by means of viscous theory, there are some notable complications which can occur. Chief among these is that ice can reach the melting point at the glacier bed, due to frictional heating or geothermal heat input, in which case water is produced, and the ice can *slide*. Thus, unlike an ordinary viscous fluid, slip can occur at the base, and this is determined by a sliding law which relates basal shear stress τ to sliding velocity u_b and also, normally, the *effective pressure* $N = p_i - p_w$, where p_i and p_w are ice and water pressures. The determination of p_w further requires a description of the subglacial hydrology, and thus the dynamics of ice is intricately coupled to other physical processes: as we shall see, this complexity leads to some exotic phenomena.

10.1 Dynamic phenomena

10.1.1 Waves on glaciers

Just as on rivers, gravity waves will propagate on glaciers. Because the flow is very slow, they only propagate one way (downstream), and at speeds comparable to the surface speed (but slightly faster). These waves are known as surface waves, as they

[2]Snowball Earth was discussed in chapter 2.

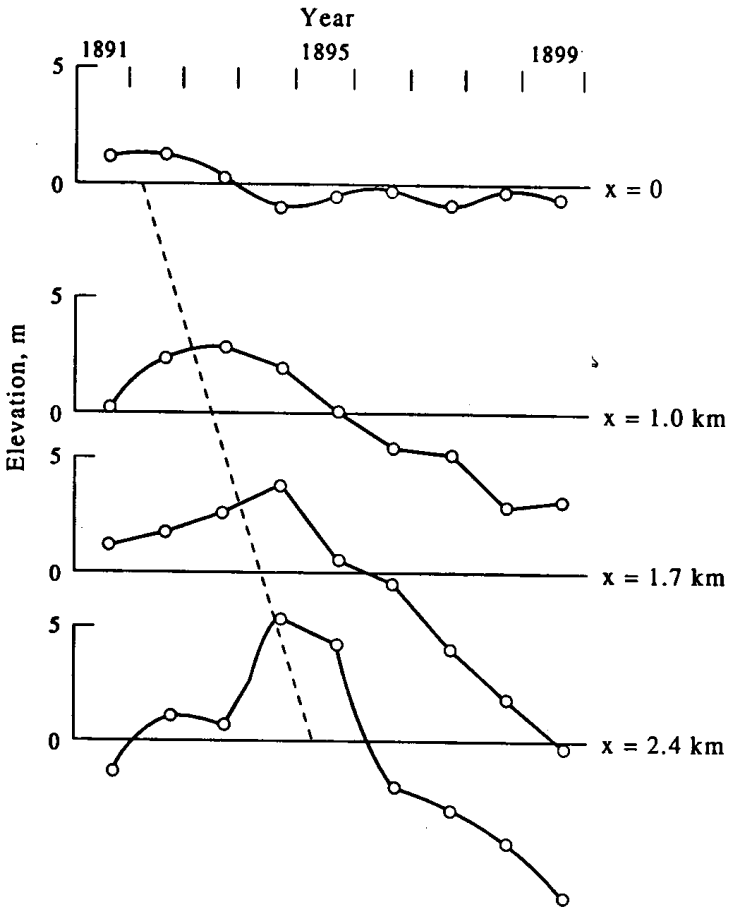

Figure 10.1: Changes of mean surface elevation of Mer de Glace, France, along four cross-profiles over a period of 9 years. The broken line corresponds to a wave velocity of 800 m/a. Reproduced from Lliboutry (1958a), by permission of the International Association of Hydrological Sciences.

are evidenced by undulations of the surface: an example is shown in figure 10.1. They are examples of *kinematic* waves, driven by the dependence of ice flux on glacier depth.

A more exotic kind of wave is the 'seasonal wave'. This has no obvious counterpart in other fluid flows. It consists of (sizeable) perturbations in the surface velocity field which propagate down glacier at speeds in the order of 20-150 times the surface speed. There is no significant surface perturbation, and these waves must in fact be caused by variations of the basal sliding speed due to annual fluctuations in the basal water pressure. Although well-known and reported at the turn of the century, little attention has been paid to these waves in recent years. Figure 10.2 shows measurements of Hodge on Nisqually Glacier which indicates the rapid passage of a velocity wave downstream.

Mention should also be made of wave ogives, although we will not deal with them here. They are bands (also known as Forbes bands) which propagate below ice-falls,

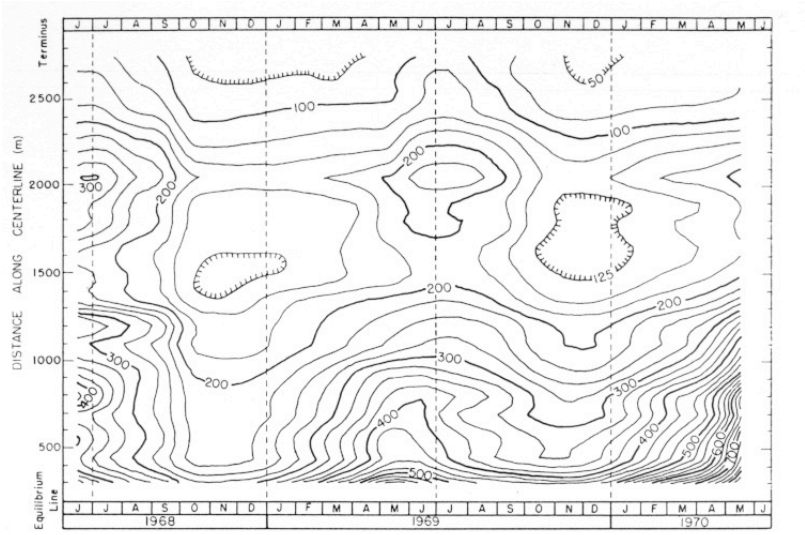

Figure 10.2: The measured surface speed of Nisqually Glacier, Mt. Rainier, as a function of time and distance. The contour interval is 25 mm d^{-1}. The maximum and minimum speeds occur progressively later with distance down-glacier; this represents a "seasonal wave" in the ice flow. Reproduced from Hodge (1974), and reprinted from the Journal of Glaciology with permission of the International Glaciological Society.

and are due to the annual ablation cycle.

10.1.2 Surges

Perhaps the most spectacular form of wave motion is the glacier *surge*. Surges are large scale relaxation oscillations of the whole length of a glacier. They are roughly periodic, with periods of the order of 20–100 years. During a long quiescent phase, the glacier is over-extended and thin. Ice accumulation causes the glacier to thicken upstream, while the over-extended snout thins and retreats. Eventually, a critical thickness is reached, and the glacier slumps rapidly downslope again. These surges will typically last only a year or two, during which time the velocity may increase a hundred-fold. The glacier snout can then advance by several kilometres.

A typical (and much studied) example is the Variegated Glacier in Alaska. Its surge periodicity is about twenty years, while its surges last about two years. The glacier, of length twenty kilometres and depth four hundred metres, advances some six kilometres during its surge, at measured speeds of up to 65 metres per *day*. Such large velocities can only occur by basal sliding, and detailed observations during the 1982–3 surge showed that the surge was mediated by an alteration in the basal drainage system, which had the effect of raising water pressure dramatically. A dynamic model suggests, in fact, that the oscillations are caused by the competitive interaction between the basal sliding law and the hydraulics of the subglacial drainage system. When the ice is relatively thin (hence the driving shear stress is low) the

Figure 10.3: Variegated Glacier at the beginning of a surge, 29 August, 1964. Photograph by Austin Post, U.S. Geological Survey.

drainage occurs through a network of channels incised into the ice at the glacier bed called Röthlisberger channels. These allow effective drainage at quite low water pressures (hence high effective pressures) and thus also low ice velocities. At higher driving stresses, however, an instability forces the channel system to close down, and the basal water is forced into cavities which exist between the ice and bedrock protuberances (such cavities are well-known to exist). The water flow is reduced, and the sudden increase in water pressure causes a sudden increase in ice velocity — the surge. The transition front between the linked cavity drainage system and the channel system is nucleated near the maximum depth, and propagates rapidly both upstream and downstream, at (measured) speeds on the order of hundreds of metres per hour. At the end of the surge, the channel drainage system is re-established. Figures 10.3 and 10.4 show an aerial view of Variegated Glacier in pre- and post-surge states.

Our understanding of the Variegated surges relies on the concept of drainage switch between channelised flow and linked cavities, implicitly for ice flowing over (hard) bedrock. A rather different situation appears to operate in Trapridge Glacier, another well-studied surging glacier, in the Yukon. Here the glacier is cold in its interior (unlike the temperate (at the melting point) Variegated Glacier); and rests on a thick ($\sim$ 6 metres) layer of *till*, sometimes more graphically called *boulder clay* — a non-uniform mixture of angular rock fragments in a finer-grained, clay-rich groundmass (see figure 10.5). Till has a bimodal grain size distribution, and is produced by

Figure 10.4: Variegated Glacier at the end of a surge, 22 August, 1965. Photograph by Austin Post, U.S. Geological Survey.

the erosion of brittle underlying bedrock, and is evacuated by the slow motion of the ice downstream.

The sequence of events which appears to be occurring as Trapridge thickens is that, firstly, the basal ice reaches melting point (and the till thaws). When this happens, the till becomes deformable, and the basal ice can slide over the bed by riding on the deforming till. The rate at which this occurs depends on the till rheology, where opinion is currently divided as to whether a viscous or plastic rheology is the more appropriate.[3] What does seem to be clear is that the water pressure will have a major effect. Increasing saturation causes increasing water pressure, which pushes the sediment grains apart and allows them to move more freely, so that in effect enhanced water production causes enhanced sliding. In turn, increased sliding causes increased frictional heating, so that there is a positive feedback which potentially can cause runaway and consequent surging behaviour. Whether the effect is strong enough is not obvious, but we shall examine a simple model which suggests that it may be.

[3]Note the use of the word 'appropriate'. As a saturated, granular material, somewhat like soil, there is little argument that a plastic rheology accommodating a yield stress is the most apposite description; such a description does not in itself provide an answer to such questions as to whether till deforms with depth (i. e., shears), or whether discrete slip occurs at the ice-till interface.

Figure 10.5: Subglacial till in a coastally exposed drumlin at Scordaun, Killough, Co. Down, Northern Ireland.

10.1.3 Ice streams

Although ice sheets also flow under the horizontal pressure gradients induced by the glaciostatic pressures beneath their sloping surfaces, they rest on essentially unsloping bases, and therefore have no advective component in their dynamics. Thus ice sheets do not, at least on the large scale, exhibit wave motion: the governing equations are essentially diffusive in character. On a more local scale, however, ice sheets have interesting phenomena of their own.

Principal among these may be ice streams. Ice sheets do not tend to drain uniformly to the margin from their central accumulation zones, but rather the outflows from catchment areas are concentrated into fast-moving ice streams. Examples are the Lambert Glacier in Antarctica and Jakobshavn Isbrae in Greenland, a fast-moving

(more than 10 kilometres per year) outlet glacier.[4] These ice streams gain their speed by carving out deep channels through which they flow. Indeed, there is an obvious positive feedback here. The deeper an ice flow, the larger the driving basal stress, and the warmer the basal ice (due to increased frictional heat and decreased conductive heat loss), and hence the softer the ice. Both of these effects contribute to enhanced ice flow, which can explain the formation of such channels, since the erosive power of ice flow increases with the basal velocity and the basal shear stress. Indeed, flow of ice over a plane bed is subject to a lateral instability (much as overland flow of surface water is unstable to the formation of rills and gullies).

A similar kind of mechanism may operate when ice flows over deforming sediments, as in the Siple Coast of West Antarctica. Here, it is found that the flow is concentrated into five ice streams, A, B, C, D, and E, which are characterised by their heavily crevassed appearance. Ice stream B is now known as the Whillans ice stream, in memory of the glaciologist Ian Whillans. Following this, the other ice streams have also been named after individuals; specifically, A is Mercer, C is Kamb, D is Bindschadler and E is MacAyeal. The flow in these ice streams is very rapid and is due to basal sliding over the underlying sediment (except for the Kamb ice stream C, which appears to have 'switched off' several hundred years ago). Measurements on the Whillans ice stream indicate that the basal water pressure is high (within 0.4 bar of the overburden pressure), and that it is underlain by some eight metres of saturated till. A similar instability to that concerning ice flow over hard bedrock may explain the streaming nature of the flow. Where ice flow is larger, there is increased water production. *If* the drainage system is such that increased water production leads to increased water pressure (as one might expect, e.g. for a Darcy flow), then the higher water pressure decreases the viscosity of the till, and hence enhances the ice flow further. This is an instability mechanism, and the limiting factor is that when ice flow increases, there is increased heat loss from the base, which acts to limit the increase of melt rate.

10.1.4 Ice shelf instability

Where continental ice sheets are not diminished by ablation, the ice will flow to the continental margin, where it will spill into the ocean. This, for example, is the case in Antarctica, where it is so cold that ordinary mass wastage of the ice is virtually absent. As a result, *ice shelves* are formed, which are tongues of floating ice connected to the grounded ice at the *grounding line*. The grounding line is a dynamical free boundary, whose location determines the hold up of land ice, and its determination is therefore of some interest as regards sea level changes.

Over the past several decades, various arguments have been put forward to suggest that ice shelves are inherently unstable and liable to collapse. This idea was originally put forward in consideration of the West Antarctic Ice Sheet (WAIS), much of the grounded part of which lies on a submarine bed. If the WAIS were to collapse

[4] Jakobshavn has undergone a remarkable acceleration in recent years, doubling its speed from 6 to 12 kilometres a year in the ten years between 1992 and 2003.

completely, global sea level would rise by some six metres, inundating many coastal cities.

The basic physical mechanism for this putative catastrophic collapse is a positive feedback between grounding line retreat and ice flow rate. Since ice shelves are not resisted at their base, they can plausibly flow more rapidly, and the consequent drawdown effect will lower ice elevation, thus allowing further grounding line retreat. The debate has been fuelled by the remarkable collapse of the Larsen B Ice Shelf on the Antarctic Peninsula in 2002, which is thought to be due to a climatic warming trend over recent decades. However, as we shall see below, it is by no means trivial to pose a theoretically coherent model for grounding line motion, and the issue of stability remains not fully resolved.

10.1.5 Tidewater glaciers

If the position of the grounding line indicates a balance between inland ice flow and ice shelf evacuation, the actual mechanism of break up involves mass wastage by calving icebergs. Indeed, in the absence of ablation, calving is the way in which marine ice sheets (i. e., those terminating in the sea) satisfy mass balance.

Glaciers which terminate in the sea are called *tidewater glaciers*, and are susceptible to a similar kind of catastrophic retreat to that which may be important for ice shelves. They also lose mass by calving, but are distinguished from ice shelves by the fact that the ice is grounded right to the margin. Instability is promoted by the fact that the calving rate increases with depth of water. If a tidewater glacier advances (in a cold climate), it will push a ridge of moraine ahead of it, snowplough style. In a stationary state, the water depth at the calving front will then be less than it is away from the margin, because of this moraine. Then, if the glacier snout retreats due, for example, to a warming trend, the snout will suddenly find itself in deeper water. The resultant increased calving rate can then lead to a catastrophic retreat. Just such a rapid retreat was observed in the Columbia Glacier in Alaska, which retreated some 12 km in twenty years from 1982, and it seems such rapid retreat is a common behavioural feature of tidewater glaciers in conditions of warmer climates.

10.1.6 Jökulhlaups

It will be clear by now that basal water is tremendously important in determining the nature of ice flow. Equally, the basal water system can fluctuate independently of the overlying ice dynamics, most notably in the outburst floods called jökulhlaups. In Iceland, in particular, these are associated with volcanoes under ice caps, where high rates of geothermal heat flux in the confines of a caldera cause a growing subglacial lake to occur, Eventually this overflows, causing a subglacial flood which propagates downglacier, and whose subsequent emergence at the glacier terminus releases enormous quantities of water over the southern coastal outwash plains. These floods carry enormous amounts of volcanic ash and sediments, which create vast beaches of black ash. Despite their violence, the ice flow is hardly disturbed. Jökulhlaups are essentially internal oscillations of the basal drainage system. They are initiated when the

rising subglacial lake level causes leakage over a topographic rim, and the resultant water flow leads to an amplifying water flow by the following mechanism. Water flow through a channel in ice enlarges it by meltback of the walls due to frictional heating. The increased channel size allows increased flow, and thus further enlargement. The process is limited by the fact that the ice tends to close up the channel due to the excess overburden pressure over the channel water pressure, and this is accentuated when the channel is larger. In effect, the opening of the valve by the excess lake pressure is closed by the excess ice pressure. These floods occur more or less periodically, every five to ten years in the case of one of the best known, that of Grímsvötn under Vatnajökull in South-east Iceland. A theory for their formation is the subject of chapter 11.

10.2 The shallow ice approximation

10.2.1 Glaciers

We consider first the motion of a glacier in a (linear) valley. We take the x axis in the direction of the valley axis, z upwards and transverse to the mean valley slope, and y across stream. The basic equations are those of mass and momentum conservation, which for an incompressible ice flow (neglecting inertial terms) are

$$\begin{aligned} \boldsymbol{\nabla}.\mathbf{u} &= 0, \\ 0 &= -\boldsymbol{\nabla} p + \boldsymbol{\nabla}.\boldsymbol{\tau} + \rho\mathbf{g}, \end{aligned} \tag{10.1}$$

where $\mathbf{g}$ is the gravity vector, p is the pressure, and $\boldsymbol{\tau}$ is the deviatoric part of the stress tensor. These are supplemented by the energy equation, which can be written in the form

$$\rho c_p(T_t + \mathbf{u}\,.\boldsymbol{\nabla} T) = k\nabla^2 T + \tau_{ij}\dot{\varepsilon}_{ij}, \tag{10.2}$$

where ρ is ice density, c_p is specific heat, and k is thermal conductivity. The summation convention is employed in writing the viscous dissipation term.[5] We focus for the present on the mass and momentum equations, and will deal with the energy equation later.

The stress and strain rate are related by

$$\tau_{ij} = 2\eta\,\dot{\varepsilon}_{ij}, \tag{10.3}$$

where η is the effective viscosity, and $\dot{\varepsilon}_{ij}$ is the strain rate

$$\dot{\varepsilon}_{ij} = \frac{1}{2}\left(\frac{\partial u_i}{\partial x_j} + \frac{\partial u_j}{\partial x_i}\right). \tag{10.4}$$

The most common choice of flow law is known as Glen's law, that is

$$\dot{\varepsilon}_{ij} = A(T)\tau^{n-1}\tau_{ij}, \tag{10.5}$$

[5]The summation convention is essentially a device for omitting summation signs; it asserts that summation is implied over repeated suffixes; thus $\tau_{ij}\dot{\varepsilon}_{ij}$ means $\sum_{i,j} \tau_{ij}\dot{\varepsilon}_{ij}$.

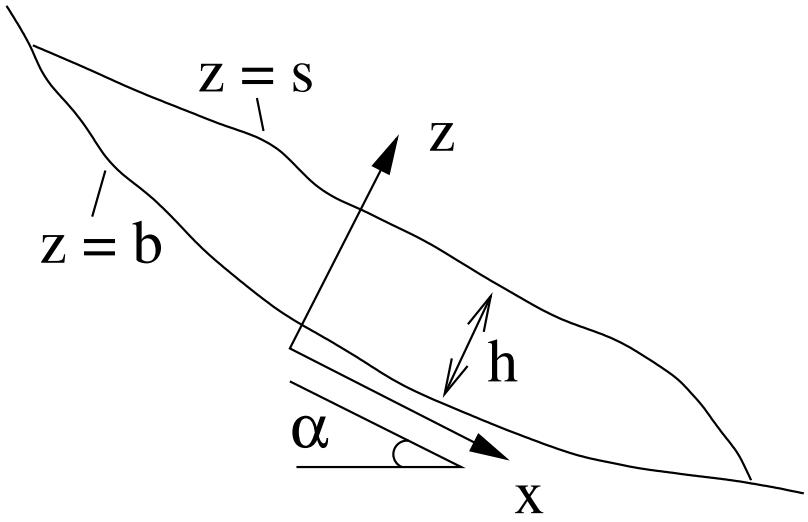

Figure 10.6: Typical profile of a valley glacier

where the second stress invariant is given by $2\tau^2 = \tau_{ij}\tau_{ij}$ (using the summation convention) and $A(T)$ is a temperature dependent rate factor which causes A to vary by about three orders of magnitude over a temperature range of 50 K: variation of A is thus significant for ice sheets (which may be subject to such a temperature range), but less so for glaciers. If we adopt the configuration shown in figure 10.6, then $\mathbf{g} = (g\sin\alpha, 0, -g\cos\alpha)$, where α is the mean valley slope downhill.

Boundary conditions for the flow are conditions of equal normal stress at the top surface $z = s(x, y, t)$; that is $\boldsymbol{\sigma}_n = -p_a\mathbf{n}$, where p_a is atmospheric pressure, or in coordinate form, $\sigma_{ij}n_j = -p_a n_i$, where $\mathbf{n} \propto (-s_x, -s_y, 1)$:

$$\begin{aligned} (-p + \tau_{11})s_x + \tau_{12}s_y - \tau_{13} &= -p_a s_x, \\ \tau_{12}s_x + (-p + \tau_{22})s_y - \tau_{23} &= -p_a s_y, \\ \tau_{13}s_x + \tau_{23}s_y - (-p + \tau_{33}) &= p_a. \end{aligned} \tag{10.6}$$

At the base $z = b(x, y, t)$, we prescribe the velocity:

$$u = u_b, \quad v = v_b, \quad w = ub_x + vb_y; \tag{10.7}$$

(u_b, v_b) is the (horizontal) sliding velocity, whose form is discussed later (as are appropriate temperature conditions). Finally, the kinematic condition on the free surface $z = s$ is

$$w = s_t + us_x + vs_y - a, \tag{10.8}$$

where a is the prescribed surface accumulation: positive for ice accumulation from snowfall, negative for ice ablation by melting.

A major simplification ensues by adopting what has been called the *shallow ice approximation*.[6] It is the lubrication theory idea that the depth $d \ll$ the glacier length

[6]The term arose during a discussion about glacier dynamics one tea time in the Mathematical Institute, Oxford, in 1976. It was invented in keeping with the fluid mechanical description of long waves known as shallow water theory.

l, and is adopted as follows. We scale the variables by putting

$$\begin{aligned}
&u \sim U;\ v, w \sim \varepsilon U;\\
&x \sim l;\ y, z, b, s \sim d; \quad t \sim l/U;\\
&\tau_{13}, \tau_{12} \sim [\tau];\ A \sim [A];\ a \sim [a];\\
&p - p_a - (\rho g \cos\alpha)(s - z) \sim \varepsilon[\tau];\\
&\tau_{11}, \tau_{22}, \tau_{33}, \tau_{23} \sim \varepsilon[\tau],
\end{aligned} \tag{10.9}$$

where

$$\varepsilon = \frac{d}{l} \tag{10.10}$$

is the aspect ratio, and we anticipate $\varepsilon \ll 1$. The choice of d and $[\tau]$ has to be determined self-consistently; we choose l from the given spatial variation of accumulation rate, and we choose U via $\varepsilon U = [a]$, which balances vertical velocity with accumulation rate. If we choose $[\tau] = \rho g d \sin\alpha$, and define

$$\mu = \varepsilon \cot\alpha, \tag{10.11}$$

then the scaled momentum equations are

$$\begin{aligned}
\frac{\partial \tau_{12}}{\partial y} + \frac{\partial \tau_{13}}{\partial z} &= -1 + \mu \frac{\partial s}{\partial x} + \varepsilon^2 \left(\frac{\partial p}{\partial x} - \frac{\partial \tau_{11}}{\partial x} \right),\\
\frac{\partial s}{\partial y} &= \frac{\varepsilon^2}{\mu} \left[-\frac{\partial p}{\partial y} + \frac{\partial \tau_{12}}{\partial x} + \frac{\partial \tau_{22}}{\partial y} + \frac{\partial \tau_{23}}{\partial z} \right],\\
\frac{\partial p}{\partial z} &= \frac{\partial \tau_{13}}{\partial x} + \frac{\partial \tau_{23}}{\partial y} + \frac{\partial \tau_{33}}{\partial z}.
\end{aligned} \tag{10.12}$$

The boundary conditions (10.7) and (10.8) are unchanged in form, and the stress conditions at the top surface $z = s(x, y, t)$ (10.6) become

$$\begin{aligned}
\varepsilon^2(-p + \tau_{11}) s_x + \tau_{12} s_y - \tau_{13} &= 0,\\
\tau_{12} s_x + (-p + \tau_{22}) s_y - \tau_{23} &= 0,\\
\tau_{13} s_x + \tau_{23} s_y - (-p + \tau_{33}) &= 0.
\end{aligned} \tag{10.13}$$

To get some idea of typical magnitudes, use values $d \sim 100$ m, $l \sim 10$ km, $\tan\alpha \sim 0.1$; then $\varepsilon \sim 10^{-2}$, $\mu \sim 10^{-1}$, so that to leading order $s = s(x, t)$ and

$$\frac{\partial \tau_{12}}{\partial y} + \frac{\partial \tau_{13}}{\partial z} = -1 + \mu \frac{\partial s}{\partial x}; \tag{10.14}$$

we retain the μ term for the moment.

The final relation to choose d (and hence also $[\tau]$) is determined by effecting a balance in the flow law. If the viscosity scale is $[\eta]$, then we choose

$$[\tau] = \frac{[\eta] U}{d}. \tag{10.15}$$

For example, for Glen's law, we can choose $[\eta] = \dfrac{1}{2[A][\tau]^{n-1}}$, from which we find

$$d = \left[\frac{[a]l}{2[A](\rho g \sin\alpha)^n}\right]^{1/(n+2)}, \tag{10.16}$$

which leads, using typical choices of the parameters given in table 10.1, to values of d comparable to those observed ($d = 128$ m).

Symbol	Definition	Glacier value	Ice sheet value
$[a]$	accumulation rate	1 m y^{-1}	0.1 m y^{-1}
$[A]$	flow rate constant	0.2 bar^{-n} y^{-1}	
c_p	specific heat	2 kJ kg^{-1} K^{-1}	
E	activation energy	139 kJ $mole^{-1}$	
g	gravity	9.8 m s^{-2}	
G	geothermal heat flux	60 mW m^{-2}	
k	thermal conductivity	2.2 W m^{-1} K^{-1}	
l	length	10 km	3,000 km
L	latent heat	3.3×10^5 J kg^{-1}	
n	Glen exponent	3	
R	gas constant	8.3 J $mole^{-1}$ K^{-1}	
$\sin\alpha$	slope	0.1	n/a
T_M	melting temperature	273 K	
ΔT	surface temperature deficit	20 K	50 K
ρ	ice density	917 kg m^{-3}	

Table 10.1: Typical values of constants for ice flow in glaciers and, where different, ice sheets. The activation energy for ice flow is the value appropriate between $-10°$ and $0°$ C. For temperatures less than $-10°$, $E = 60$ kJ mol^{-1}. For shear-dominated flows such as ice sheets, it is the warmer value which is more relevant.

The two important shear stresses are given by

$$\tau_{13} = \eta\left(\frac{\partial u}{\partial z} + \varepsilon^2\frac{\partial w}{\partial x}\right), \quad \tau_{12} = \eta\left(\frac{\partial u}{\partial y} + \varepsilon^2\frac{\partial v}{\partial x}\right), \tag{10.17}$$

and the second stress invariant τ is given by

$$\tau^2 = \tau_{13}^2 + \tau_{12}^2 + \varepsilon^2\left[\tfrac{1}{2}\left(\tau_{11}^2 + \tau_{22}^2 + \tau_{33}^2\right) + \tau_{23}^2\right]; \tag{10.18}$$

for Glen's flow law, the dimensionless viscosity is

$$\eta = \frac{1}{A(T)\tau^{n-1}}, \tag{10.19}$$

where $A(T)$ is the scaled (with $[A]$) temperature dependent rate factor. If we now put $\varepsilon = 0$ (the shallow ice approximation) we see that

$$\tau \approx \eta|\boldsymbol{\nabla} u|, \tag{10.20}$$

where $\boldsymbol{\nabla} = (\partial/\partial y, \partial/\partial z)$, and for Glen's law,

$$\eta = A^{-1/n} |\boldsymbol{\nabla} u|^{-(n-1)/n} \tag{10.21}$$

(note $n = 1$ for a Newtonian flow; Glen's law usually assumes $n = 3$); the determination of velocity distribution in a cross section S of a glacier then reduces to the elliptic equation for u in S (putting $\mu = 0$ and $\varepsilon = 0$ in $(10.12)_1$):

$$\boldsymbol{\nabla}.[\eta\{A, |\boldsymbol{\nabla} u|\}\boldsymbol{\nabla} u] = -1 \quad \text{in} \quad S, \tag{10.22}$$

with appropriate boundary conditions for no slip at the base being $u = 0$ on $z = b$, and the no stress condition at $z = s$ is, from $(10.13)_1$ and (10.17) with $s_y \approx 0$ and $\varepsilon = 0$, $\partial u/\partial z = 0$. The scalar s (independent of y) is determined through prescription of the downslope ice volume flux, $\displaystyle\int_S u \, dy \, dz = Q$, which will depend on x and t, but can be presumed to be known. In general, this problem requires numerical solution. Analytic solutions are available for constant A and a semi-circular cross section, but the free boundary choice of s cannot then be made.

Most studies of wave motion and other dynamic phenomena ignore lateral variation with y, and in this case (with $\tau_{13} = 0$ on $z = s$) (10.14) gives

$$\tau_{13} = (1 - \mu s_x)(s - z), \tag{10.23}$$

and Glen's law is, approximately,

$$\frac{\partial u}{\partial z} = A(T) \, |\tau_{13}|^{n-1} \, \tau_{13} = A(T) \, |1 - \mu s_x|^{n-1} \, (1 - \mu s_x)(s - z)^n. \tag{10.24}$$

If $A = 1$ is constant, then two integrations of (10.24) give the ice flux $Q = \displaystyle\int_b^s u \, dz$ as

$$Q = u_b H + |1 - \mu s_x|^{n-1} \, (1 - \mu s_x) \frac{H^{n+2}}{n + 2}, \tag{10.25}$$

where $H = s - b$ is the depth, and u_b is the sliding velocity. Integration of the mass conservation equation, together with the basal velocity condition (10.7) and the kinematic surface boundary condition (10.8), then leads to the integral conservation law

$$\frac{\partial H}{\partial t} + \frac{\partial Q}{\partial x} = a, \tag{10.26}$$

where a is the dimensionless accumulation rate. (10.26) is an equation of convective diffusion type, with the diffusive term being that proportional to μ. For a glacier, it is reasonable to assume that $1 - \mu s_x > 0$, meaning that the ice surface is always inclined downhill, and in this case the modulus signs in (10.25) are redundant. In essence, this unidirectionality of slope is what distinguishes a glacier from an ice cap or ice sheet.

Note that if transverse variations were to be included, we should solve

$$\frac{\partial S}{\partial t} + \frac{\partial Q}{\partial x} = a, \tag{10.27}$$

where S is the cross sectional area, and Q would be given by $Q = \displaystyle\int_S u \, dS$, where u solves (10.22) in the cross section S, together with appropriate boundary conditions.

10.2.2 Ice sheets

A model for ice sheets can be derived in much the same way — typical aspect ratios are 10^{-3} — but there is no 'downslope' gravity term $\rho g \sin\alpha$ (effectively $\alpha = 0$), and the appropriate balance determines the driving shear stress at the base in terms of the surface slope. Effectively, the advection term is lost and $\mu = 1$. Another difference is that $x \sim y \sim l$ (~ 3000 km) while $z \sim 3$ km is the only small length scale.

We will illustrate the scaling in two dimensions; the three dimensional version is relegated to the exercises (question 10.4). In two dimensions, we write the deviatoric stresses as

$$\tau_{11} = -\tau_{33} = \tau_1, \quad \tau_{13} = \tau_3. \tag{10.28}$$

Then the governing equations are

$$\begin{aligned} u_x + w_z &= 0, \\ 0 &= -p_x + \tau_{1x} + \tau_{3z}, \\ 0 &= -p_z + \tau_{3x} - \tau_{1z} - \rho g, \\ \dot{\varepsilon}_{ij} &= A\tau^{n-1}\tau_{ij}. \end{aligned} \tag{10.29}$$

The surface stress boundary conditions are, on $z = s$,

$$\begin{aligned} (-p + \tau_1)s_x - \tau_3 &= -p_a s_x, \\ \tau_3 s_x - (-p - \tau_1) &= p_a; \end{aligned} \tag{10.30}$$

at the base $z = b(x, y, t)$, we prescribe the velocity:

$$u = u_b, \quad w = ub_x; \tag{10.31}$$

and on $z = s$, the kinematic condition is

$$w = s_t + us_x - a. \tag{10.32}$$

We scale the variables by putting

$$\begin{aligned} &u \sim U;\ w \sim [a]; \\ &x \sim l;\ z, b, s \sim d; \quad t \sim l/U; \\ &\tau_3 \sim [\tau];\ A \sim [A];\ a \sim [a]; \\ &p - p_a - \rho_i g(s - z) \sim \varepsilon[\tau]; \\ &\tau_1 \sim \varepsilon[\tau], \end{aligned} \tag{10.33}$$

where

$$\varepsilon = \frac{d}{l}. \tag{10.34}$$

An appropriate balance of terms is effected by choosing

$$U = 2[A][\tau]^n d = \frac{[a]}{\varepsilon}, \quad [\tau] = \rho g d\varepsilon, \tag{10.35}$$

and this leads to

$$d = \left(\frac{[a] l^{n+1}}{2[A](\rho g)^n} \right)^{\frac{1}{2(n+1)}}, \tag{10.36}$$

and thus

$$\varepsilon = \left(\frac{[a]}{2[A](\rho g)^n l^{n+1}} \right)^{\frac{1}{2(n+1)}}, \tag{10.37}$$

and the typical values of the constants in table 10.1 do lead to a depth scale of the correct order of magnitude, $d = 3595$ m, so that $\varepsilon \sim 10^{-3}$.

The corresponding dimensionless equations are

$$\begin{aligned} u_x + w_z &= 0, \\ 0 &= -s_x + \tau_{3z} + \varepsilon^2 \left[-p_x + \tau_{1x} \right], \\ 0 &= -p_z + \tau_{3x} - \tau_{1z}, \\ \left(u_z + \varepsilon^2 w_x \right) &= A\tau^{n-1}\tau_3, \\ 2u_x &= A\tau^{n-1}\tau_1, \\ \tau^2 &= \tau_3^2 + \varepsilon^2 \tau_1^2, \end{aligned} \tag{10.38}$$

and the boundary conditions are, on $z = s$:

$$\begin{aligned} \tau_3 + \varepsilon^2 (p - \tau_1) s_x &= 0, \\ \tau_3 s_x + p + \tau_1 &= 0, \\ w &= s_t + u s_x - a; \end{aligned} \tag{10.39}$$

at the base $z = b(x, y, t)$:

$$u = u_b, \quad w = u b_x. \tag{10.40}$$

The shallow ice approximation puts $\varepsilon = 0$, and then we successively find

$$\tau_3 = -s_x (s - z), \quad \tau = |s_x| (s - z), \tag{10.41}$$

whence

$$p + \tau_1 = \left[s s_x \right]_x (s - z) + \tfrac{1}{2} (z^2 - s^2) s_{xx}, \tag{10.42}$$

and, if we assume that $A = 1$ is constant, the ice flux is

$$\int_b^s u \, dz = u_b H + \frac{H^{n+2}}{n+2} |s_x|^{n-1} \left(-s_x \right), \tag{10.43}$$

so that conservation of mass leads to

$$\frac{\partial H}{\partial t} = \frac{\partial}{\partial x} \left[\frac{H^{n+2}}{n+2} |s_x|^{n-1} s_x - H u_b \right] + a, \tag{10.44}$$

a nonlinear diffusion equation for the depth H, since $s = H + b$.

The three-dimensional version of this equation is (with $\boldsymbol{\nabla} = (\partial/\partial x,\ \partial/\partial y)$)

$$H_t = \boldsymbol{\nabla} . \left[\left\{ \frac{|\boldsymbol{\nabla} s|^{n-1} H^{n+2}}{n+2} \boldsymbol{\nabla} s \right\} - H \mathbf{u}_b \right] + a. \tag{10.45}$$

The term in the sliding velocity $\mathbf{u}_b$ is apparently a convective term, but in fact the sliding law usually has $\mathbf{u}_b$ in the direction of shear stress, whence $\mathbf{u}_b \propto -\boldsymbol{\nabla} s$, and this term also is diffusive.

Boundary conditions

Normally one would expect a boundary condition to be applied for (10.45) at the margin of the ice sheet, whose location itself may not be known. For an ice sheet that terminates on land, this condition would be $H = 0$ at the margin, but since the diffusion equation (10.45) is degenerate, in the sense that the diffusion coefficient vanishes where $H = 0$, no extra condition to specify the margin location is necessary, other than requiring that the ice flux also vanish where $H = 0$.

A different situation pertains for a marine ice sheet which terminates (and is grounded), let us suppose, at the edge of the continental shelf. Then the margin position is known, and the ice thickness and flux are finite. In this case, the appropriate condition is to prescribe H at the margin, on the basis that the ice (approximately) reaches flotation there.

A more representative condition for marine ice sheets occurs when the grounded ice extends into an ice shelf before the continental shelf edge is reached. Extended ice shelves occur in the Antarctic ice sheet, two notable examples being the Ronne-Filchner ice shelf and the Ross ice shelf. The grounding line where the ice changes from grounded ice to floating ice is a free boundary whose location must be determined. The appropriate boundary condition for the ice sheet at the grounding line is bound up with the mechanics of the ice shelf, whose behaviour is altogether different; the mechanics of ice shelves is studied in section 10.2.6, and the problem of determining the grounding line is studied in section 10.2.7.

10.2.3 Temperature equation

Although the isothermal models are mathematically nice, they are apparently not quantitatively very realistic. For a glacier, probably the neglect of variation of the rate parameter $A(T)$ in the flow law is as important as the assumption of a two-dimensional flow, although the possible coupling of temperature to water production and basal sliding is also significant. For ice sheets, temperature variation is unquestionably significant, and cannot in practice be neglected.

Boundary conditions

The ice temperature is governed by the energy equation (10.2), and it must be supplemented by suitable boundary conditions. At the ice surface, an appropriate boundary condition follows from consideration of energy balance, much as in chapter 3, but for purposes of exposition, we suppose that the ice surface temperature is equal to a prescribed air temperature, thus

$$T = T_A \quad \text{at} \quad z = s. \tag{10.46}$$

The boundary conditions at the base are more complicated. While the ice is frozen, we prescribe a geothermal heat flux G, and presume the ice is frozen to the base, so that there is no slip, thus

$$-k\frac{\partial T}{\partial n} = G, \quad T < T_M, \quad u = 0 \quad \text{at} \quad z = b, \tag{10.47}$$

where T_M is the melting temperature, which depends weakly on pressure; $\mathbf{n}$ is the unit normal pointing upwards at the base. Classically, one supposes that when T reaches T_M, a lubricating Weertman film separates the ice from the bed, allowing slip to take place, so that we have a sliding velocity $u = u_b$, in which, for example, u_b is a function of basal shear stress τ_b. The details of the calculation of this sliding velocity are detailed in section 10.3. For the moment it suffices to point out that the transition from no sliding to a full sliding velocity must occur over a narrow range of temperature near the melting point, when only a partial water film is present. In this régime, there is no net production of water at the base, the temperature is essentially at the melting point, and there is sliding, but this is less than the full sliding velocity u_b; we call this the sub-temperate régime:

$$-k\frac{\partial T}{\partial n} = G + \tau_b u, \quad T = T_M, \quad 0 < u < u_b. \tag{10.48}$$

The term $\tau_b u$ represents the frictional heat delivered to the base by the work of sliding.[7]

When the water film is completely formed, there is net water production at the base, and the sliding velocity reaches its full value; this is the temperate régime:

$$0 < -k\frac{\partial T}{\partial n} < G + \tau_b u, \quad T = T_M, \quad u = u_b. \tag{10.49}$$

In all the above régimes, the ice above the bed is cold. When the heat flux $-k\dfrac{\partial T}{\partial n}$ reaches zero, the ice above the bed becomes temperate and moist, containing water. In this case the energy equation must be written as an equation for the enthalpy

$$h = c_p\,(T - T_M) + Lw, \tag{10.50}$$

where L is latent heat, and w is the mass fraction of water inclusions, and the inequalities $T \leq T_M$ in the above conditions can be replaced by the inequalities $h \leq 0$. Proper formulation of the correct thermal boundary condition when $h > 0$ now requires an appropriate formulation for the enthalpy flux q_n when $w > 0$, and this requires a description of moisture transport in the moist ice. This goes some way beyond our present concerns, and is not pursued further here.

Non-dimensionalisation

With variables scaled as in the previous section for an ice sheet, the temperature equation for an ice sheet may be written approximately as

$$T_t + \mathbf{u}.\boldsymbol{\nabla} T = \frac{\alpha\tau^2}{\eta} + \beta T_{zz}, \tag{10.51}$$

[7] An alternative formulation combines the frozen and sub-temperate régimes by allowing the sliding velocity to be a function of temperature near the melting point. This may be a simpler formulation to use in constructing numerical solutions.

where $T - T_M$ is scaled with ΔT (a typical surface temperature below melting point). The stress invariant τ is related to the horizontal velocity $\mathbf{u}_H = (u, v)$ by

$$\tau \approx \eta \left| \frac{\partial \mathbf{u}_H}{\partial z} \right| = (s - z)|\boldsymbol{\nabla} s|, \tag{10.52}$$

since the horizontal stress vector $\boldsymbol{\tau} = (\tau_{13}, \tau_{23})$ satisfies

$$\boldsymbol{\tau} = \eta \frac{\partial \mathbf{u}_H}{\partial z} = -(s - z)\boldsymbol{\nabla} s. \tag{10.53}$$

The parameters α and β are given by

$$\alpha = \frac{gd}{c_p \Delta T}, \ \beta = \frac{\kappa}{d[a]}, \tag{10.54}$$

where d is the depth scale, c_p is the specific heat, g is gravity, $\kappa = \dfrac{k}{\rho c_p}$ is the thermal diffusivity, and $[a]$ is accumulation rate. Using the values in table 10.1, together with $d = 3{,}500$ m, we find that typical values for an ice sheet are $\alpha \sim 0.3$, $\beta \sim 0.1$. We see that viscous heating (the α term) is liable to be significant, while thermal conduction is small or moderate.

The dimensionless forms of the temperature boundary conditions (10.46)–(10.49) take the form

$$T = T_A \quad \text{at} \quad z = s, \tag{10.55}$$

where the scaled surface temperature T_A is negative and $O(1)$. At the base $z = b$, we have

$$\begin{aligned} -\frac{\partial T}{\partial n} &= \Gamma, \quad T < 0, \quad u = 0, \\ -\frac{\partial T}{\partial n} &= \Gamma + \frac{\alpha \tau_b u}{\beta}, \quad T = 0, \quad 0 < u < u_b, \\ 0 < -\frac{\partial T}{\partial n} &< \Gamma + \frac{\alpha \tau_b u}{\beta}, \quad T = 0, \quad u = u_b, \end{aligned} \tag{10.56}$$

where

$$\Gamma = \frac{Gd}{k \Delta T}. \tag{10.57}$$

For values of the parameters in table 10.1, and with $d = 3{,}500$ m, we have $\Gamma \approx 1.9$, so that the geothermal heat flux is significant, and temperature variation is important.

The dimensional rate factor in the flow law is modelled as

$$A = A_0 \exp\left(-\frac{E}{RT}\right), \tag{10.58}$$

and in terms of the non-dimensional temperature, this can be written in the form

$$A = [A] \exp\left[\frac{E}{RT_M}\left\{1 - \left(1 + \frac{\Delta T}{T_M} T\right)^{-1}\right\}\right], \tag{10.59}$$

where

$$[A] = A_0 \exp\left(-\frac{E}{RT_M}\right). \tag{10.60}$$

Assuming $\Delta T \ll T_M$, we can write (10.58) in the approximate form

$$A \approx e^{\gamma T}, \tag{10.61}$$

where now A is the dimensionless rate factor, and

$$\gamma = \frac{E\Delta T}{RT_M^2}. \tag{10.62}$$

Using the values for the activation energy E and gas constant R in table 10.1, we find $\gamma \approx 11.2$. Because this relatively large value occurs in an exponent, its largeness is enhanced.[8]

The temperature equation for a (two-dimensional) valley glacier is the same as (10.51), although in the definition of α, we replace d by $l \sin\alpha$. With the previous scalings, (10.52) is corrected by simply replacing $|\boldsymbol{\nabla} s|$ in the last expression by $|1 - \mu s_x|$). Although the scales are different, typical values of α and β (from table 10.1) are $\alpha \sim 0.25$, $\beta \sim 0.29$, and thus of significance. On the other hand, geothermal heat is of less importance, with a typical estimate being $\Gamma \approx 0.17$.[9]

10.2.4 A simple non-isothermal ice sheet model

The fact that the ice sheet model collapses to a simple non-linear diffusion equation (10.45) when the rate coefficient is independent of temperature raises the question of whether any similar simplification can be made when temperature dependence is taken into account. The answer to this is yes, provided some simplifying approximations are made. Before doing this, we revisit the non-dimensionalisation in (10.33). The balance of terms in (10.35) is based on the assumption that shearing is important throughout the thickness of the ice. However, this is not entirely accurate. The largeness of the rheological coefficient γ implies that shearing will be concentrated near the bed, where it is warmest. This effect is amplified by the smallness of β, which means that temperature gradients may be confined to a thin basal thermal boundary layer, and also by the largeness of the Glen exponent n, which increases the shear near the bed. To allow for shearing being restricted to a height of $O(\nu) \ll 1$ above the bed, we adjust the balance in (10.35) by choosing

$$U = 2[A][\tau]^n \nu d, \tag{10.63}$$

[8] However, the value of E is smaller below $-10°$ C, which serves to modify the severity of the temperature dependence of A at cold temperatures.

[9] This raises an interesting issue in the modelling of glaciers. So little heat is supplied geothermally that it seems difficult to raise the ice temperature much above the surface average value anywhere. In practice, the presence of crevasses allows meltwater and rainfall to access the glacier bed, and the re-freezing of even a modest depth of water enormously enhances the effective heat supplied to the bed via the latent heat released. For example, a meltwater supply of 10 cm per year to the bed raises the effective value of Γ to 2.9.

with the other choices remaining the same. The change to the depth scale in (10.36) is obtained by replacing $[A]$ by $\nu[A]$. We will choose ν below. Note that If $\nu = 0.1$, then the depth scale is increased by a factor of $10^{1/8} \approx 1.33$ to 4,794 m, still appropriate for large ice sheets.

The shallow ice approximation then leads to the model

$$\begin{aligned} T_t + \mathbf{u}\,.\boldsymbol{\nabla} T &= \frac{\alpha}{\nu}\tau^{n+1}e^{\gamma T} + \beta T_{zz}, \\ \nu\frac{\partial \mathbf{u}}{\partial z} &= \tau^{n-1}\boldsymbol{\tau} e^{\gamma T}, \\ H_t + \boldsymbol{\nabla}.\left\{\int_b^s \mathbf{u}\,dz\right\} &= a, \\ \boldsymbol{\tau} &= -(s-z)\boldsymbol{\nabla} s, \end{aligned} \tag{10.64}$$

where $H = s - b$ is the depth, $\mathbf{u} = \mathbf{u}_H = (u, v)$ is the horizontal velocity, and α, β and γ retain their earlier definitions in (10.54) and (10.62).

We now suppose that $\gamma \gg 1$ and $\beta \ll 1$. The temperature then satisfies the approximate equation

$$T_t + \mathbf{u}\,.\boldsymbol{\nabla} T = 0, \tag{10.65}$$

where also $(10.64)_2$ implies the plug flow $\mathbf{u} = \mathbf{u}(x, y)$. This 'outer' equation is valid away from the base, where there must be a basal boundary layer and a shear layer in order to satisfy velocity and temperature boundary conditions.

For simplicity, let us consider the particular case of steady flow over a flat bed, so that $b = 0$, $H = s$, and time derivatives are ignored. The vertical velocity for the plug flow is

$$w \approx -z\Delta, \quad \Delta = u_x + v_y, \tag{10.66}$$

so that T satisfies

$$uT_x + vT_y - z\Delta T_z = 0. \tag{10.67}$$

In two dimensions, it is easy to solve this, because there is a stream function. For example, if $v \equiv 0$, then the general solution is $T = f(zu)$. Similarly, if $u \equiv 0$, then $T = f(zv)$. It is not difficult to see that the general solution for a two-dimensional flow is then $T = f(z|\mathbf{u}|)$.

This suggests that we seek solutions in the form

$$T = f(zU), \quad U = U(x, y). \tag{10.68}$$

Note that U is defined up to an arbitrary multiple. Substituting this into (10.67), we find that U satisfies the equation

$$\left(\frac{u}{U}\right)_x + \left(\frac{v}{U}\right)_y = 0, \tag{10.69}$$

whence there is a function χ such that

$$u = U\chi_y, \quad v = -U\chi_x. \tag{10.70}$$

Note that $(10.64)_{2,4}$ imply that

$$\mathbf{u} = -K\boldsymbol{\nabla} s \tag{10.71}$$

for some scalar K, and therefore (10.70) implies that $\boldsymbol{\nabla} s.\boldsymbol{\nabla}\chi = 0$, and the level sets of s and χ form an orthogonal coordinate system. In particular, the coordinate $-s$ points down the steepest descent paths of the surface $z = s$, while the coordinate χ tracks anti-clockwise round the contours of s. Note that for a steady flow in which a is finite, there can be no minima of s, and the flow is everywhere downhill. In general, the contours of s are closed curves, and the coordinates $-s$, χ are like generalised polar coordinates. Complications arise if there are saddles, but these simply divide the domain into different catchments, each of which can be treated separately.

If we change to independent coordinates s and χ, then we find, after some algebra,

$$\frac{\partial}{\partial s}\left(\frac{U}{|\mathbf{u}|}\right) = -\frac{K}{|\mathbf{u}|^3}\left(uv_\chi - vu_\chi\right). \tag{10.72}$$

Let θ be the angle of the flow direction to the x axis, so that $\tan\theta = \dfrac{v}{u}$. Calculating the derivative of θ, we then find that the equation (10.72) takes the form

$$\frac{\partial}{\partial s}\left(\frac{U}{|\mathbf{u}|}\right) = -\frac{1}{|\boldsymbol{\nabla} s|}\frac{\partial\theta}{\partial\chi}, \tag{10.73}$$

and this is our basic equation to determine U. Note that in a two-dimensional flow where $\dfrac{\partial}{\partial\chi} = 0$, we regain $U = |\mathbf{u}|$ as before.

A more user-friendly version of (10.73) follows from the following geometrical considerations. From (10.70), we have $|\boldsymbol{\nabla}\chi| = \dfrac{|\mathbf{u}|}{U}$, and since s and χ are orthogonal, it follows that

$$\frac{d\chi}{d\sigma} = \frac{|\mathbf{u}|}{U} \tag{10.74}$$

on level contours of s, where σ is arc length measured anti-clockwise. Now the curvature of a level s contour[10] is defined by

$$\kappa = \frac{d\theta}{d\sigma}. \tag{10.75}$$

Therefore $\dfrac{\partial\theta}{\partial\chi} = \dfrac{\kappa U}{|\mathbf{u}|}$; in addition distance ξ at the base below a steepest descent path on the surface satisfies $d\xi = -\dfrac{ds}{|\boldsymbol{\nabla} s|}$, and therefore (10.73) can be written in the form

$$\frac{\partial}{\partial\xi}\left(\frac{U}{|\mathbf{u}|}\right) = \frac{U\kappa}{|\mathbf{u}|}, \tag{10.76}$$

[10]Strictly this is twice the mean curvature, since in three dimensions the other radius of curvature of the level s contours is infinite.

with solution

$$U = |\mathbf{u}| \exp\left[\int^{\xi} \kappa \, d\xi\right]. \tag{10.77}$$

The constant of integration can be chosen arbitrarily.

Given a surface $z = s(x, y)$, we find the level contours and the steepest descent paths, and we compute from the geometry of the contours their curvature κ. On any steepest descent path, (10.77) then gives U, and the function f is determined by the requirement that the surface temperature

$$T_s = f(sU). \tag{10.78}$$

Along any flow path, sU is a monotone increasing function of $-s$ (see question 10.5), and therefore (10.78) determines f uniquely. Question 10.6 shows a worked example in the particular case of a cylindrically symmetric ice sheet. Typically, with surface temperatures being lower at higher elevation, the outer temperature profiles thus constructed are inverted, i. e., they are colder at depth. There is then an inversion near the base, where a thermal boundary layer reverses the temperature gradient.

Thermal boundary layer structure

We now consider the equations (10.64) near the base of the ice sheet. We will restrict our attention to the case where the ice is at the melting point, but where sliding is negligible. It is straightforward to deal with other cases also.

Away from the base, the temperature satisfies (10.68). More specifically (see question 10.5), we can write the outer solution in the form

$$T = f\left(\frac{z}{s}\int_s^{s_0} \frac{a}{J}\, ds\right), \tag{10.79}$$

where the integral is along a flow line $\chi =$ constant, and J is the Jacobian

$$J = -\frac{\partial(s, \chi)}{\partial(x, y)} > 0 \tag{10.80}$$

of the transformation from (x, y) to $(-s, \chi)$. Here s_0 is the surface elevation at the ridge forming the ice divide where the flow line starts.

Insofar as we might suppose the surface temperature decreases with increasing elevation, it is reasonable to suppose that f is an increasing function of its argument, and thus the temperature in (10.79) increases with height. As $z \to 0$, $T \to f(0) < 0$, and there is a temperature inversion in a thermal boundary layer through which $T \to 0$. In this layer, the plug flow velocity is unaffected, as the exponential terms are negligible. We write

$$z = \beta^{1/2} Z, \tag{10.81}$$

so that the temperature equation takes the approximate form

$$uT_x + vT_y - Z\Delta T_Z = T_{ZZ}. \tag{10.82}$$

It is convenient again to write this in terms of the coordinates s, χ, Z, when the equation becomes

$$-J\left[UT_s - ZU_sT_Z\right] = T_{ZZ}, \tag{10.83}$$

with boundary conditions

$$\begin{aligned} T &= 0 \quad \text{on} \quad Z = 0, \\ T &\to f(0) \quad \text{as} \quad Z \to \infty. \end{aligned} \tag{10.84}$$

We can simplify this by defining

$$X = \int_s^{s_0} \frac{ds}{J}, \quad \Psi = ZU, \tag{10.85}$$

which reduces the problem to

$$\Psi_Z T_X - \Psi_X T_Z = T_{ZZ}. \tag{10.86}$$

A further Von Mises transformation to independent variables (X, Ψ) reduces this to a diffusion equation, for which a similarity solution is appropriate, and this is given by

$$T = f(0)\text{erf}\left[\frac{ZU}{2\sqrt{\Xi}}\right], \tag{10.87}$$

where

$$\Xi = \int_0^X U\, dX = \int_s^{s_0} \frac{U\, ds}{J}. \tag{10.88}$$

A uniform approximation is then given by

$$T = f\left(\frac{z}{s}\int_s^{s_0} \frac{a}{J}\, ds\right) - f(0)\text{erfc}\left\{\frac{zU}{2\sqrt{\beta\Xi}}\right\}. \tag{10.89}$$

To illustrate the consequent temperature profiles, we make simplifying assumptions. For a one-dimensional flow in the x–direction, we have $\chi = y$, $J = -s_x$, $U = u$. Suppose $a = 1$, $u = x$, $s = 1 - x^2$ and that the surface temperature is $T|_s = -s$.We then find that $f(x) = -(1 - x^2)$, and thence

$$T = -\left[1 - \left(\frac{zx}{1 - x^2}\right)^2\right] + \text{erfc}\left[\frac{z}{\sqrt{2\beta}}\right]. \tag{10.90}$$

Figure 10.7 shows two profiles at distances of $x = 0.1$ and $x = 0.5$ along the flow line, which resemble the sorts of profiles which are typically measured (and which are also found in direct numerical simulations).

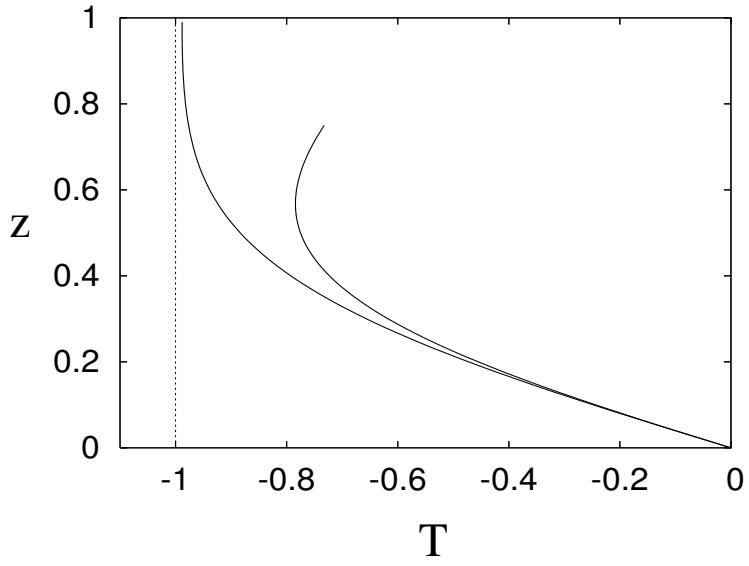

Figure 10.7: Typical temperature profiles at $x = 0.1$ and $x = 0.5$ for the uniform approximation (10.89), for the particular assumptions in (10.90). The value of $\beta = 0.1$.

Shear layer

Embedded within the thermal boundary layer is a thinner shear layer of thickness $O(\nu)$, to be determined. From the thermal boundary layer solution (10.87), we have $T \sim \dfrac{f(0)UZ}{\sqrt{\pi\Xi}}$ as $Z \to 0$; additionally we require $T \sim \dfrac{1}{\gamma}$ in the shear layer in order that there be non-zero shear. Thus we define

$$\theta = \gamma T, \quad \nu = \frac{\sqrt{\beta}}{\gamma}, \tag{10.91}$$

which confirms that $\nu \ll \sqrt{\beta}$, and thus the shear layer is indeed embedded within the thermal boundary layer. Defining $z = \nu\zeta$, the shear layer equations become, to leading order,

$$\begin{aligned} \boldsymbol{\tau} &= -s\boldsymbol{\nabla}s, \\ \frac{\partial \mathbf{u}}{\partial \zeta} &= \tau^{n-1}\boldsymbol{\tau}e^{\theta}, \\ 0 &= \mathcal{A}\tau^{n+1}e^{\theta} + \theta_{\zeta\zeta}, \end{aligned} \tag{10.92}$$

where

$$\mathcal{A} = \frac{\alpha}{\sqrt{\beta}}. \tag{10.93}$$

Using the values $\alpha \sim 0.3$, $\beta \sim 0.1$, then $\mathcal{A} \approx 1$, and it is sensible to suppose formally that $\alpha \sim \sqrt{\beta}$, so that $\mathcal{A} \sim O(1)$. Suitable boundary conditions for the equations are

then (supposing sliding is negligible)

$$\begin{aligned} \mathbf{u} = 0, \quad \theta = 0 \quad &\text{at} \quad \zeta = 0, \\ \theta \sim \frac{f(0)U\zeta}{\sqrt{\pi\Xi}} \quad &\text{as} \quad \zeta \to \infty. \end{aligned} \tag{10.94}$$

Integrating the temperature equation in the form $\theta_{\zeta\zeta} + \mathcal{A}\boldsymbol{\tau}.\mathbf{u}_\zeta = 0$, we find that indeed $\mathbf{u} = -K\boldsymbol{\nabla}s$, where

$$K = \frac{\theta_\zeta|_\infty^0}{\mathcal{A}s|\boldsymbol{\nabla}s|^2}. \tag{10.95}$$

Direct integration of the temperature equation gives the solution in the form

$$\theta = -2\ln\left[B\cosh\left(\sqrt{\frac{\lambda}{2}}\frac{\zeta}{B} + C\right)\right], \tag{10.96}$$

where

$$\lambda = \mathcal{A}\tau^{n+1}. \tag{10.97}$$

Applying the boundary conditions, we find after some algebra that, if we define $f(0) = -T_R$, then

$$K = \frac{T_R U(1 - \tanh C)}{\sqrt{\pi\Xi}\mathcal{A}s|\boldsymbol{\nabla}s|^2}, \tag{10.98}$$

where

$$\cosh C = \frac{T_R U}{\sqrt{2\lambda\pi\Xi}}. \tag{10.99}$$

(10.98) defines K implicitly and non-locally along a flow line, since (10.77) implies that $U \propto K$, and thus (10.88) implies that Ξ involves an integral of K. Given s, we can determine K and hence $\mathbf{u}$, and this can be used to evolve the surface via the diffusion equation

$$s_t = \boldsymbol{\nabla}.(sK\boldsymbol{\nabla}s) + a. \tag{10.100}$$

This is not strictly accurate, since the (outer) temperature is assumed stationary. However, the outer temperature is only involved in the determination of the velocity field through the prescription of the ridge temperature $-T_R$. If the ridges are stationary, or if the ridge temperature is constant, then the derivation above remains appropriate; if not, T_R must be determined as well.

To illustrate how K is determined, consider the two-dimensional case, where x is in the direction of flow. We then have $\chi = y$, $J = -s_x$, $\kappa = 0$, $X = x$, $U = u$, $\Xi = \displaystyle\int_0^x u\,dx$. In addition, suppose that $T_R = 1$ and that C is sufficiently large that $1 - \tanh C \approx 2e^{-2C} \approx \frac{1}{2}\mathrm{sech}^2 C$. Formally this is the case if $\mathcal{A} \ll 1$. Define

$$L = 2\sqrt{\Xi}; \tag{10.101}$$

we then find that

$$KL' = \sqrt{\pi}s^n|\boldsymbol{\nabla}s|^{n-1}. \tag{10.102}$$

In addition, $U = \frac{1}{2}LL' = K|\boldsymbol{\nabla} s|$; eliminating K, we can derive the differential equation for L

$$LL'^2 = 2\sqrt{\pi} s^n |\boldsymbol{\nabla} s|^n, \tag{10.103}$$

subject to $L(0) = 0$. Solving this, we can then determine K from (10.102).

More generally, with L still defined by (10.101) and $T_R = 1$, (10.98) and (10.99) lead to

$$K = \frac{LL_X}{2W|\boldsymbol{\nabla} s|} = \frac{L_X - \{L_X^2 - 2\pi \mathcal{A} s^{n+1} |\boldsymbol{\nabla} s|^{n+1}\}^{1/2}}{\sqrt{\pi}\mathcal{A} s |\boldsymbol{\nabla} s|^2}, \tag{10.104}$$

where

$$W = \exp\left\{ \int_0^\xi \kappa \, d\xi \right\}. \tag{10.105}$$

Solving for L_X, we find

$$L_X^2 = \frac{8\sqrt{\pi} W^2 \tau^n}{L(4W - \sqrt{\pi}\mathcal{A}\tau)}; \tag{10.106}$$

both L and hence K can be determined from (10.106).

Reverting to two-dimensional flow for a moment, we might suppose that for sufficiently small x, $u \sim x$. Since with $X = x$ and $W = 1$, $u = \frac{1}{2}LL_x$, this suggests $L \sim x$, and $L_x \approx L'$ is constant. From (10.106) (with also τ small), we then have

$$L \approx \frac{2\sqrt{\pi}\tau^n}{L'^2} \tag{10.107}$$

(note that this is only consistent with $L \sim x$ if $\tau \sim x^{1/n}$). From (10.104), we then have

$$K \approx \frac{\sqrt{\pi}}{L'} s^n |s'|^{n-1}, \tag{10.108}$$

and (10.100) takes the form

$$s_t = \mathcal{K} \frac{\partial}{\partial x} \left[s^{n+1} |s_x|^{n-1} s_x \right] + a, \tag{10.109}$$

where

$$\mathcal{K} = \frac{\sqrt{\pi}}{L'}. \tag{10.110}$$

One can show (cf. (10.118) below) that for small x, we indeed have $\tau \sim x^{1/n}$ as required, so that this approximation is consistent. The value of L' is determined by the boundary condition at the margin. For example, if we suppose (10.109) applies all the way to the margin at $x = 1$, where $s = 0$, then we can show for the steady state ice sheet that

$$s(0) = s_0 = \left(\frac{2n+1}{n+1} \right)^{n/(2n+1)}, \tag{10.111}$$

and that $u \approx \dfrac{\sqrt{\pi} x}{L' s_0}$; consistency with $u \approx \frac{1}{2}LL' \approx \frac{1}{2}L'^2 x$ then implies thsat

$$L' = \left(\frac{2\sqrt{\pi}}{s_0} \right)^3, \quad \mathcal{K} = \left(\frac{\pi s_0}{2} \right)^{1/3}. \tag{10.112}$$

The success of this approach suggests an extension to the three-dimensional model (10.104). If we suppose L_X and W are approximately constant, then we find

$$L \approx \frac{8\sqrt{\pi}W^2\tau^n}{L_X^2(4W - \sqrt{\pi}\mathcal{A}\tau)}, \quad K \approx \frac{4\sqrt{\pi}W\tau^n}{L_X|\boldsymbol{\nabla} s|(4W - \sqrt{\pi}\mathcal{A}\tau)}, \tag{10.113}$$

and thus (10.100) takes the form

$$s_t = \boldsymbol{\nabla}.\,[D\boldsymbol{\nabla} s] + a, \tag{10.114}$$

where

$$D = \frac{\sqrt{\pi}}{L_X}\frac{s^{n+1}|\boldsymbol{\nabla} s|^{n-1}}{\left\{1 - \dfrac{\mathcal{A}\sqrt{\pi}s|\boldsymbol{\nabla} s|}{4W}\right\}}. \tag{10.115}$$

10.2.5 Using the equations

Nonlinear diffusion

The derivation of (10.114) shows that for a temperature-dependent ice flow law, one reasonably obtains a nonlinear diffusion equation to govern the ice sheet evolution. Similarly, for flow over a flat base, $h = 0$, with no sliding, the isothermal ice sheet equation (10.45) is just

$$s_t = \boldsymbol{\nabla}.\left[\frac{s^{n+2}|\boldsymbol{\nabla} s|^{n-1}}{n+2}\boldsymbol{\nabla} s\right] + a, \tag{10.116}$$

which for Glen's flow law would have $n = 3$. This is a degenerate nonlinear diffusion equation, and has singularities at ice margins ($s = 0$) or divides (where $\boldsymbol{\nabla} s/|\boldsymbol{\nabla} s|$ is discontinuous). In one space dimension, we have near a margin $x = x_m(t)$ where $a < 0$ (ablation), assuming zero ice flux there,

$$\begin{aligned} s &\sim (a/|\dot{x}_m|)(x_m - x) \text{ if } \dot{x}_m < 0 \text{ (retreat)}, \\ s &\sim \left(\frac{2n+1}{n}\right)^{\frac{n}{2n+1}} [(n+1)\dot{x}_m]^{\frac{1}{2n+1}}(x_m - x)^{\frac{n}{2n+1}} \text{ if } \dot{x}_m > 0 \text{ (advance)}. \end{aligned} \tag{10.117}$$

This is the common pattern for such equations: margin retreat occurs with finite slope, while for an advance, the slope must be infinite. Consequently, there is a waiting time between a retreat and a subsequent advance, while the front slope grows.

Near a divide $x = x_d$, where $s_x = 0$ and $a > 0$, s is given by

$$s \sim s_0(t) - \left(\frac{n}{n+1}\right)\left[\frac{(n+2)(a - \dot{s}_0)}{s_0^{n+2}}\right]^{1/n}|x - x_d|^{(n+1)/n}, \tag{10.118}$$

and thus the curvature is infinite. Singularities of these types need to be taken into account in devising numerical methods.

Thermal runaway

One of the interesting possibilities of the thermomechanical coupling between flow and temperature fields is the possibility of thermal runaway, and it has even been suggested that this may provide an explanation for the surges of certain thermally regulated glaciers. The simplest model is that for a glacier, with exponential rate factor, thus

$$T_t + \mathbf{u}.\boldsymbol{\nabla} T = \alpha \tau^{n+1} e^{\gamma T} + \beta T_{zz}, \tag{10.119}$$

where the stress is given by

$$\tau = s - z. \tag{10.120}$$

The simplest configuration is the parallel sided slab in which s = constant, $\mathbf{u} = (u(z), 0, 0)$, so that

$$\frac{\partial T}{\partial t} = \alpha (s-z)^{n+1} e^{\gamma T} + \beta \frac{\partial^2 T}{\partial z^2}, \tag{10.121}$$

with (say)

$$T = -1 \text{ on } z = s, \; T_z = -\Gamma \text{ on } z = 0. \tag{10.122}$$

For given s, (10.121) will exhibit thermal runaway for large enough α, and $T \to \infty$ in finite time. As the story goes, this leads to massive melting and enhanced sliding, thus 'explaining' surges. The matter is rather more complicated than this, however. For one thing, s would actually be determined by the criterion that, in a steady state, the flux $\displaystyle\int_0^s u\, dz$ is prescribed, $= B$ say, where B would be the integrated ice accumulation rate from upstream ($= \displaystyle\int a\, dx$).

Thus even if we accept the unrealistic parallel slab 'approximation', it would be appropriate to supplement (10.121) and (10.122) by requiring s to satisfy

$$\int_0^s u\, dz = B. \tag{10.123}$$

Since the flow law gives

$$\frac{\partial u}{\partial z} = (s-z)^n e^{\gamma T}, \tag{10.124}$$

we find, if $u = 0$ on $z = 0$, that (10.123) reduces to

$$\int_0^s (s-z)^{n+1} e^{\gamma T} dz = s. \tag{10.125}$$

Thermal runaway is associated with multiple steady states of (10.121), in which case we wish to solve

$$\begin{aligned} 0 &= \alpha (s-z)^{n+1} e^{\gamma T} + \beta T_{zz}, \\ T &= -1 \text{ on } z = s, \\ T_z &= -\Gamma \text{ on } z = 0, \\ T_z &= -\left[\Gamma + \frac{\alpha B}{\beta}\right] \text{ on } z = s. \end{aligned} \tag{10.126}$$

Putting $\xi = s - z$, we solve

$$T_{\xi\xi} = -\mathcal{A}\xi^{n+1}e^{\gamma T},$$
$$T - 1, \quad T_\xi = \Gamma + \mathcal{A}B \quad \text{on} \quad \xi = 0, \tag{10.127}$$

where

$$\mathcal{A} = \frac{\alpha}{\beta}, \tag{10.128}$$

as an initial value problem. T_ξ is monotone decreasing with increasing ξ, and thus there is a unique value of s such that $T_\xi = \Gamma$ there. It follows that there is a unique solution to the free boundary problem, and in fact it is linearly stable. It then seems that thermal runaway is unlikely to occur in practice.

A slightly different perspective may allow runaway, if we admit non-steady ice fluxes. Formally, we can derive a suitable model if $\mathcal{A} = O(1)$, $\beta \to \infty$. In this case, we can expect T to tend rapidly to equilibrium of (10.121), and then s reacts more slowly via mass conservation, thus

$$s_t + q_x = a,$$
$$q = \frac{1}{\mathcal{A}}[T_z]_0^s. \tag{10.129}$$

An x-independent version of (10.129), consistent with the previous discussion, is

$$\frac{\partial s}{\partial t} = B - q(s), \tag{10.130}$$

and this *will* allow relaxation oscillations if $q(s)$ is multivalued as a function of s — which will be the case. Surging in this sense is conceivable, but the limit $\beta \to \infty$ is clearly unrealistic, and unlikely to be attained. The earlier conclusion is the more likely.

It is also possible to study thermal runaway using the more realistic approach involving a basal shear layer, as in section 10.2.4, and allowing for the separate thermal boundary conditions in (10.56). Although multiple solutions are possible, they are in reality precluded by the transition from one basal thermal régime to another as the basal ice warms. In the last thermal régime, where the basal ice becomes temperate, the dependence of the flow law on moisture content could also allow a runaway, but one which now would involve excess moisture production. Whether this can occur will depend on whether the resultant drainage to the basal stream system can be carried away subglacially, but this process requires a description of water flow within and below the glacier.

10.2.6 Ice shelves

When an ice sheet flows to the sea, as mostly occurs in Antarctica, it starts to float at the *grounding line*, and continues to flow outwards as an *ice shelf*. The dynamics of ice shelves can be described by an approximate theory, but this is very different from that appropriate to ice sheets.

We begin with the equations in the form (10.38) and (10.39), as scaled for the ice sheet. These must be supplemented by conditions on the floating base $z = b$. To be specific, we take the level $z = 0$ to be sea level. The water depth at $z = b$ is thus $-b$, and the resulting hydrostatic pressure must balance the normal stress in the ice. In addition, there is no shear stress. The general form of the (vector) stress balance condition at an interface of this type which supports only a pressure p_i is (cf. (10.6))

$$\boldsymbol{\sigma}.\,\mathbf{n} = -p_i\mathbf{n}, \tag{10.131}$$

and in addition to this there is a kinematic boundary condition. When written in terms of the ice sheet scales, these boundary conditions become

$$\begin{aligned} -\tau_3 + \varepsilon^2(-p+\tau_1)b_x &= (s+\delta b)b_x, \\ s &= -\delta b - \varepsilon^2\left[\tau_3 b_x + p + \tau_1\right], \\ w &= b_t + ub_x - m, \end{aligned} \tag{10.132}$$

in which m is the bottom melting rate, and the parameter δ is given by

$$\delta = \frac{\rho_w - \rho_i}{\rho_i}, \tag{10.133}$$

where ρ_i and ρ_w are ice and water densities. The second of these conditions, the flotation condition, essentially says that 90% of the ice is below the surface, as in Archimedes' principle.

Whereas the dominant force balance in the ice sheet is between shear stress and horizontal pressure gradient, and longitudinal stresses are negligible, this is not true in the ice shelf, where the opposite is true: shear stress is small, and the primary balance is between longitudinal stress and horizontal pressure gradient. Therefore the equations must be rescaled in order to highlight this fact. The issue is complicated by the presence of two small parameters $\delta \sim 0.1$ and $\varepsilon \sim 10^{-3}$.

We suppose that the length scale for the ice shelf is $x \sim \lambda$ (relative to the horizontal ice sheet scale), and that the depth scale is $z \sim \nu$, and we anticipate that $\nu \ll 1$. We then find that a suitable balance of terms reflecting the dominance of longitudinal stresses is given by writing

$$\begin{gathered} x \sim \lambda, \quad z, b \sim \nu, \quad u \sim \frac{1}{\nu}, \quad w \sim \lambda, \\ p, \tau_1 \sim \frac{\delta\nu}{\varepsilon^2}, \quad \tau_3 \sim \frac{\delta\nu^2}{\lambda}, \quad \tau \sim \frac{\delta\nu}{\varepsilon}, \quad s \sim \delta\nu. \end{gathered} \tag{10.134}$$

The governing equations become

$$\begin{aligned} u_x + w_z &= 0, \\ 0 &= -s_x + \tau_{3z} - p_x + \tau_{1x}, \\ 0 &= -p_z - \tau_{1z} + \omega^2\tau_{3x}, \\ \left(u_z + \omega^2 w_x\right) &= \omega^2\tau^{n-1}\tau_3, \\ 2u_x &= \tau^{n-1}\tau_1, \\ \tau^2 &= \omega^2\tau_3^2 + \tau_1^2, \end{aligned} \tag{10.135}$$

and the appropriate boundary conditions are, on the top surface $z = \delta s$:

$$\begin{aligned} \tau_3 + \delta(p - \tau_1)s_x &= 0, \\ p + \tau_1 + \delta\omega^2\tau_3 s_x &= 0, \\ w &= \lambda\delta\nu s_t + \delta u s_x - \lambda a; \end{aligned} \tag{10.136}$$

and on the base $z = b$:

$$\begin{aligned} \tau_3 + (p - \tau_1)b_x &= (s + b)b_x, \\ s + b &= -\left(p + \tau_1 + \omega^2\tau_3 b_x\right), \\ w &= \nu\lambda b_t + u b_x - \lambda m; \end{aligned} \tag{10.137}$$

in these equations,

$$\omega = \frac{\nu\varepsilon}{\lambda} \ll 1. \tag{10.138}$$

The length scale is as yet essentially arbitrary; observations suggest $\lambda \lesssim 1$. The parameter ν is defined by the constraint that longitudinal stress balances longitudinal strain rate, and this determines

$$\nu = \frac{\varepsilon}{\delta}\left(\frac{\delta}{\lambda A}\right)^{1/(n+1)}, \tag{10.139}$$

where, if A varies with temperature, it is the ice upper surface (lowest) value that should be used.[11]

We let $\omega \to 0$ in these equations; it follows that $u \approx u(x,t)$, $\tau \approx |\tau_1|$, whence $\tau_1 \approx \tau_1(x,t)$; $p + \tau_1 \approx 0$, so that $\tau_{3z} \approx s_x - 2\tau_{1x}$, and thus

$$\tau_3 \approx (s_x - 2\tau_{1x})(z - \delta s) + 2\delta\tau_1 s_x. \tag{10.140}$$

Applying the boundary conditions at $z = b$, we have

$$s = -b, \quad 2\tau_1 b_x = (s_x - 2\tau_{1x})(b - \delta s) + 2\delta\tau_1 s_x, \tag{10.141}$$

whence, integrating, we find

$$\tau_1 = -\tfrac{1}{4}b, \tag{10.142}$$

and the integration constant (for $(10.141)_2$) is taken to be zero on applying an averaged force balance at the ice shelf front (see question 10.7). Thus we finally obtain the stretching equations, noting that the ice thickness $H \approx -b$ to $O(\delta)$,

$$u_x = \tfrac{1}{2}\left(\tfrac{1}{4}H\right)^n, \quad \nu\lambda H_t + (uH)_x = \lambda(a - m); \tag{10.143}$$

the second equation is that of mass conservation, and is derived by integrating the mass continuity equation. Note that the time scale for mass adjustment is $O(\nu\lambda) \ll 1$, so that the ice shelf responds rapidly to changes in supply. We might suppose that

[11] This is opposite to the situation in an ice sheet, where it is the warmest (basal) ice which is rate-controlling.

the choice of length scale λ would be such that $\lambda(a-m) = O(1)$, but in fact it is more likely that the extent of an ice shelf is determined by the rate of calving at the front, which is not treated here. Typical basal melt rates are comparable to accumulation rates, of the order of ten centimetres a year in some models.

Suitable initial conditions for H and u would follow from continuity of ice flux and depth across the grounding line, but the position of the grounding line $x = x_G$ is not apparently determined. Let us anticipate that suitable conditions on H and u are that

$$u \to 0, \quad Hu \to q_I \quad \text{as} \quad x \to x_G; \tag{10.144}$$

assuming steady conditions, it follows from (10.143) that

$$Hu = q_I + \int_{x_G}^{x} (a - m)\, dx. \tag{10.145}$$

The solution for u follows by quadrature. In the particular case that $a = m$ (and in any case as $x \to x_G$), we have $Hu = q_I$, and thus

$$u = \left\{ \frac{(n+1)}{2} \left(\frac{q_I}{4} \right)^n \right\}^{1/(n+1)} (x - x_G)^{1/(n+1)}. \tag{10.146}$$

In order to find a condition for q_I and for the position of x_G, we need to consider the region near the grounding line in more detail, and this is done in the following subsection.

10.2.7 The grounding line

In the transition region, we need to retain terms which are of importance in both ice sheet and ice shelf approximations. This requires us to rescale the ice sheet scaled variables in the following way:

$$x - x_G \sim \gamma, \quad z, b \sim \beta, \quad s \sim \delta\beta, \quad u \sim \frac{1}{\beta}, \quad w \sim \frac{1}{\gamma},$$

$$t \sim \beta, \quad p, \tau_1 \sim \frac{\delta\beta}{\varepsilon^2}, \quad \tau_3 \sim \frac{\delta\beta^2}{\gamma}, \quad \tau \sim \frac{\delta\beta}{\varepsilon}, \tag{10.147}$$

where x_G is the grounding line position; the parameters β and γ are defined by

$$\beta = \left(\frac{\varepsilon}{\delta} \right)^{\frac{n}{n+2}} \frac{1}{A^{\frac{1}{n+2}}}, \quad \gamma = \beta\varepsilon. \tag{10.148}$$

This rescaling reintroduces the full Stokes equations. Denoting the rescaled variables (except time) by capitals, and writing

$$x - x_G(t) = \gamma X, \quad t = \beta t^*, \tag{10.149}$$

we derive the model

$$\begin{aligned} U_X + W_Z &= 0, \\ 0 &= -S_X + T_{3Z} - P_X + T_{1X}, \\ 0 &= -P_Z - T_{1Z} + T_{3X}, \\ U_Z + W_X &= T^{n-1} T_3, \\ 2U_X &= T^{n-1} T_1, \\ T^2 &= T_3^2 + T_1^2. \end{aligned} \tag{10.150}$$

The boundary conditions are the following. On the surface $Z = \delta S$,

$$\begin{aligned} T_3 + \delta(P - T_1) S_X &= 0, \\ P + T_1 + \delta T_3 S_X &= 0, \\ W &= \delta(\gamma S_{t^*} - \dot{x}_G S_X) + \delta U S_X - \gamma a, \end{aligned} \tag{10.151}$$

where $\dot{x}_G = \dfrac{dx_G}{dt^*}$. On the base $Z = B$, when $X > 0$,

$$\begin{aligned} -T_3 + (-P + T_1) B_X &= (S + B) B_X, \\ S + B &= -\left[P + T_1 + T_3 B_X\right], \\ W &= \gamma B_{t^*} - \dot{x}_G B_X + U B_X - \gamma m, \end{aligned} \tag{10.152}$$

and when $X < 0$,

$$W = 0, \quad U = 0, \tag{10.153}$$

where we assume that the sliding velocity is zero for grounded ice[12]

To leading order, we can approximate the top surface boundary conditions as $\gamma \to 0$ and also $\delta \to 0$ by

$$T_3 = P + T_1 = W = 0 \quad \text{on} \quad Z = 0. \tag{10.154}$$

The kinematic condition at the shelf base is approximately

$$W = -\dot{x}_G B_X + U B_X \quad \text{on} \quad Z = B. \tag{10.155}$$

In addition, the solution must be matched to the outer (sheet and shelf) solutions. We consider first the ice sheet behaviour as $x \to x_G$. We suppose that the ice sheet is described in one dimension by (10.45), thus

$$H_t = -q_x + a, \tag{10.156}$$

where the ice flux is (in ice sheet scaled variables)

$$q = \frac{(s - b)^{n+2} (-s_x)^n}{n + 2}. \tag{10.157}$$

[12]This simple assumption is not very realistic, since it is most likely that in the vicinity of the grounding line, the basal ice will be at the melting point, and the sliding velocity will be non-zero. Where ice streams go afloat, the velocity is almost entirely due to basal sliding.

We can carry out a local analysis near x_G similar to those in section 10.2.5. As $x \to x_G$, $s - b \to 0$ (since $s - b \sim \beta \ll 1$), but the ice flux is non-zero; in this case we find that always

$$H = s - b \sim C(x_G - x)^{\frac{n}{2(n+1)}}, \quad q \sim q_G = \left(\frac{n}{2(n+1)}\right)^n \frac{C^{2n+2}}{n+2}. \tag{10.158}$$

When the surface slope is computed from this, we find that the requisite matching condition for the slope written in terms of the transition zone scalings is that

$$S_X \sim -\frac{nC}{2(n+1)} \frac{1}{(-\delta X)^{\frac{n+2}{2(n+1)}}} \quad \text{as} \quad X \to -\infty. \tag{10.159}$$

Clearly the presence of the small parameter δ does not allow direct matching of the transition zone to the ice sheet.

The problem is easily resolved, however. There is a 'joining' region in which $X = \tilde{X}/\delta$, $S = \tilde{S}/\delta$, and then also $P, T_1, W \sim \delta$; the resultant set of equations is easily solved (it is a shear layer like the ice sheet), and we find

$$\tilde{S} = B_G + \left[(-B_G)^{2(n+1)/n} - \frac{2(n+1)}{n}\{(n+2)q_G\}^{1/n}\tilde{X}\right]^{n/(2n+2)}, \tag{10.160}$$

where $B = B_G$ at $x = x_G$. Expanding this as $\tilde{X} \to 0$, we find that the matching condition for S in the transition zone as $X \to -\infty$ is

$$S \sim -\Lambda X, \tag{10.161}$$

where

$$\Lambda = \frac{\{(n+2)q_G\}^{1/n}}{(-B_G)^{(n+2)/n}}. \tag{10.162}$$

A final simplification to the transition zone problem results from defining

$$\Pi = P + S; \tag{10.163}$$

to leading order in γ and δ, the transition problem is then

$$\begin{aligned} U_X + W_Z &= 0, \\ \Pi_X &= T_{3Z} + T_{1X}, \\ \Pi_Z &= -T_{1Z} + T_{3X}, \\ U_Z + W_X &= T^{n-1}T_3, \\ 2U_X &= T^{n-1}T_1, \\ T^2 &= T_3^2 + T_1^2, \end{aligned} \tag{10.164}$$

together with the boundary conditions

$$T_3 = W = 0 \quad \text{on} \quad Z = 0, \tag{10.165}$$

$$\begin{aligned} B &= -(\Pi + T_1 + T_3 B_X), \\ T_3(1 - B_X^2) &= 2T_1 B_X, \\ W &= (-\dot{x}_G + U)B_X \quad \text{on} \quad Z = B, \quad X > 0, \end{aligned} \tag{10.166}$$

and

$$W = U = 0 \quad \text{on} \quad Z = B_G, \quad X < 0. \tag{10.167}$$

The matching conditions to the ice sheet may be summarised as

$$\Pi_X \to -\Lambda, \quad W \to 0, \quad T_3 \to -\Lambda Z \quad \text{as} \quad X \to -\infty, \tag{10.168}$$

with the flow becoming the resultant pressure gradient driven shear flow at $-\infty$. Towards the ice shelf, a comparison of orders of magnitude shows firstly that

$$\frac{\nu}{\beta} = \left(\frac{\gamma}{\lambda}\right)^{1/(n+1)} \ll 1, \tag{10.169}$$

and that in the ice shelf, the transition scaled variables are

$$S, B \sim \frac{\nu}{\beta}, \quad W \sim \frac{\gamma}{\lambda}, \quad P, T_1 \sim \frac{\nu}{\beta}, \quad T_3 \sim \left(\frac{\nu}{\beta}\right)^2 \frac{\gamma}{\lambda}; \tag{10.170}$$

note also that the ice shelf time scale $\nu\lambda$ is much less than the transition zone time scale β, so that it is appropriate in the transition zone to assume that the far field ice shelf is at equilibrium, and thus described by (10.145) and (10.146). Bearing in mind (10.169), it follows from this that suitable matching conditions for the transition region are

$$\begin{aligned} T_1 \sim -\tfrac{1}{4}B, \qquad & U \sim MX^{1/(n+1)}, \\ W \to 0, \qquad & B \sim -\frac{q_I}{U} \quad \text{as} \quad X \to \infty, \end{aligned} \tag{10.171}$$

where

$$M = \left\{ \frac{(n+1)}{2} \left(\frac{q_I}{4}\right)^n \right\}^{1/(n+1)}, \tag{10.172}$$

and the flow becomes an extensional flow as $X \to \infty$. It follows from integration of the continuity equation between B and S that the ice flux to the ice shelf, q_I, is given by

$$q_I = q_G + \dot{x}_G B_G. \tag{10.173}$$

The top surface is defined by

$$S = (\Pi + T_1)|_{Z=0}\,, \tag{10.174}$$

and uncouples from the rest of the problem. The extra condition on $Z = B,\ X > 0$ in (10.166) should determine B providing $\dot{x}_G$ is known. This is the basic conundrum of the grounding line determination, since there appears to be no extra condition to determine $\dot{x}_G$.

The resolution of this difficulty has not yet been finally achieved. One might wonder whether there is an extra condition hiding in the matching conditions (10.168) or (10.171), but it appears not: the conditions on T_3 and W as $X \to -\infty$ imply the pressure gradient condition, while the condition on U as $X \to \infty$ implies the other three. It seems that the answer lies in the additional posing of contact conditions. Specifically, for the solution in the transition region to have physical sense, we require that the effective normal stress downwards, $-\sigma_{33} - p_w$, be positive on the grounded base, and we require the ice/water interface to be above the submarine land surface on the floating shelf base. When written in the current scaled coordinates, these conditions become

$$\begin{aligned} B + \Pi + T_1 > 0, \qquad & X < 0, \\ B > B_G, \qquad & X > 0. \end{aligned} \tag{10.175}$$

In addition, we may add to these the condition that at the grounding line, the effective normal stress is zero, whence

$$B + \Pi + T_1 = 0 \quad \text{at} \quad X = 0. \tag{10.176}$$

Numerical solutions appear to be consistent with the idea that, for any given $\dot{x}_G$, there is a unique value of Λ such that the contact conditions (10.175) and (10.176) are satisfied. If this is true, then (10.162) determines the ice sheet flux q_G at the grounding line as a function of x_G (through B_G) and $\dot{x}_G$, and this provides the extra condition (as well as $s \to b$ as $x \to x_G-$) for the determination of the grounding line position.

10.2.8 Marine ice sheet instability

Much of the interest concerning grounding line motion concerns the possible instability of marine ice sheets. A marine ice sheet is one whose base is below sea level; the major example in the present day is the West Antarctic Ice Sheet. Marine ice sheets terminate at grounding lines, from which ice shelves protrude. Depending on the slope of the submarine surface, they can be susceptible to instability, and it has been postulated that fluctuations in sea level, for example, might cause a catastrophic retreat of the grounding lines in West Antarctica, and consequent collapse of the ice sheet.

To understand why this might be so, consider an ice sheet governed by the mass conservation equation (10.156), and for simplicity (it does not affect the argument), take the ice flux $q = -H_x$, so that

$$H_t = H_{xx} + a, \tag{10.177}$$

with boundary conditions

$$\begin{aligned} H_x = 0 \quad \text{at} \quad x = 0, \\ H = H_G(x_G), \quad -H_x = q_G(H) \quad \text{at} \quad x = x_G \end{aligned} \tag{10.178}$$

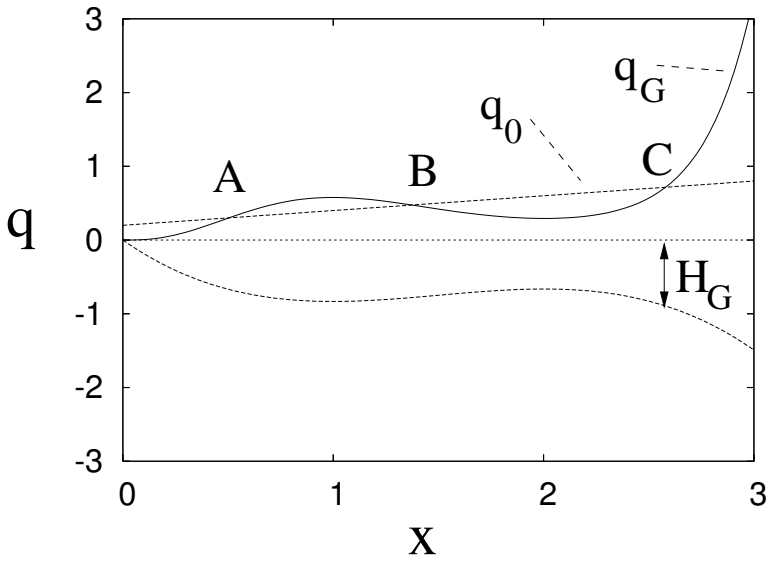

Figure 10.8: Variation of $q_G[H_G(x)]$ and the equilibrium flux $q_0 = ax$ for the bottom depth profile H_G indicated. Equilibria occur for the points of intersection of the two flux curves, with instability occurring if $q_0' > q_G'$. Thus points A and C are stable, while B is unstable. The particular functions used are $H_G = 2x - \frac{3}{2}x^2 - \frac{1}{3}x^3$, $q_G = H^3$, and $q_0 = 0.2(1 + x)$ (with the divide implicitly being at $x = -1$).

(note that we retain here the finite depth of the ice sheet at the grounding line). $H_G(x)$ represents the depth of the land subsurface below sea level, and we assume that q_G is an increasing function of H, as suggested by (10.162), if Λ is constant. There is a steady solution $H = H_0(x)$; note that since the ice sheet slopes down to the ice shelf, we have $H_0'(x_G) < H_G'(x_G)$.

Consider a situation such as that shown in figure 10.8, in which the subsurface slopes upwards for part of the domain. In this case there can be three possible equilibria, of which the middle one is unstable. The casual argument for this is the following suggestion: if x_G advances, then the ice sheet must deliver a larger flux q_0; however, assuming $q_G'(H) > 0$, then in regions where $H_G'(x) < 0$ (i. e., the bed slopes upwards towards the grounding line), the actual flux delivered is less; consequently, the ice builds up behind the grounding line, causing its further advance.

To demonstrate this mathematically, we linearise (10.177) and (10.178) about the steady state $H = H_0(x)$, $x_G = x_G^0$, by putting $H = H_0(x) + \eta$, $x_G = x_G^0 + \gamma$; the resulting linearised system for η is (eliminating γ)

$$\begin{aligned} \eta_t &= \eta_{xx}, \\ \eta_x &= 0 \quad \text{at} \quad x = 0, \\ -\eta_x &= K\eta \quad \text{at} \quad x = x_G^0, \end{aligned} \tag{10.179}$$

where

$$K = \frac{q_G'(H_G)H_G'(x_G^0) - a}{H_G'(x_G^0) - H_0'(x_G^0)}, \tag{10.180}$$

which has (stable) solutions $\eta = e^{-\lambda^2 t}\cos\lambda x$ providing $\lambda\tan\lambda x_G^0 = K$. If $K > 0$, these are the only solutions, and the steady state is stable. However, if $K < 0$, the first mode (with $\lambda x_G^0 < \frac{1}{2}\pi$) is replaced by an unstable mode $\eta = e^{\lambda^2 t}\cosh\lambda x$, where $\lambda\tanh\lambda x_G^0 = -K$. Therefore the steady state is unstable precisely if $K < 0$. Consulting (10.180), and recalling that $H_0'(x_G) < H_G'(x_G)$, it follows that the steady state is unstable if

$$\frac{dq_G}{dx_G} < a, \tag{10.181}$$

as suggested in figure 10.8. Question 10.8 generalises this result to the case where $q = -D(H, H_x)H_x$.

10.3 Sliding and drainage

The sliding law relates the basal shear stress τ_b to the basal sliding velocity u_b. The classical theory, enunciated by Lliboutry, Weertman, Nye, Kamb, and others, considers ice flowing at the base of a glacier over an irregular, bumpy bedrock. The ice is lubricated at the actual interface by the mechanism of *regelation*, or melting-refreezing, which allows a thin film (microns thick) to exist at the ice-rock interface, and allows the ice to slip. The drag is then due to two processes; regelation itself, and the viscous flow of the ice over the bedrock. Regelation is dominant for small wavelength roughness, while viscous drag is dominant for large wavelengths, and early work emphasised the importance of a controlling (intermediate) wavelength (of several centimetres). More recently, the emphasis has moved away from regelation and has been put more on consideration of the viscous flow, and we do this here, assuming no normal velocity of the ice as it slides over the bed.

A suitable model for discussion is the flow of a Newtonian fluid over a rough bedrock of 'wavelength' $[x]$ and amplitude $[y]$, given by

$$y = h_D(x) \equiv [y]h\left(\frac{x}{[x]}\right), \tag{10.182}$$

where y is now the vertical coordinate.[13] The governing equations for two-dimensional flow down a slope of angle α are

$$\begin{aligned} u_x + v_y &= 0, \\ p_x &= \rho_i g\sin\alpha + \eta\nabla^2 u, \\ p_y &= -\rho_i g\cos\alpha + \eta\nabla^2 v, \end{aligned} \tag{10.183}$$

where η is the viscosity. We suppose that the glacier has a depth of order d, thus providing a basal shear stress τ_b of order $[\tau]$, which drives a shear velocity of order $[u]$, and these are related by

$$[\tau] = \rho_i g d\sin\alpha = \frac{\eta[u]}{d}. \tag{10.184}$$

[13] Because shortly we will use z for the complex variable $x + iy$.

The basal boundary conditions are those of no shear stress and no normal flow, and take the form

$$\sigma_{nt} = \frac{\tau_2(1 - h_D'^2) - 2\tau_1 h_D'}{1 + h_D'^2} = 0, \tag{10.185}$$

where

$$\tau_1 = 2\eta u_x, \quad \tau_2 = \eta(u_y + v_x), \tag{10.186}$$

and

$$v = uh_D', \tag{10.187}$$

both (10.185) and (10.187) being applied at $y = h_D(x)$. Note also that the normal stress is

$$-\sigma_{nn} = \frac{p(1 + h_D'^2) + \tau_1(1 - h_D'^2) + 2h_D'\tau_2}{1 + h_D'^2}. \tag{10.188}$$

Because we describe a local flow near the base of the glacier, it is appropriate to apply matching conditions to the ice flow above. In particular, we require $\tau_2 \to \tau_b$ as y becomes large, and hence

$$u \sim u_b + \frac{\tau_b y}{\eta} \tag{10.189}$$

far from the bed.

We non-dimensionalise the equations by scaling

$$x, y \sim [x], \quad u, v \sim [u], \quad \tau_b = [\tau]\tau^*, \quad u_b = [u]u^*,$$

$$p = p_i + \frac{\nu[\tau]}{\sigma} P, \tag{10.190}$$

where

$$p_i = p_a + \rho_i g(y_i - y)\cos\alpha \tag{10.191}$$

is the ice overburden pressure, and $y = y_i \sim d$ is the ice upper surface (and taken as locally constant); this leads to the non-dimensional set

$$\begin{aligned} u_x + v_y &= 0, \\ \nu P_x &= \sigma^2 + \nabla^2 u, \\ \nu P_y &= \nabla^2 v, \end{aligned} \tag{10.192}$$

subject to the boundary conditions that

$$P \to 0, \quad u \sim u^* + \sigma\tau^* y \quad \text{as} \quad y \to \infty, \tag{10.193}$$

and

$$\begin{aligned} (1 - \nu^2 h'^2)(u_y + v_x) - 4\nu h' u_x &= 0, \\ v &= \nu u h', \end{aligned} \tag{10.194}$$

on the dimensionless bed $y = \nu h$ (from (10.182). The corrugation σ and the aspect ratio ν are defined by

$$\sigma = \frac{[x]}{d}, \quad \nu = \frac{[y]}{[x]}; \tag{10.195}$$

ν is a measure of the roughness of the bed.

We will assume that both ν and σ are small. In consequence, the dimensionless basal stress τ^* in (10.193) is uncoupled from the problem; however, integration of the momentum equations over the domain yields an expression for τ^*. In dimensional terms, this relation is

$$\tau_b = \frac{1}{L}\int_0^L \sigma_{n1}\, ds, \tag{10.196}$$

where the integral is over a length L of the base $y = h_D$, over which conditions are taken to be periodic (alternatively, the limit $L \to \infty$ may be taken).

Evidently, the velocity is uniform to leading order, and therefore we write

$$u = u^* + \nu U, \quad v = \nu V, \tag{10.197}$$

so that the problem reduces to

$$\begin{aligned} U_x + V_y &= 0, \\ P_x &= \frac{\sigma^2}{\nu} + \nabla^2 U, \\ P_y &= \nabla^2 V, \end{aligned} \tag{10.198}$$

with boundary conditions

$$U \sim \frac{\sigma\tau^*}{\nu} y \quad \text{as} \quad y \to \infty, \tag{10.199}$$

and

$$\begin{aligned} (1-\nu^2 h'^2)(U_y + V_x) - 4\nu h' U_x &= 0, \\ V = (u^* + \nu U)h' \end{aligned} \tag{10.200}$$

on $y = \nu h$. When written in dimensionless terms, the overall force balance (10.196) takes the form (with L now being dimensionless)

$$\frac{\sigma\tau^*}{\nu^2} = \frac{1}{L}\int_0^L [P(1+\nu^2 h'^2) + 2(1-\nu^2 h'^2)U_x + 2\nu h'(U_y + V_x)]\frac{h'\,dx}{1+\nu^2 h'^2}. \tag{10.201}$$

It is fairly clear from (10.201) that there is a distinguished limit $\sigma \sim \nu^2$, which corresponds to the situation where sliding is comparable to shearing, and it is convenient to adopt this limit as an example. We introduce a stream function ψ via

$$U = \psi_y, \quad V = -\psi_x; \tag{10.202}$$

then letting $\nu \to 0$ with $\sigma \sim \nu^2$, we derive the reduced model

$$\begin{aligned} P_x &= \nabla^2 \psi_y, \\ P_y &= -\nabla^2 \psi_x, \end{aligned} \tag{10.203}$$

together with the boundary conditions

$$P, \psi \to 0 \text{ as } y \to \infty,$$

$$\psi = -u^* h(x), \ \psi_{yy} - \psi_{xx} = 0 \text{ on } y = 0. \tag{10.204}$$

The shear stress is determined by (10.201), whence to leading order (e. g., if h is periodic with period 2π)

$$\frac{\sigma\tau^*}{\nu^2} = \frac{1}{2\pi}\int_0^{2\pi} (P + 2\psi_{xy})|_{y=0} \ h' \, dx; \tag{10.205}$$

more generally a spatial average would be used. Since the expression in brackets in (10.205) is simply (minus) the normal stress, it is therefore also equal to the scaled water pressure in the lubricating film, which from (10.190) can be written in the form

$$P + 2\psi_{xy} = -N^*, \quad N^* = \frac{\sigma(p_i - p_w)}{\nu[\tau]}. \tag{10.206}$$

The quantity N^* is the dimensionless effective pressure at the bed. We come back to this below.

A nice way to solve this problem is via complex variable theory. We define the complex variable $z = x + iy$, and note that equations (10.203) are the Cauchy-Riemann equations for the analytic function $P + i\nabla^2\psi$. Consequently, ψ satisfies the biharmonic equation, which has the general solution

$$\psi = (\bar{z} - z)f(z) - B(z) + (cc), \tag{10.207}$$

where f and B are analytic functions and (cc) denotes the complex conjugate, as does the overbar. The zero stress condition (10.204) requires $f = -\frac{1}{2}B'$, and also $B \to 0$ as $z \to \infty$ (with Im $z > 0$), and the last condition is then

$$B + \bar{B} = u^* h \quad \text{on} \quad \text{Im}\, z = 0. \tag{10.208}$$

If h is periodic, with a Fourier series

$$h = \sum_{-\infty}^{\infty} a_k e^{ikx}, \tag{10.209}$$

then B is simply given by

$$B = u^* \sum_{1}^{\infty} a_k e^{ikz} \tag{10.210}$$

(we can assume $a_0 = 0$, i. e., the mean of h is zero). However, it is also convenient to formulate this problem as a Hilbert problem. We define $L(z) = B''(z)$, which is analytic in Im $z > 0$, and then $L(z) = \overline{B''(\bar{z})}$ is analytic in Im $z < 0$. From (10.207), $\nabla^2\psi = 4\psi_{z\bar{z}} = -2(L + \bar{L})$, and therefore $P + i\nabla^2\psi + 4iL = P + 2i(L - \bar{L})$ is analytic; since this last expression is real, it is constant and thus zero, since it tends to zero as

$z \to \infty$. Applying the boundary conditions at $\operatorname{Im} z = 0$, and using the usual notation for the values on either side of the real axis, it follows that

$$\begin{aligned} L_+ + L_- &= u^* h'', \\ L_+ - L_- &= \tfrac{1}{2} i P, \end{aligned} \tag{10.211}$$

which relate the values either side of Im $z = 0$. From (10.207), we have $\psi_{xy} = i(\psi_{zz} - \psi_{\bar{z}\bar{z}}) = \frac{1}{2} i (z - \bar{z})(B''' - \overline{B'''})$, and thus $\psi_{xy}|_{y=0} = 0$; it follows that $P = -N^*$ on $y = 0$, and the drag (i. e., the sliding law) is then computed (for a 2π-periodic h) as

$$\frac{\sigma \tau^*}{\nu^2} = \frac{1}{i\pi} \int_0^{2\pi} (L_+ - L_-) h' \, dx; \tag{10.212}$$

evaluating the integral, we find

$$\frac{\sigma \tau^*}{\nu^2} = 4u^* \sum_1^\infty k^3 |a_k|^2. \tag{10.213}$$

For a linear model such as this, τ^* and thus τ_b is necessarily proportional to u^* and thus u_b. For Glen's flow law, the slip coefficient multiplying τ^* becomes $\dfrac{\sigma}{\nu^{n+1}}$. The problem can not be solved exactly, but variational principles can be used to estimate a sliding law of the form

$$\tau_b \approx R u_b^{1/n}. \tag{10.214}$$

Weertman's original sliding law drew a balance between (10.214) and the linear dependence due to regelation, and the heuristic 'Weertman's law' $\tau_b \propto u_b^{1/m}$, with $m \approx \frac{1}{2}(n+1)$ is often used.

Simplistic sliding laws such as the above have been superceded by the inclusion of cavitation. When the film pressure behind a bump decreases to a value lower than the water pressure in the local subglacial drainage system, a cavity must form, and indeed, such cavities are plentifully observed. An appropriate generalisation of (10.211) is then

$$\begin{aligned} L_+ + L_- &= u^* h'' \quad \text{in} \quad C', \\ L_+ - L_- &= -\tfrac{1}{2} i N_c \quad \text{in} \quad C, \end{aligned} \tag{10.215}$$

where the bed is divided into cavities (C) where P is known ($= -N_c$), and attached regions where h is known. One can solve this problem to find the unknown cavity shapes, and for a bed consisting of isolated bumps, $\tau_b(u_b)$ increases monotonically for small u_b, reaches a maximum, and then decreases for large u_b, as shown in figure 10.9. The decreasing portion of the curve is unstable (increasing velocity decreases drag) and is caused by the roofs of the cavities from one bump reaching the next bump.

From (10.206) it follows that N_c in (10.215) is proportional to the effective pressure $N = p_i - p_w$, specifically

$$N_c = \frac{\sigma N}{\nu[\tau]}, \tag{10.216}$$

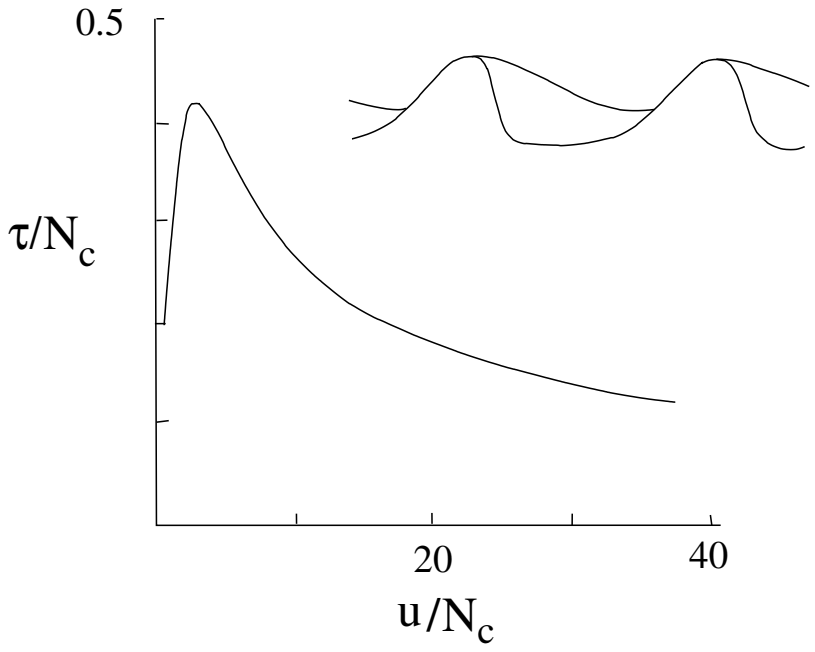

Figure 10.9: Stress versus velocity for a bed of isolated bumps. The inset shows the typical form of the separated flow on the decreasing portion of the curve, when the cavities reach the next bump.

and in fact the sliding law has the specific form $\tau_b = Nf\left(\frac{u_b}{N}\right)$. For a nonlinear Glen's law, the generalisation must take the form

$$\tau_b = Nf\left(\frac{u_b}{N^n}\right). \tag{10.217}$$

The reason for this is that one can scale the problem in the nonlinear case using $p - p_i, \tau_{ij} \sim N$, $\mathbf{u} \sim A[x]N^n$, $\mathbf{x} \sim [x]$, and the consequent sliding law must be of the form (10.217) (assuming the regelative component is small). In particular, note that the fraction s of uncavitated bed must be a decreasing function of $\Lambda = \dfrac{u_b}{N^n}$.

The multivaluedness of $u_b(\tau_b)$ is very suggestive of surging — but is it realistic? Consideration of more realistic (non-periodic) beds suggests that the multi-valuedness remains so long as the the peak roughness amplitude is relatively constant. However, if there are increasing large bumps—pinning points, riegels—one might expect that $f(\cdot)$ in (10.217) will be an increasing function of its argument, since when smaller bumps start to be drowned, larger ones will take up the slack. A plausible sliding law then has $f(\xi)$ increasing as a power of ξ, whence we can obtain (for example)

$$\tau_b = cu_b^r N^s, \tag{10.218}$$

where we would expect $r, s > 0$. More specifically, (10.217) would suggest $s = 1 - rn$, and also that $r \approx \frac{1}{n}$ would be appropriate at low u_b, where cavitation is absent. When cavitation occurs, one would then expect lower stresses, so that $r < \frac{1}{n}$. There

is in fact some experimental and field evidence consistent with laws of this type, with $r \approx s \approx \frac{1}{3}$, for example. More detailed theoretical studies suggest that $f(\Lambda)$ will eventually reach a maximum which is determined by the largest wavelength bumps.

An apparently altogether different situation occurs when ice slides over wet, deforming till. If the till is of thickness d_T and has (effective) viscosity η_T, then an appropriate sliding law would be

$$\tau_b = \frac{\eta_T u_b}{d_T}. \tag{10.219}$$

In fact, till is likely to have a nonlinear rheology, and also in accordance with Terzaghi's principle of soil mechanics, one would expect η_T to depend on effective pressure N. One possible rheology for till[14] gives the strain rate as

$$\dot{\varepsilon} = A_T \frac{\tau^a}{N^b}, \tag{10.220}$$

in which case the sliding law would be again of the form (10.218), with $c = (A_T d_T)^{-1/a}$, $r = 1/a$, $s = b/a$. If the till is taken to be plastic, then we would have $r = 0$, $s = 1$, corresponding to (10.220) when $a = b \gg 1$. Thus there are some good reasons to choose (10.218) as an all purpose sliding law, and this points up the necessity of a subglacial hydraulic theory to determine N.

10.3.1 Röthlisberger channels

Subglacial water is generated both by basal melt (of significance in ice sheets) and from run-off of surface melt or rainfall through crevasses and *moulins*, which access the glacier bed. Generally the basal water pressure p_w is measured to be below the overburden ice pressure p_i, and the resulting positive effective pressure $N = p_i - p_w$ tends to cause any channels in the ice to close up (by creep of the ice). In fact, water is often seen to emerge from outlet streams which flow through large tunnels in the ice, and the theory which is thought to explain how such channels remain open asserts that the channel closure rate is balanced by melt back of the channel walls by frictional heating due to the water flow.

The classical theory of subglacial drainage is due to Röthlisberger, and is described below. Much more detail, including the effects of time dependence in the model, is provided in chapter 11. Here we discuss only the determination of effective pressure in steady state conditions. We consider a single channel of cross sectional area S, through which there is a water flux Q. We take Q as being determined by external factors such as surface meltwater runoff; this is appropriate for glaciers, but not for ice sheets, where Q must be determined by subglacial melting (we come back to this later). If the flow is turbulent, then the Manning law for flow in a straight conduit is

$$\rho_w g \sin\alpha - \frac{\partial p}{\partial s} = \frac{f_1 Q^2}{S^{8/3}}, \tag{10.221}$$

[14]The choice of a suitable till rheology is problematic, since till is a granular material, and therefore has plastic behaviour, i. e., a yield stress. It is a matter of current interest whether any kind of viscous rheology is actually appropriate. Further discussion is given in the notes.

where ρ_w is water density, g is gravity, s is distance down channel, α is the local bed slope, and we write $p = p_w$ for water pressure; f_1 is a roughness coefficient related to the Manning friction factor.[15] If we suppose that the frictional heat dissipated by the turbulent flow is all used to melt the walls, then

$$mL = Q\left[\rho_w g \sin\alpha - \frac{\partial p}{\partial s}\right], \tag{10.222}$$

where L is the latent heat, and m is the mass of ice melted per unit length per unit time.

The last equation to relate the four variables S, Q, p and m stems from a kinematic boundary condition for the ice, and represents a balance between the rate at the which the ice closes down the channel, and the rate at which melting opens it up:

$$\frac{m}{\rho_i} = KS(p_i - p)^n; \tag{10.223}$$

here m/ρ_i is the rate of enlargement due to melt back, while the term on the right hand side represents ice closure due to Glen's flow law for ice; the parameter K is proportional to the flow law parameter A.

Elimination of m and S yields a second order ordinary differential equation for the effective pressure $N = p_i - p$, which can be solved numerically. However, it is also found that typically $\partial p/\partial s \ll \rho_w g \sin\alpha$ (in fact, we expect $\partial p/\partial s \sim \rho_w g d/l$, so that in the notation of (10.11), the ratio of these terms is of $O(\varepsilon)$); the neglect of the $\partial p/\partial s$ term in (10.221) and (10.222) is singular, and causes a boundary layer of size $O(\varepsilon)$ to exist near the terminus in order that p decrease to atmospheric pressure.[16] Away from the snout, then

$$S \approx \left[\frac{f_1 Q^2}{\rho_w g \sin\alpha}\right]^{3/8}, \; KSN^n \approx \frac{Q\rho_w g \sin\alpha}{\rho_i L}, \tag{10.224}$$

thus

$$N \approx \beta Q^{1/4n}, \tag{10.225}$$

where

$$\beta = \left[\frac{\rho_w g \sin^{11/8}\alpha}{\rho_i L K G^{3/8} n'^{3/4}}\right]^{1/n} \tag{10.226}$$

is a material parameter which depends (inversely) on roughness. Taking $\rho_w = 10^3$ kg m^{-3}, $\rho_i = 917$ kg m^{-3}, $g = 9.81$ m s^{-2}, $L = 3.3 \times 10^5$ J kg^{-1}, $K = 0.5 \times 10^{-24}$ Pa^{-n} s^{-1}, $n = 3$, $\sin\alpha = 0.1$, $G = 6.57$ and $n' = 0.04$ m$^{-1/3}$ s, we find $\beta \approx 24.7$ bar

[15] Retracing our steps to (4.17), we see that $f_1 = \rho_w g n'^2 G$, where the geometrical factor $G = \left(\frac{l^2}{S}\right)^{2/3} = 6.57$ for a full semi-circular channel; l is the wetted perimeter.

[16] At least, this would be the boundary condition if the channel were full all the way to the margin. In practice, this is not the case. Glacial streams typically emerge from a cavern which is much larger than the stream, and in this case it is appropriate to specify that the channel pressure is atmospheric where the ice pressure is positive. In any case, the Röthlisberger theory makes no sense if $p = p_i$, since then we would have $m = 0$ and thus $Q = 0$.

$(\mathrm{m}^3\ \mathrm{s}^{-1})^{-1/12}$, so that $N \approx 30$ bars when $Q = 10\ \mathrm{m}^3\ \mathrm{s}^{-1}$. Since $p_i = 9$ bars for a 100 metre deep glacier, it is clear that the computed N may exceed p_i. In this case, p must be atmospheric and there will be open channel flow. It is likely that seasonal variations are important in adjusting the hydraulic régime.

Arterial drainage

A feature of the Röthlisberger system is the surprising fact that as the water pressure is increased (so N decreases), the water flux *decreases*. This is opposite to our common expectation. A consequence of this is that the channels, like Greta Garbo, want to be alone; if one puts two channels of equal size and equal effective pressures side by side, each carrying a water flux Q, then a perturbation $\Delta Q > 0$ in the flow of one channel will cause an increase in N, and thus a decrease in water pressure, relative to the other channel. Because the bed of a glacier will be leaky, this allows the now smaller channel to drain towards the bigger one, and thus the smaller one will close down. This process, the formation of larger wavelength pattern from smaller scales, is known as coarsening, and occurs commonly in systems such as granular flows, river system development and dendritic crystal growth, and is not fully understood, although the apparent mechanism may be clear (as here).

A consequence of this coarsening is that we expect a channelised system to form a branched, arborescent network, much like a subaerial river system. The difference is that tributaries oblique to the ice flow will tend to be washed away by the ice flow, so that only channels more or less parallel to the ice flow will be permanent features. Presumably, tributary flow will thus be facilitated by the presence of bedrock steps and cavities, which can shield the tributaries from the ice flow.

10.3.2 Linked cavities

The channelised drainage system described above is not the only possibility. Since water will also collect in cavities, it is possible for drainage to occur entirely by means of the drainage between cavities. A simple way to characterise such a drainage system is via a 'shadowing function' s which is the fraction of the bed which is cavity-free. From our discussion following (10.217), s is a monotonically decreasing function of

$$\Lambda = \frac{u}{N^n}, \tag{10.227}$$

where u is the sliding velocity. If P is the normal ice stress over the cavity-free part of the bed, then a force balance over the bed suggests that

$$p_i = sP + (1 - s)p, \tag{10.228}$$

where p is the water pressure in the cavities and $p_i = N + p$ is the far-field ice pressure. We imagine a system of cavities linked by Röthlisberger-type orifices.[17] If there are n_K such cavities across the width of a glacier, then the total water flow Q divides into

[17] The cavities are the veins, and the orifices are the arteries, of the subglacial plumbing system.

$\frac{Q}{n_K}$ per channel, subjected to a local effective pressure $P - p = \frac{N}{s}$. Röthlisberger dynamics then dictates that the effective pressure is given by

$$\frac{N}{s(\Lambda)} = \delta N_R, \tag{10.229}$$

where N_R is given by (10.225), Λ by 10.227, and

$$\delta = \left(\frac{1}{n_K}\right)^{1/4n} < 1. \tag{10.230}$$

Linked cavity drainage thus operates at a higher pressure than a channelised drainage system. This very simple description is at best qualitatively true, but it is very powerful (and therefore tempting), as we shall see.

Stability

If there are two different styles of drainage, one may ask which will occur in practice? For the linked cavity system, the answer to this lies in the inverse to our discussion of arterial drainage above. A linked cavity system is an example of a distributed drainage system, and if we denote the corresponding effective pressure by N_K (satisfying (10.229)), then the system will be stable if $N_K'(Q) < 0$. In this case, any local enlargement of an inter-cavity passage will relax stably back to the distributed system.

It is convenient to define $L(\Lambda)$ via

$$L = \ln\left(\frac{1}{s}\right); \tag{10.231}$$

L is a monotonically increasing function of Λ, and for illustrative purposes we will take it, for the moment, as linear (this is inessential to the argument). Calculation of N_K' (see question 10.10) shows that

$$-\frac{N_K'}{N_K}(n\Lambda L' - 1) = \frac{N_R'}{N_R}, \tag{10.232}$$

and thus the linked cavity system is stable if

$$\Lambda > \Lambda_c = \frac{1}{nL'}. \tag{10.233}$$

If $\Lambda < \Lambda_c$, then local perturbations will cause inter-cavity passages to grow, forming channels which will eventually coarsen to result in a single central Röthlisberger artery.

More generally, the effective pressure defined by (10.229) can be written in the form

$$n_K^{1/4n} N \exp\left[L\left(\frac{u}{N^n}\right)\right] = \beta Q^{1/4n}, \tag{10.234}$$

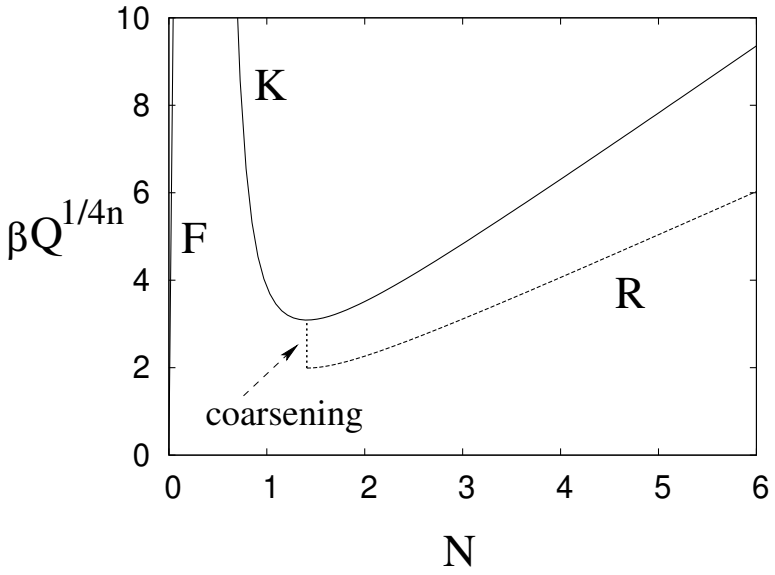

Figure 10.10: Illustrative form of the drainage effective pressure given by (10.234) relating effective pressure N to water flow Q through a field of linked cavities. The specific functions used in the figure are $L(\Lambda) = \dfrac{1 - e^{-k\Lambda}}{k}$, $\Lambda = \dfrac{u}{N^n}$, with $k = 0.2$, $u = 1$, $n = 3$. For the curve labelled K (which is the continuation of that labelled F) $n_K = 200$, while for the lower (R) curve $n_K = 1$. The three components of the curve represent F: patchy film flow; K: linked cavities; R: Röthlisberger channel. To the right of the minimum of the curve (here at $N \approx 1.41$), $\Lambda < \Lambda_c$, and the drainage channels coarsen, leading to the single Röthlisberger channel R. To the left of the minimum, distributed drainage is stable, and this takes the form of linked cavities K for $N > 0$. However, if $N \to 0$, we suppose that some of the bed remains in contact with ice, thus the shadowing function remains positive, and this allows a film flow F as the water flux decreases to zero.

which yields a family of curves (depending on the number n_K of channels) which relate N to water flow Q: see figure 10.10. All of these curves have their turning point at $\Lambda = \Lambda_c$. To the left of these minima, $\Lambda > \Lambda_c$ and a distributed system is preferred, with n_K increasing (fine-graining) until limited by the cavity spacing. To the right of the minima, coarsening will occur until a single channel ($n_K = 1$) occurs.

A question arises, what happens at very low water fluxes, when (10.234) suggests no corresponding value of N if L is linear. In reality, we expect that at very low water fluxes, water will trickle along the bed in a patchy film, while the ice is in effective contact with the larger clasts of the bed. If this is the case, then it indicates that s, and thus also L, should saturate at large Λ. The effect of this is then to cause Q given by (10.234) to reach a maximum at small N, and then decrease sharply to zero. This gives us a third branch, which we associate with film flow, when there is insufficient water flux to develop proper orifice flow between cavities.

In this view of the drainage system, there is really no difference between streams

and cavities, or between linked cavities and Röthlisberger channels and patchy films; the only distinction is of one of degree. Intrinsic to our conceptual description is an assumption of bimodality of bed asperity size. The small scale granularity of the bed allows a trickling flow at small Q, while the larger bumps allow cavities and inter-cavity orifices; but while this assumption is a useful imaginative convenience, it is probably inessential.

10.3.3 Canals

A further possible type of drainage is that of a system of canals. This refers to situations where ice flows over a layer of subglacial sediments, which will commonly take the form of till, with its bimodal mixture of fine particles and coarse clasts. If the basal ice is temperate and there is subglacial water, then it is commonly thought that the permeability will be sufficiently low that some sort of subglacial stream system must develop.[18] If the till is very stiff, then this can take the form of Röthlisberger channels. On the other hand, if the till is erodible, then the channels may become incised downwards into the sediments. It is this situation which we now try and describe.

Because there are now two different wetted perimeters, both the ice and the till dynamics must be considered. That for the ice is similar to the Röthlisberger channel, except that we do not assume that the channel is semi-circular. Rather, we identify a mean width w and a depth h. The semi-circular case is recovered if $h \sim w$. We take the cross-sectional area to be

$$S = wh. \tag{10.235}$$

If we assume a Manning flow law in the canal, then (cf. (4.18))

$$\tau = \frac{\rho_w g n'^2 u^2}{R^{1/3}}, \tag{10.236}$$

where u is the mean velocity, and

$$R = \frac{S}{l} \tag{10.237}$$

is the hydraulic radius, with l being the wetted perimeter; we take

$$l \approx 2w, \tag{10.238}$$

which will serve for both wide and semi-circular channels.

The rate of ice melting is

$$\dot{m}_i = \frac{\tau u w}{L}, \tag{10.239}$$

while a force balance yields

$$\tau l \approx \rho_i g S S_i, \tag{10.240}$$

[18]This may not always be necessary; shear and consequent fracture of the till may allow higher permeability pathways, and consequent drainage to bedrock, if there is a basal aquifer. However, this scenario seems unlikely for a deep till layer which only deforms in its uppermost part.

where S_i is the ice surface slope (this ignores the relatively small difference between ice and water densities, and also the gradient of effective pressure). We suppose that melting balances ice closure, so that

$$\dot{m}_i = \rho_i K w^2 N^n, \tag{10.241}$$

where K is a shape-dependent closure rate coefficient; (10.241) is appropriate for both semi-circular and wide channels. Finally, the water flux is

$$Q = Su. \tag{10.242}$$

Counting equations, we see that only one further equation is necessary to determine N in terms of Q, and this involves a description of the sediment flow. Eliminating subsidiary variables, we find

$$w^2 = \frac{2^{4/3}\rho_w n'^2 Q^2}{\rho_i S_i h^{10/3}}, \quad K w^2 N^n = \frac{g S_i Q}{2L}, \tag{10.243}$$

which can be compared with (10.224). In particular, if we take $w \approx h$, then we regain the Röthlisberger relation (10.225), with

$$\beta = \left[\frac{g S_i}{2KL} \left(\frac{\rho_i S_i}{2^{4/3}\rho_w n'^2} \right)^{3/8} \right]^{1/n}, \tag{10.244}$$

comparable to (10.226).

Now we consider the appropriate choice of depth for a canal. On the face of it, there is little difference between the combined processes of thermal erosion (melting) and ice creep, and sediment erosion and till creep. But there *is* a difference, and that lies in the rôle played by gravity. The shape of sub-aerial river channels is mediated by the fact that non-cohesive sediments cannot maintain a slope larger than the angle of repose, and when subject to a shear stress, the maximum slope is much less. Consequently, river beds tend to be relatively flat, and rivers are consequently wide and shallow. Therefore, if subglacial till is erodible, as we expect, the resulting channel will tend to have a depth which is not much greater than that which provides the critical stress for transporting sediment. As an approximation, we might thus take

$$\tau \approx \tau_c = \mu_c \Delta\rho_{sw} g D_s, \tag{10.245}$$

where $\mu_c \approx 0.05$ is the critical Shields stress, and D_s is a representative grain size, probably of the small size particles. In this case, the depth of the canal is given by

$$h \approx h_c = \frac{2\mu_c \Delta\rho_{sw} D_s}{\rho_i S_i}. \tag{10.246}$$

Using values $\mu_c = 0.05$, $\Delta\rho_{sw} = 1.6 \times 10^3$ kg m^{-3}, $\rho_i = 0.917 \times 10^3$ kg m^{-3}, $D_s \lesssim 10^{-3}$ m, $S_i = 10^{-3}$, we find $h \lesssim 20$ cm.

If we assume that the channel depth is controlled by sediment erosion as in (10.246), then the relations in (10.243) give

$$N = \frac{\gamma}{Q^{1/n}}, \tag{10.247}$$

where

$$\gamma = \left[\frac{\rho_i g S_i^2 h_c^{10/3}}{2^{7/3} K L \rho_w n'^2} \right]^{1/n}. \tag{10.248}$$

Using similar values as before with $h_c = 0.2$ m, we find $\gamma \approx 0.32$ bar $(\mathrm{m}^3\ \mathrm{s}^{-1})^{1/3}$.

There are two important consequences of (10.247). The first is that N decreases with Q, so that, unlike Röthlisberger channels, canals as described here will form a distributed system, just like the linked cavity system; in effect there is little difference other than a semantic one between the two systems. The second consequence is that for any reasonable values of Q, say 0.1–10 $\mathrm{m}^3\ \mathrm{s}^{-1}$, the effective pressure is much less than that of a channelled system, in a typical range 0.1–0.6 bars, similar to that found on the Siple Coast ice streams. The inverse dependence of N on Q also has an important dynamic effect on the ice flow, as we discuss below in section 10.4.3.

An issue of concern in this description is that we have apparently ignored the details of sediment creep and canal bank erosion, despite the apparent equivalence with the processes of ice creep and thermal erosion. We will have more to say on this in section 10.5.2, but for the moment we simply observe that in our theoretical description, we have arbitrarily assumed that the ice surface is (relatively) flat. The rough basis for this assumption lies in our expectation that it will be appropriate if the till is much softer than the ice, but in order to quantify this, it is necessary to write down a model which allows description of both the upper ice/water interface and the lower water/sediment interface. The basis for such a model is given in section 10.5.2, when we (briefly) discuss the formation of eskers.

10.3.4 Ice streams

A modification of the discussion of ice shelves occurs when we consider an appropriate model for ice streams. Ice streams, in particular those on the Siple Coast of Antarctica, are characterised by small surface slopes and high velocities. On ice streams such as the Whillans ice stream B, the depth $d_i \sim 10^3$ m and the ice surface slope is $\sim 10^{-3}$, so that the basal shear stress is ~ 0.1 bar. If we suppose that the effective viscosity $\eta_i = \dfrac{1}{2A\tau^{n-1}} \approx 6$ bar y, and take the velocity scale as $U \sim 500$ m y^{-1}, then the corresponding shear stress scale $\eta_i U/d_i \sim 3$ bar: evidently motion is largely by sliding. We thus introduce a new dimensionless parameter λ, which is the ratio of the magnitude of the actual basal stress to the shear stress scale:

$$\lambda = \frac{\tau_0 d_i}{\eta_i U}, \tag{10.249}$$

where $\tau_0 = \rho_i g d_i \varepsilon$ is the basal stress scale, ε being the aspect ratio. Using the values quoted above, we may estimate $\lambda \sim 0.03$.

We follow the exposition in section 10.2.2 (and its three-dimensional modification in question 10.4), with the distinction that the shear stresses are scaled as $\tau_{13}, \tau_{23} \sim \tau_0$, while the longitudinal stresses are scaled as $p - p_a - \rho_i g(s-z), \tau_{12}, \tau_{11}, \tau_{22}, \tau_{33} \sim \dfrac{\eta_i U}{l}$; then the scaled model (10.38) takes the form

$$\begin{aligned}
u_x + v_y + w_z &= 0, \\
\tau_{13,z} &= s_x + \frac{\varepsilon^2}{\lambda}\left[p_x - \tau_{11,x} - \tau_{12,y}\right], \\
\tau_{23,z} &= s_y + \frac{\varepsilon^2}{\lambda}\left[p_y - \tau_{12,x} - \tau_{22,y}\right], \\
p_z - \tau_{33,z} &= \lambda(\tau_{13,x} + \tau_{23,y}), \\
u_z + \varepsilon^2 w_x &= \lambda A \tau^{n-1} \tau_{13}, \\
v_z + \varepsilon^2 w_y &= \lambda A \tau^{n-1} \tau_{23}, \\
u_y + v_x &= A\tau^{n-1}\tau_{12}, \\
2u_x &= A\tau^{n-1}\tau_{11}, \\
2v_y &= A\tau^{n-1}\tau_{22}, \\
2w_z &= A\tau^{n-1}\tau_{33}, \\
\tau^2 &= \tau_{13}^2 + \tau_{23}^2 + \frac{\varepsilon^2}{\lambda^2}\left[\tfrac{1}{2}\tau_{11}^2 + \tfrac{1}{2}\tau_{22}^2 + \tfrac{1}{2}\tau_{33}^2 + \tau_{12}^2\right].
\end{aligned} \tag{10.250}$$

This allows for a temperature-dependent rate factor A, but we will now suppose $A = 1$. The boundary conditions are, on $z = s$:

$$\begin{aligned}
\tau_{13} &= \frac{\varepsilon^2}{\lambda}\left[\left(-p + \tau_{11}\right) s_x + \tau_{12} s_y\right], \\
\tau_{23} &= \frac{\varepsilon^2}{\lambda}\left[\tau_{12} s_x + \left(-p + \tau_{22}\right) s_y\right], \\
p - \tau_{33} &= \lambda(-\tau_{13} s_x - \tau_{23} s_y), \\
w &= s_t + u s_x + v s_y - a,
\end{aligned} \tag{10.251}$$

while at the base $z = b(x, y, t)$:

$$(u, v) = \mathbf{u}_b, \quad w = u b_x + v b_y. \tag{10.252}$$

The dimensionless form of the sliding law (10.218) can be written as

$$\tau_b = R u_b^r, \tag{10.253}$$

where $u_b = |\mathbf{u}_b|$, and R is a dimensionless roughness factor which depends on effective pressure N. By choice of λ, we may suppose $R \lesssim O(1)$ in streaming flow, but we can also describe shear flow with little or no sliding by having $R \gg 1$. The corresponding vector form of (10.253) is

$$\boldsymbol{\tau}_b = R u_b^{r-1} \mathbf{u}_b, \tag{10.254}$$

where, correct to terms of $O(\varepsilon^2)$, $\boldsymbol{\tau}_b = (\tau_{13}, \tau_{23})$.

When $\lambda \ll 1$, it is possible to use a different form of approximation (to the shallow ice approximation where $\lambda = 1$) which includes the longitudinal stress terms. This is called the membrane stress approximation. To derive it, we reconsider (10.250). Without approximation, we can integrate the vertical normal stress equation to give

$$p = -(\tau_{11} + \tau_{22}) - \lambda \left[\frac{\partial}{\partial x} \int_z^s \tau_{13}\, dz + \frac{\partial}{\partial y} \int_z^s \tau_{23}\, dz \right], \tag{10.255}$$

and substituting this into the shear stress equations, they take the form, again without approximation,

$$\begin{aligned} \tau_{13,z} &= s_x - \frac{\varepsilon^2}{\lambda}(2\tau_{11,x} + \tau_{12,y} + \tau_{22,x}) - \varepsilon^2 \left(\frac{\partial^2}{\partial x^2} \int_z^s \tau_{13}\, dz + \frac{\partial^2}{\partial x \partial y} \int_z^s \tau_{23}\, dz \right), \\ \tau_{23,z} &= s_y - \frac{\varepsilon^2}{\lambda}(\tau_{11,y} + \tau_{12,x} + 2\tau_{22,y}) - \varepsilon^2 \left(\frac{\partial^2}{\partial x \partial y} \int_z^s \tau_{13}\, dz + \frac{\partial^2}{\partial y^2} \int_z^s \tau_{23}\, dz \right). \end{aligned} \tag{10.256}$$

The membrane stress approximation is based on the limit $\varepsilon \ll 1$, independently of the size of λ, and consists in essence of the neglect of the integral terms in (10.256), thus we have

$$\begin{aligned} \tau_{13,z} &= s_x - \frac{\varepsilon^2}{\lambda}[2\tau_{11,x} + \tau_{12,y} + \tau_{22,x}], \\ \tau_{23,z} &= s_y - \frac{\varepsilon^2}{\lambda}[\tau_{11,y} + \tau_{12,x} + 2\tau_{22,y}]. \end{aligned} \tag{10.257}$$

If, in addition, we suppose that $\lambda \ll 1$, then it follows from (10.250)[19] that $\left|\frac{\partial \mathbf{u}}{\partial z}\right| \ll 1$, and thus $\mathbf{u} \approx \mathbf{u}_b$, and is a function of x and y. Thus, so also are the stresses τ_{11}, τ_{12} and τ_{22}, and so we can integrate (10.257) using (10.251) to obtain

$$\begin{aligned} \tau_{13} &= -(s-z)s_x + \frac{\varepsilon^2}{\lambda}\left[\frac{\partial}{\partial x}\{(2\tau_{11} + \tau_{22})(s-z)\} + \frac{\partial}{\partial y}\{\tau_{12}(s-z)\} \right], \\ \tau_{23} &= -(s-z)s_y + \frac{\varepsilon^2}{\lambda}\left[\frac{\partial}{\partial x}\{\tau_{12}(s-z)\} + \frac{\partial}{\partial y}\{(\tau_{11} + 2\tau_{22})(s-z)\} \right]. \end{aligned} \tag{10.258}$$

As a matter of fact we can argue that (10.258) is still approximately true even if $\lambda \sim O(1)$, as follows. The corrective stress terms of $O(\varepsilon^2/\lambda)$ are small unless horizontal gradients of $\mathbf{u}$ are large, and the only way in which this can occur is if the sliding velocity changes rapidly in space. It follows that in regions where the corrective stresses are important, they can be accurately approximated by using the sliding velocity in computing them. There is no loss of accuracy in doing this everywhere, since the terms are in any case small when the sliding velocity is not

[19] We presume that $\mathbf{u} = (u, v) \sim O(1)$.

changing rapidly. By evaluating (10.258) at the bed, we obtain a closed model for the sliding velocity, in the form

$$\begin{aligned}\tau_1 &= -Hs_x + \frac{\varepsilon^2}{\lambda}\left[\frac{\partial}{\partial x}\{(2\tau_{11}+\tau_{22})H\} + \frac{\partial}{\partial y}\{\tau_{12}H\}\right], \\ \tau_2 &= -Hs_y + \frac{\varepsilon^2}{\lambda}\left[\frac{\partial}{\partial x}\{\tau_{12}H\} + \frac{\partial}{\partial y}\{(\tau_{11}+2\tau_{22})H\}\right],\end{aligned} \tag{10.259}$$

where $H = s - b$ is the depth, and $(\tau_1, \tau_2) = \boldsymbol{\tau}_b$ is the basal shear stress, given by (10.254). This is the membrane stress approximation, in which the membrane stresses τ_{11}, τ_{12} and τ_{22} are given in terms of the sliding velocity (u, v); in the case that $\lambda \ll 1$, so that shearing is negligible, H is determined by conservation of mass in the form

$$\frac{\partial H}{\partial t} + \frac{\partial (Hu)}{\partial x} + \frac{\partial (Hv)}{\partial y} = a, \tag{10.260}$$

where a is the accumulation rate.

On the Siple Coast, fast flow alternates with inter-ice stream regions where ice flow is small, and sliding is small or negligible. In building a model for the mechanics of ice streams, it is thus advisable to allow for regions where shear flow is important. Luckily, it is easy to do this in the present context. In consideration of (10.258), we can reasonably assume that the ice surface does not change abruptly. In that case, we can remove the depth terms from inside the derivatives, and we can write (10.258) in the form

$$(\tau_{13}, \tau_{23}) \approx (s - z)\mathbf{g}, \tag{10.261}$$

where

$$\mathbf{g} = -\boldsymbol{\nabla} s + \frac{\varepsilon^2}{\lambda}\mathbf{G}, \tag{10.262}$$

and

$$\mathbf{G} = \left(\frac{\partial}{\partial x}\{2\tau_{11}+\tau_{22}\} + \frac{\partial \tau_{12}}{\partial y}, \frac{\partial \tau_{12}}{\partial x} + \frac{\partial}{\partial y}\{\tau_{11}+2\tau_{22}\}\right). \tag{10.263}$$

In seeking a correction to (10.260) when shearing is important, we can now invert our earlier argument. The correction will only be important when sliding is small, and consequently when longitudinal stresses are small. In this case, τ does not vary rapidly, and we can take

$$\tau = Hg; \tag{10.264}$$

(10.263) can then be simplified to the form

$$\mathbf{G} \approx \frac{1}{\tau^{n-1}}\left(\nabla^2 \mathbf{u} + 3\boldsymbol{\nabla}\Delta\right), \tag{10.265}$$

where Δ is the dilatation

$$\Delta = \boldsymbol{\nabla}.\,\mathbf{u}. \tag{10.266}$$

Just as in the shallow ice approximation, we can integrate (10.261) twice to obtain the generalisation of (10.260) in the form

$$\frac{\partial H}{\partial t} + \boldsymbol{\nabla}. \left\{ H\mathbf{u} + \frac{\lambda H^{n+2}}{n+2}\, g^{n-1}\mathbf{g} \right\} = a. \tag{10.267}$$

Together with the membrane stress approximation (10.259) and the sliding law (10.254), which can be combined to give (approximately)

$$\boldsymbol{\tau} = Ru^{r-1}\mathbf{u} = H\mathbf{g}, \tag{10.268}$$

(10.267) allows for a unified description of flow in which both ice streams and non-ice stream flow are accurately described, at least for isothermal ice (i. e., constant A); $\mathbf{g}$ is defined by (10.262), and $\mathbf{G}$ by (10.263).[20]

A simple model of an ice stream

We give here a simple model of an ice stream such as those in the Siple Coast. We take axes x downstream and y cross-stream, and we suppose the velocity is purely in the x-direction, is independent of depth z, and varies only with the transverse coordinate y, thus $\mathbf{u} = (u(y), 0)$. We suppose $H = 1$ and $-\boldsymbol{\nabla} s = (\alpha, 0)$, where a reasonable value of $\alpha = 0.1$. Then the basal stress is $\boldsymbol{\tau} = (\tau_1, 0)$, and we have the system

$$\begin{aligned} \tau_1 = Ru^r &= \alpha + \frac{\varepsilon^2}{\lambda}\frac{\partial \tau_{12}}{\partial y}, \\ \tau^2 &= \tau_1^2 + \frac{\varepsilon^2}{\lambda^2}\tau_{12}^2, \\ \tau_{12} &= \frac{u_y}{\tau^{n-1}}. \end{aligned} \tag{10.269}$$

For the basal sediments on the Siple coast, for example beneath the Whillans ice stream, a yield stress may be relevant, in which case we might have $r = 0$ and $R \approx 0.01$. Then we suppose that $\tau_1 \ll \dfrac{\varepsilon}{\lambda}\tau_{12}$, so that

$$\tau \approx \frac{\varepsilon}{\lambda}\tau_{12}. \tag{10.270}$$

It then follows that

$$\tau \approx \left(\frac{\varepsilon}{\lambda} |u_y|^{\frac{1}{n}-1} u_y \right), \quad \tau_{12} = \left(\frac{\lambda}{\varepsilon} \right)^{1-\frac{1}{n}} |u_y|^{\frac{1}{n}-1} u_y, \tag{10.271}$$

and thus that u satisfies the equation

$$Ru^r = \alpha + \frac{\varepsilon^{1+\frac{1}{n}}}{\lambda^{\frac{1}{n}}} \frac{\partial}{\partial y} \left(|u_y|^{\frac{1}{n}-1} u_y \right). \tag{10.272}$$

[20]Note that τ in (10.264) is the second stress invariant, while $\boldsymbol{\tau}$ in (10.268) is the basal shear stress.

We define $y = \nu Y$, where

$$\nu = \frac{\varepsilon}{\lambda^{\frac{1}{n+1}} \alpha^{\frac{n}{n+1}}}, \tag{10.273}$$

and suppose that $R \ll \alpha$, connoting weak basal till. u then satisfies the equation

$$0 \approx 1 + \frac{\partial}{\partial Y} \left(|u_Y|^{\frac{1}{n}-1} u_Y \right), \tag{10.274}$$

and suitable boundary conditions are that

$$u = 0 \quad \text{on} \quad Y = \pm L, \tag{10.275}$$

where L can be determined if we specify the normalising condition $u(0) = 1$. Adopting this, the solution is

$$u = 1 - \frac{|Y|^{n+1}}{n+1}, \tag{10.276}$$

and the dimensional ice stream width is then

$$L_{is} = 2d_i \left(\frac{n+1}{\lambda \alpha^n} \right)^{\frac{1}{n+1}}, \tag{10.277}$$

where d_i is ice depth. Taking $d_i = 1{,}000$ m, we can find an ice stream width of 40 km if, for example, we take $\alpha = 0.1$, $\lambda = 0.025$.

Note that in $(10.269)_1$, we have $\frac{\varepsilon}{\lambda}\tau_{12} \sim \frac{\alpha\nu}{\varepsilon}$, so that our earlier assumption that τ_1 $(\sim R) \ll \frac{\varepsilon}{\lambda}\tau_{12}$ is valid if $R \ll \frac{\alpha\nu}{\varepsilon}$, and thus certainly if $\nu \gtrsim \varepsilon$, as is confirmed by (10.273).

10.4 Waves, surges and mega-surges

10.4.1 Waves on glaciers

Waves on glaciers are most easily understood by considering an isothermal, two-dimensional model. We suppose the base is flat ($h = 0$), so that equations (10.25) and (10.26) give

$$H_t + \left[\{1 - \mu H_x\}^n \frac{H^{n+2}}{n+2} + u_b H \right]_x = B'(x), \tag{10.278}$$

where $B'(x) = a$ is the accumulation rate, and $\mu \sim 0.1$. If we firstly put $\mu = 0$ and also $u_b = 0$, then

$$H_t + H^{n+1} H_x = B'(x), \tag{10.279}$$

which has the steady state

$$\frac{H_0^{n+2}}{n+2} = B(x). \tag{10.280}$$

With $B' > 0$ in $x < x_f$ (say) and $B' < 0$ in $x > x_f$ ($x = x_f$ is then the *firn line*), (10.280) defines a concave profile like that in figure 10.6. (10.279) is clearly

hyperbolic, and admits wave-like disturbances which travel at a speed H^{n+1}, which is in fact $(n+1)$ (≈ 4) times the surface speed. If we take an initial condition at $t=0$ corresponding to a balance function $B(x)-\varepsilon D(x)$, where $\varepsilon \ll 1$, then the solution using the method of characteristics subject to an upstream boundary condition of

$$H = 0 \quad \text{at} \quad x = 0 \tag{10.281}$$

is

$$\frac{H^{n+2}}{n+2} = B(x) - \varepsilon D(\sigma),$$

$$t = \int_{\sigma}^{x} \frac{dx'}{[(n+2)\{B(x') - \varepsilon D(\sigma)\}]^{(n+1)/(n+2)}}. \tag{10.282}$$

The characteristics of (10.279) propagate downstream and reach the snout (where $H=0$) in finite time. (10.282) is somewhat unwieldy, and it is useful to approximate the characteristic solution for small ε. However, if we use the blunt approach, where we write $H = H_0 + \varepsilon h$, a straightforward linearisation of (10.279) shows that h grows unboundedly near the snout of the glacier. This unphysical behaviour occurs because the linearisation artificially holds the snout position fixed; mathematically, the linearisation is invalid near the snout where $H_0 = 0$ and the assumption $\varepsilon h \ll H_0$ breaks down. An apparently uniformly valid approximation can be obtained, however, by linearising the characteristics:

$$H_t + H_0^{n+1} H_x \approx B'(x). \tag{10.283}$$

For $H \approx H_0$, the general solution is

$$H = H_0(x) + \phi(\xi - t), \tag{10.284}$$

where

$$\xi = \int_0^x \frac{dx}{H_0^{n+1}(x)} \tag{10.285}$$

is a characteristic spatial coordinate (note ξ is finite at the snout). (10.284) clearly reveals the travelling wave characteristic of the solution.

Margin response

However, although (10.284) is better than the blunt approach, it is not really good enough, as it still only defines the solution within the confines of the steady state solution domain determined by (10.285). The more methodical way to deal with the singularity of the solution at the snout is to allow margin movement by using the method of strained coordinates. That is to say, we change coordinates to

$$x = s + \varepsilon x_1(s,\tau) + \ldots, \quad t = \tau. \tag{10.286}$$

The equation (10.279) now takes the form

$$H_\tau + H^{n+1} H_s = B' + \varepsilon(x_{1\tau} + H^{n+1} x_{1s}) H_s + \ldots, \tag{10.287}$$

and analogously to (10.282), we pose the initial condition

$$\frac{H^{n+2}}{n+2} = B(s) - \varepsilon D(s) \quad \text{at} \quad \tau = 0. \tag{10.288}$$

In addition, we pose the boundary condition

$$H = 0 \quad \text{at} \quad s = 0, \tag{10.289}$$

which also forces

$$x_1 = 0 \quad \text{at} \quad s = 0. \tag{10.290}$$

We also require that x_1 is such that

$$H = 0 \quad \text{at} \quad s = 1, \tag{10.291}$$

this being the position of the snout when $D = 0$, i. e., $B(1) = 0$.

We put

$$H = H_0 + \varepsilon h + \ldots, \tag{10.292}$$

and hence find that

$$\frac{H_0^{n+2}}{n+2} = B(s), \tag{10.293}$$

and, using ξ defined by (10.285) (but with s as the upper limit) as the space variable, we have

$$\left(H_0^{n+1}h\right)_\tau + \left(H_0^{n+1}h\right)_\xi = \left(x_{1\tau} + x_{1\xi}\right) H_0'(\xi), \tag{10.294}$$

and the initial condition is

$$H_0^{n+1}h = -D \quad \text{at} \quad \tau = 0. \tag{10.295}$$

The boundary condition of $h = 0$ at $s = 0$ is irrelevant here, because there is only a perturbation in the initial condition, so that for $\tau > \xi$, $h = 0$ and the steady solution is restored.

The solution of (10.294) can be written as

$$\begin{aligned} H_0^{n+1}h &= -D(\xi - \tau) + U(\xi, \tau), \\ x_1 &= \int_0^\tau P(\eta + \xi - \tau, \eta)\, d\eta + x_1^0(\xi - \tau), \end{aligned} \tag{10.296}$$

where U satisfies

$$\begin{aligned} U_\tau + U_\xi &= P(\xi, \tau) H_0'(\xi), \\ U &= 0 \quad \text{at} \quad \tau = 0. \end{aligned} \tag{10.297}$$

The method of strained coordinates proceeds by choosing x_1 in order that h is no more singular than H_0. Since $H_0 \sim \xi_1 - \xi$ as $\xi \to \xi_1$, where

$$\xi_1 = \int_0^1 \frac{ds}{H_0^{n+1}(s)}, \tag{10.298}$$

we have to choose U so that the right hand side of $(10.296)_1$ is $O[(\xi_1 - \xi)^{n+2}]$ as $\xi \to \xi_1$. For $n = 3$, for example, this requires choosing the $n + 2 = 5$ conditions

$$U = D(\xi_1 - \tau),\ U_\xi = D'(\xi_1 - \tau), \ldots, U_{\xi\xi\xi\xi} = D^{\text{iv}}(\xi_1 - \tau) \quad \text{at} \quad \xi = \xi_1. \tag{10.299}$$

As is well known, any such function will do, its importance being locally near $\xi = \xi_1$. Given U, $(10.297)_1$ defines P, and then $(10.296)_2$ defines the straining, and thus the margin position. To find U, it is convenient to solve the partial differential equation (assuming $n + 2 = 5$)

$$U_\tau = U_{10\xi}, \tag{10.300}$$

subject to the five boundary conditions in (10.299), together with, for example,

$$U = U_\xi = \ldots = U_{4\xi} = 0 \quad \text{at} \quad \xi = \xi_f, \tag{10.301}$$

where ξ_f denotes the firn line position where $H_0'(\xi_f) = 0$. The point of choosing a tenth order equation is to ensure decay away from $\xi = \xi_1$, which is cosmetically advantageous; the point of choosing ξ_f in (10.301) is to ensure that P remains bounded; again, this is largely cosmetic and one might simply replace ξ_f by ∞.

The upstream boundary condition

We have blithely asserted that

$$H = 0 \quad \text{at} \quad x = 0, \tag{10.302}$$

as seems fine for the diffusionless equation (10.279). Let us examine this more closely, assuming the diffusional model (10.278) with no sliding, in steady state form:

$$\frac{(1 - \mu H_x)^n H^{n+2}}{n + 2} = B(x), \tag{10.303}$$

where we have already integrated once, applying the condition that the ice flux is zero at the glacier head $x = 0$, where $B = \displaystyle\int_0^x a(x')\,dx' = 0$. If we ignore μ, this seems fine, but if $\mu \neq 0$, then we can rewrite (10.303) as

$$\mu H_x = 1 - \left\{ \frac{(n + 2)B}{H^{n+2}} \right\}^{1/n}. \tag{10.304}$$

Consideration of the direction of trajectories in the (x, H) plane shows that there is no trajectory which has $H(0) = 0$. The only alternative allowing zero flux at the head is $\mu H_x = 1$ there (physically, a horizontal surface), but then the depth is necessarily non-zero.

We have seen this problem before (see question 4.10). Consideration of (10.304) shows that there is a unique value of $H_0 > 0$ such that if $H(0) = H_0$, then $\dfrac{H^{n+2}}{n + 2} \sim B(x)$ for $x \gg \mu$, as is appropriate. Based on our earlier experience, we might expect that a boundary layer in which longitudinal stresses are important would provide a mechanism for the transition from $H = 0$ to $H = H_0$. This is indeed the case (see question 10.11), but the resultant compressive boundary layer appears to be very unphysical. The theoretical description of the head of a glacier therefore remains problematical.

Shock formation

An issue which complicates the small perturbation theory above is the possible formation of shocks. Characteristics $x(\sigma, t)$ in (10.282) intersect if $\dfrac{\partial x}{\partial \sigma} = 0$. Computing this we find

$$\frac{\partial x}{\partial \sigma} = \frac{H^{n+1}(x,\sigma)}{H^{n+1}(\sigma,\sigma)} - \varepsilon(n+1)D'(\sigma)H^{n+1}(x,\sigma)\int_\sigma^x \frac{dx'}{H^{2n+3}(x',\sigma)}. \tag{10.305}$$

From this unwieldy expression, it is clear that for small ε, shocks will always form near the snout if $D' > 0$ somewhere, which is the condition for local advance of the glacier. More generally, glacier advances are associated with steep fronts, while retreats have shallower fronts, as is commonly observed.

Shocks can form away from the snout if H is increased locally (e. g., due to the surge of a tributary glacier). The rôle of the term in μ is then to diffuse such shocks. A shock at $x = x_s$ will propagate at a rate

$$\dot{x}_s = \frac{[H^{n+2}]^+_-}{(n+2)[H]^+_-}, \tag{10.306}$$

where $[\ \ ]^+_-$ denotes the jump across x_s. When the shock reaches the snout, it then propagates at a speed $H_-^{n+1}/(n+2)$, which is *slower* than the surface speed.

In the neighbourhood of a shock (with $u_b = 0$), we put

$$x = x_s + \nu X, \tag{10.307}$$

so that

$$\frac{\partial H}{\partial t} - \frac{\dot{x}_s}{\nu}\frac{\partial H}{\partial X} + \frac{1}{\nu}\left[\left\{1 - \frac{\mu}{\nu}H_X\right\}^n \frac{H^{n+2}}{n+2}\right]_X = B'(x_s + \nu X); \tag{10.308}$$

if ν is small, the profile rapidly relaxes to the steady travelling wave described by

$$\dot{x}_0 H_X = \left[\{1 - H_X\}^n \frac{H^{n+2}}{n+2}\right]_X, \tag{10.309}$$

providing we choose $\nu = \mu$, which thus gives the width of the shock structure. (10.309) can be solved by quadrature (see question 10.15). In practice the shock width is relatively long, so steep surface wave shocks due to this mechanism are unlikely (but they can form for other reasons, for example in surges, when longitudinal stresses become important).

Seasonal waves

Although they constitute the more dramatic phenomenon, the seasonal wave has attracted much less attention than the surface wave, perhaps because there are less obvious comparable analogies. The surface wave is essentially the same as the surface wave in a river, while the seasonal wave bears more resemblance to a compression wave in a metal spring, even though the ice is essentially incompressible.

Apparently the waves are induced through seasonal variations in velocity, which are themselves associated with variations in meltwater supply to the glacier bed, so that a natural model for the ice flow would involve only sliding, thus (non-dimensionally)

$$H_t + (Hu)_x = a, \tag{10.310}$$

where u is the sliding velocity. If the natural time scale for glacier flow is $t_i \sim 100$ y, while the seasonal time scale is $t_s = 1$ y, then it is appropriate to rescale the time as

$$t = \varepsilon T, \quad \varepsilon = \frac{t_s}{t_i} \ll 1, \tag{10.311}$$

so that H satisfies

$$H_T = \varepsilon \left[a - (Hu)_x \right]; \tag{10.312}$$

this immediately explains why there is no significant surface perturbation during passage of the seasonal wave.

To study the velocity perturbation, we suppose that the sliding velocity depends on the basal shear stress τ (which varies little by the above discussion) and effective pressure N. If, for example, basal drainage is determined by a relation such as (10.225), then essentially $u = u(Q)$, so that waves in u are effectively waves in Q, i. e., waves in the basal hydraulic system.

Suppose that mass conservation in the hydraulic system is written non-dimensionally as

$$\phi S_T + Q_x = M, \tag{10.313}$$

where M is the basal meltwater supply rate,

$$\phi = \frac{t_h}{t_s} \tag{10.314}$$

is the ratio of the hydraulic time scale t_h to the seasonal time scale t_s, and a force balance relation such as (10.221) (cf. (10.224)) suggests $S = S(Q)$. If, for simplicity, we take $\phi S'(Q) = \kappa$ as constant, then the solution of (10.313) subject to a boundary condition of

$$Q = 0 \quad \text{at} \quad x = 0 \tag{10.315}$$

is

$$Q = \frac{1}{\kappa}[J(T) - J(T - \kappa x)], \tag{10.316}$$

where

$$J(T) = \int_0^T M(T')\, dT'. \tag{10.317}$$

(10.316) clearly indicates the travelling wave nature of the solution.

The diagram in figure 10.2, sometimes called a Hodge diagram, depicts a seasonal wave through the propagation of the constant velocity contours down glacier. The constant velocity contours are represented as functions $x(Q, t)$ (if we suppose u depends on Q). Higher Q causes higher N in Röthlisberger channels, and thus lower

velocity, as seen in figure 10.2. A crude representation of the data is thus as a family of curves

$$x = A(Q) + X[T - \theta(Q)], \tag{10.318}$$

where A increases with Q and θ also increases with Q.

To illustrate how (10.316) mimics this, we first note that for non-negative melt-water supply rates M, J is monotonically increasing and thus invertible, whence we can write (10.316) in the form

$$x = \frac{1}{\kappa}\left[T - J^{-1}\{J(T) - \kappa Q\}\right]. \tag{10.319}$$

Suppose, for example that $M = 1 + m(T)$ where m is small and has zero mean, so that

$$J(T) = T + j(T), \quad j(T) = \int_0^T m(T')\,dT'; \tag{10.320}$$

it follows that

$$J^{-1}(u) \approx u - j(u), \tag{10.321}$$

and thus

$$x \approx Q - \frac{1}{\kappa}\left[j(T) - j(T - \kappa Q)\right]. \tag{10.322}$$

This is sufficiently similar to the putative (10.318) to suggest that this mechanism may provide an explanation for seasonal waves. According to (10.322), the dimensionless wave speed is $v_s^* \sim \dfrac{1}{\kappa}$, and thus the dimensional wave speed $v_s \sim \dfrac{l}{t_h}$. In figure 10.3, we see typical ice velocities of 100 m y^{-1} compared with a seasonal wave speed of some 15 km y^{-1}. Assuming a time scale of 60 y for a six kilometre long glacier, this would suggest a hydraulic time scale of about five months. On the face of it, this seems very long, but in fact the relevant hydraulic time scale should be that over which the water pressure in the cavity system can respond to changes in the channel pressure, which will be a lot longer than the adjustment time for the channel itself.

10.4.2 Surges

It has long been suggested that the fast velocities during surges could only be caused by rapid sliding. Therefore it is sufficient for our purpose to analyse the mass conservation equation in the form

$$H_t + (Hu)_x = B'(x), \tag{10.323}$$

where u is the sliding velocity. Also, it has been thought that if the sliding velocity were a multi-valued function of basal stress τ_b (i. e., $\tau_b(u)$ has a decreasing portion) then, since $\tau_b = H(1 - \mu s_x) \approx H$, this would cause the ice flux $Q = uH$ to be multi-valued, as shown in figure 10.11. In this case we might expect relaxation oscillations to occur for values of B intermediate between the two noses of $Q(H)$. Two fundamental questions arise. Firstly, is there any genuine reason why $\tau_b(u)$ should

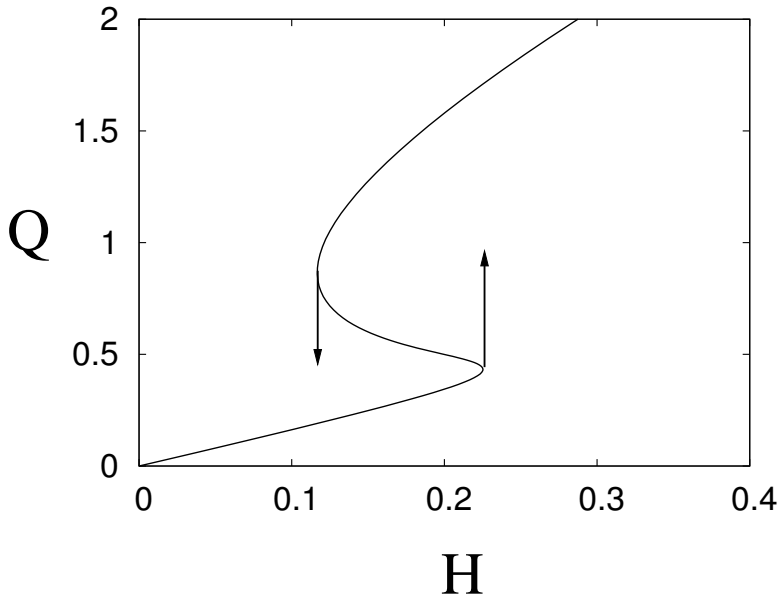

Figure 10.11: A multi-valued flux-depth relation can cause oscillatory surges.

be non-monotone, and secondly, how would such a relaxation oscillator work in the spatially dependent case? In particular, it would seem necessary to have a secondary variable, whose rapid change can facilitate the relaxation between the different solution branches (cf. figure 1.6 and equations (1.25)).

The discussion in section 10.2 suggested the possibility of non-monotone $\tau_b(u)$ for flow over a periodic bed. However, it is arguable whether real beds have this feature[21], in which case we may suppose that τ increases with both u and N. What observations of the 1982–3 surge of Variegated Glacier showed, however, was that there is a switch in drainage pattern during its surge. There are (at least) two possible modes of drainage below a glacier. Röthlisberger channels, as described in section 10.2, can form a branched arterial drainage system. In this case the value of the effective pressure at the bed N is determined by the water flow, $N = N_R$, say. Alternatively, there may be no channel system, and the water at the bed fills the cavities behind bed protuberances, and drains by a slower leakage between cavities. This is the linked cavity régime described in section 10.3.2; it operates at a higher water pressure and thus lower effective pressure, N_c, than in the channel drainage. The crucial factor which enables surges to take place is the switching mechanism, and this depends on the ice flow over the cavities.

We now combine the form of the sliding law $\tau_b = Nf(u/N^n)$, as discussed in section 10.2, with a drainage system consisting either of Röthlisberger channels or linked cavities, the choice of which depends on the value of $\Lambda = u/N^n$, with the

[21] An exception may be the very steep 'hanging glaciers', where the periodic behaviour consists of complete detachment of the glacier snout following tensile fracture.

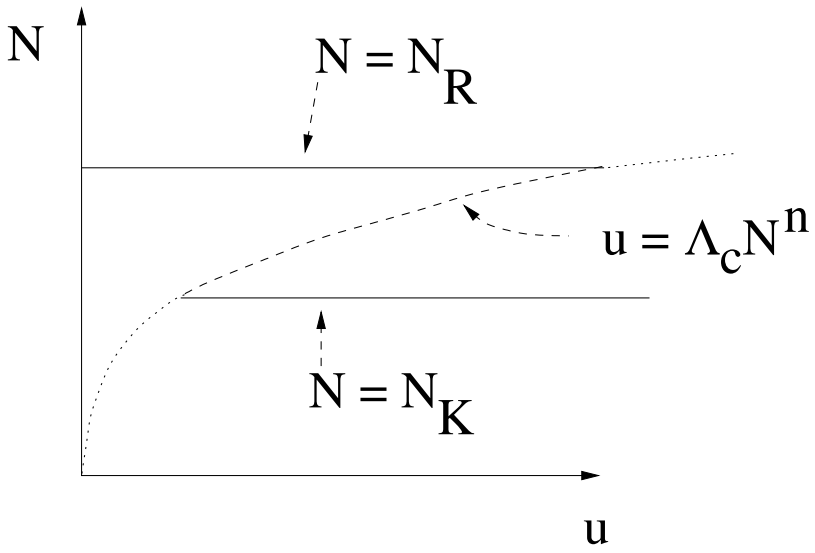

Figure 10.12: N is a multi-valued function of u.

transition between drainage systems occurring at the critical value Λ_c. That is,

$$\begin{aligned} N = N_R, \qquad & u/N^n < \Lambda_c; \\ N = N_c, \qquad & u/N^n > \Lambda_c. \end{aligned} \tag{10.324}$$

If this is written as a function $N(u)$, it is multi-valued, as shown in figure 10.12. As a consequence of this, the sliding law is indeed multi-valued, and hence $Q(H)$ has the form shown in figure 10.13.

There are two critical values of Q in figure 10.13, denoted Q_+, Q_-: these are the values at the noses of the curve (where also $H = H_+, H_-$). If $B(x) < Q_+$, then an equilibrium glacier profile exists in which $Q = B(x)$. However, if the maximum value of B, $B_{\max}$, is greater than Q_+, then such a stable equilibrium cannot occur, and the glacier surges.

The sequence of events in a surge is then as follows. The glacier grows from a quiescent state in which $Q < Q_+$ on the lower (slow) branch everywhere. When the maximum depth reaches H_+, there is a *reservoir* zone where $H > H_-$. The ice flux at H_+ jumps to the upper (fast) branch by switching drainage pattern, and this switch propagates upstream and downstream to where $H = H_-$. These *activation waves* propagate at rates of hundreds of metres per *hour* (and in effect have been observed). Once the activation waves have propagated to the boundaries of the reservoir zone, the ice flow is described by the fast mode on the upper branch, and the activated reservoir zone propagates rapidly downstream, possibly overriding the stagnant snout and propagating forwards as a front. In terms of figure 10.13, the surge terminates when H reaches H_- everywhere, and deactivation waves propagate inwards from the boundaries of the exhausted reservoir zone to re-establish the channel drainage system. There then follows another quiescent phase where the maximum value of H increases from H_- to H_+ before the next surge is initiated.

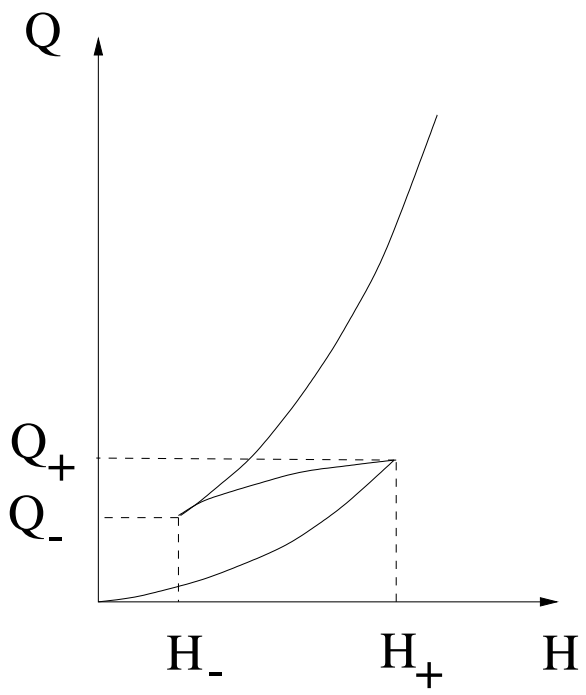

Figure 10.13: Q is a multi-valued function of H

10.4.3 Sliding and ice streams

It is not known for certain why the ice flow on the Siple Coast of Antarctica, which flows out to the floating Ross ice shelf, segregates itself into the five distinct ice streams A to E. The picture which one has of this region is of a gently sloping (slope $\alpha \sim 10^{-3}$) kilometer thick ice sheet which flows in the ice streams at typical rates of 500 m y^{-1}. Such rapid velocity can only be due to basal sliding, and the seismic evidence indicates that the ice is underlain by several metres of wet till. One might expect that a sliding law of the form advocated previously is appropriate, that is

$$\tau_b = c u_b^r N^s, \tag{10.325}$$

with r and s positive. The issue then arises as to how to prescribe N. Recall from section 10.2 that for drainage through Röthlisberger channels, an appropriate law is $N = \beta Q_w^{1/4n}$, where Q_w is water flux. When ice flows over till, an alternative system of drainage is that of distributed 'canals' incised in the subglacial till. For such a system, an appropriate law is $N = \gamma Q_w^{-1/n}$, and the low values of effective pressure in this relation are more representative of measured basal pressures on Whillans ice stream, for example.

In this case an interesting feedback exists. In Antarctic ice streams, there is little, if any, surface melt reaching the bed, and the basal water flow is due to melting there. The quantity of meltwater produced per unit area per unit time is given by the melt velocity

$$v_m = \frac{G + \tau_b u_b - g}{\rho_w L}, \tag{10.326}$$

where ρ_w is water density, L is latent heat, G is geothermal heat flux, and g is the basal heat flux into the ice. This assumes the base is at the melting point. Thus we expect the basal water flux $Q_w \propto G + \tau_b u_b - g$, and so Q_w increases with u_b (the dependence of g on u_b is likely to be weaker — boundary layer theory would suggest $g \sim u_b^{1/2}$). If also N decreases with Q_w, then N decreases as u_b increases. But this causes further increase of u_b via the sliding law. This positive feedback can lead to a runaway phenomenon which we may call hydraulic runaway.

To get a crude idea of how this works, we denote the ice thickness as h and the surface slope as S_i. If the velocity is u, then the ice flux per unit width is

$$Q = hu; \tag{10.327}$$

the basal shear stress is

$$\tau = Rh = cu^r N^s, \tag{10.328}$$

where we define

$$R = \rho_i g S_i; \tag{10.329}$$

we suppose

$$N = \gamma Q_w^{-p}, \tag{10.330}$$

and that

$$Q_w = b[G + \tau u - g], \tag{10.331}$$

where, from (10.326), we define

$$b = \frac{l_i l_s}{\rho_w L}, \tag{10.332}$$

in which l_i is the ice flow line length scale and l_s is the stream spacing, and the heat flux to the ice is given by

$$g = au^{1/2}, \tag{10.333}$$

corresponding to a heat flux through a thermal boundary layer. Consequently

$$h = \frac{fu^r}{[G + Rhu - au^{1/2}]^m}, \tag{10.334}$$

where

$$m = ps, \quad f = \frac{c\gamma^s}{Rb^m}. \tag{10.335}$$

It is not difficult to see from (10.334) if f is low enough (equivalently, the friction coefficient c is low enough), that u and hence the ice flux Q will be a multivalued function of h, as shown in figure 10.14. In fact, application of realistic parameter values suggests that such multi-valued flux laws are normal. More specifically, we choose estimates for the parameters as follows. We use exponents $p = r = s = \frac{1}{3}$ and thus $m = \frac{1}{9}$, and then $c = 0.017$ bar$^{2/3}$ m$^{-1/3}$ y$^{1/3}$, based on a sliding law (10.328) with $\tau = 0.1$ bar, $N = 0.4$ bar and $u = 500$ m y^{-1}. Other parameter values are $\gamma = 0.3$ bar (m^3 s^{-1})$^{1/3}$, $S_i = 10^{-3}$, $\rho_i = 0.917 \times 10^3$ kg m^{-3}, $g = 9.8$ m s^{-2}, $G = 0.06$ W m^{-2}, $\rho_w = 10^3$ kg m^{-3}, $L = 3.3 \times 10^5$ J kg^{-1}, and in addition we choose $l_i = 10^3$ km, $l_s = 330$ m; from these we find $R = 3 \times 10^{-7}$ W m^{-4} y, $b = 1$ J^{-1} m^5, and

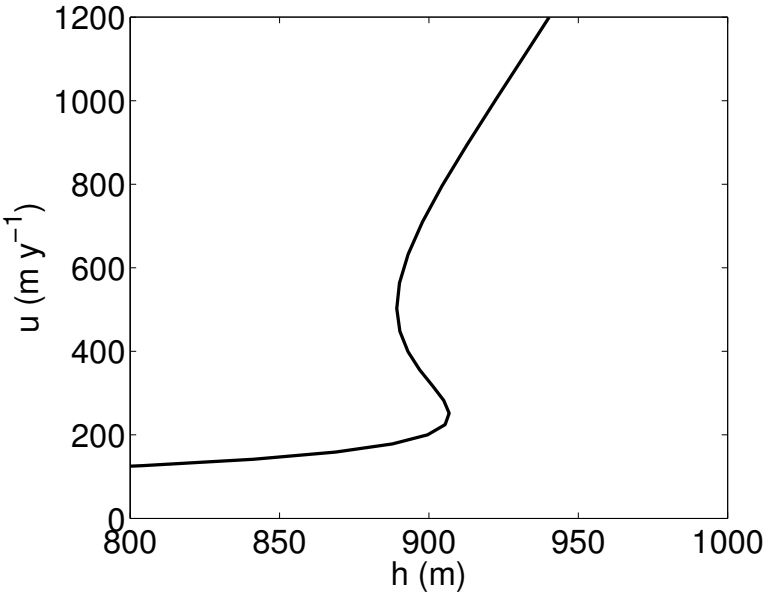

Figure 10.14: Thermal feedback causes a multi-valued ice flux. The solution of (10.334) is plotted using a value of the critical parameter $f = 70$ W$^{1/9}$ m$^{4/9}$ y$^{1/3}$. Other values are as described in the text. I am indebted to Ian Hewitt for his production of this figure.

thus $f = 126$ W$^{1/9}$ m$^{4/9}$ y$^{1/3}$. Finally, we choose the value of a based on an assumed magnitude of $g \approx \dfrac{4k\Delta T}{d_i}$, where ice depth is $d_i = 10^3$ m, thermal conductivity is $k = 2.2$ W m^{-1} K^{-1}, and surface temperature below freezing is $\Delta T = 20°$ K; with $u = 500$ m y^{-1}, this gives $a = 0.8 \times 10^{-2}$ W m$^{-5/2}$ y$^{1/2}$. Figure 10.14 plots velocity versus depth with these parameter values, except that we take $f = 70$ W$^{1/9}$ m$^{4/9}$ y$^{1/3}$, and question 10.14 provides approximate analytic solutions for the different branches.

If, indeed, hydraulic feedback can cause a multi-valued relationship between ice velocity and depth, what then happens in a region such as the Siple Coast of West Antarctica? We suppose that the ice flux is determined by conditions upstream, so that if the ice flux per unit width is q, and the width of the discharge region is W, then

$$Wq = B, \tag{10.336}$$

where B is the volume flux of ice discharged. If the flow law is multi-valued, then there exists a range (q_-, q_+) of q such that the ice flow is unstable (see question 10.14). If $B/W < q_-$, then a uniform slow moving ice flow is possible. Similarly, if $B/W > q_+$, a uniform fast moving ice stream is possible. What if $q_- < B/W < q_+$? A uniform ice flow is now unstable, and we may expect a spatial instability to occur, whereby ice streams spontaneously form, as is in fact observed. Such an instability would be mediated by transitions in water pressure, since basal water will flow from fast streams at high water pressure to slower ice at low water pressure. This generates

a lateral enthalpy flux, and in a steady state this can be balanced by a heat flux in the ice in the opposite direction, since cooling (g) is less effective at lower u, therefore the slow ice is warmer near the base than the ice streams.

10.4.4 Heinrich events and the Hudson strait mega-surge

What if the drainage channel of an ice sheet over deforming till is relatively narrow? By analogy with the pattern formation mechanism in reaction-diffusion equations, one would expect that a multivalued flux-depth relation would not allow separate streams to form if the channel width is too small, and in this case we would expect periodic surges to occur down the channel, if the prescribed mass flux corresponds to a velocity on the unstable position of figure 10.14.

A situation of this type appears to have occurred during the last ice age. The Laurentide ice sheet which existed in North America drained the ice dome which lay over Hudson Bay out through the Hudson Strait, a 200 km wide trough which discharged the ice (as icebergs) into the Labrador sea and thence to the North Atlantic.

Hudson Bay is underlain by soft carbonate rocks, mudstones, which can be mobilised when wet. It has been suggested that the presence of these deformable sediments, together with the confined drainage channel, led to the occurrence of semi-periodic surges of the Hudson Strait ice stream. The evolution of events is then as follows. When ice is thin over Hudson Bay, the mudstones may be frozen at the base, there is little, if any, sliding and very little ice flow. Consequently, the ice thickens and eventually the basal ice warms. The basal muds thaw, and sliding is initiated. If the friction is sufficiently low (i. e., c and thus f is small), then the multi-valued sliding law of figure 10.14 is appropriate, and if the accumulation rate is large enough, cyclic surging will occur. During a surge, the flow velocity increases dramatically, and there results a massive iceberg flux into the North Atlantic. On the lower branch of figure 10.14, water production is virtually absent, Q_w is low in (10.331) since the flow is slow and the geothermal and viscous heat at the base can be conducted away by the ice. The low value of Q_w gives high N, consistent with low u. On the upper branch, however, viscous heat dominates, and Q_w is large, N is small, also consistent with a high u.

At the end of a surge, the rapid ice drawdown causes the water production to drop, and the rapid velocities switch off. This may be associated with re-freezing of the basal mudstones.

When water saturated soils freeze, frost heave occurs by sucking up water to the freezing front via capillary action, and this excess water freezes (at least for fine grained clays and silts) in a sequence of discrete ice lenses. Heaving can occur at a typical rate of perhaps a metre per year, though less for fine grained soils, and the rate of heave is suppressed by large surface loads. Calculations suggest a surge period of perhaps a hundred years, with a drawdown of a thousand metres, and a recovery period on the order of 5,000–10,000 years. During the surge, the rapidly deforming basal muds will dilate (in the deforming horizon, likely to be only a metre or so thick). At the termination of a surge, this layer re-consolidates, and we can expect the total heave to be a certain (small) fraction of the frost penetration depth. In effect, the

ice lenses freeze the muds into the ice stream, so that when the next surge phase is initiated, some of this frozen-in basal sediment will be transported downstream, and thence rafted out into the North Atlantic in iceberg discharge.

As discussed in chapter 2, there is evidence that this rather glamorous sequence of events actually occurs. Heinrich events are layers of ice-rafted debris in deep-sea sediment cores from the North Atlantic which indicate (or are consistent with) massive iceberg discharges every 7000 years or so. In addition, oxygen isotope concentrations in ice cores from Greenland indicate that severe cooling cycles occurred during the last ice age. These cooling events may be caused by a switch-off of North Atlantic deep water (NADW) circulation — effectively switching off the convective heat transport from equatorial latitudes and thus cooling the atmosphere. It seems that sequences of these cooling cycles are terminated by Heinrich events, in the sense that following Heinrich events the climate warms dramatically, perhaps after some delay. There are two reasons why this should be so. On the one hand, the sudden reduction in ice thickness should warm the air above, and also it can be expected that a massive iceberg (and thus freshwater) flux to the North Atlantic acts as a source of thermal buoyancy, which first slows down and subsequently restarts a vigorous North Atlantic circulation. Rather than being lumbering beasts, glaciers and ice sheets show every sign of being dynamically active agents in shaping the climate and the earth's topography.

10.5 Drumlins and eskers

There are a number of bedforms associated with the motion of ice sheets, and in this section we will discuss two of them, drumlins and eskers. Drumlins are small hills[22], generally of oval shape, which corrugate the landscape, as shown in figures 10.15 and 10.16. They are formed ubiquitously under ice sheets, and take a range of shapes, depending presumably on the basal ice conditions. Ribbed moraines, also called Rogen moraines after the area in Sweden (Lake Rogen) where such features were first described, are transverse furrows like a washboard, with the undulations (presumed) perpendicular to the former ice flow. They are analogous to the transverse dunes described in chapter 5, and as we shall see, are supposed to be formed by an analogous instability mechanism.

The three-dimensional drumlins of figure 10.15 may then arise through a secondary transverse instability, perhaps as some parameter associated with ice flow changes. What certainly happens under former fast moving ice streams is that drumlins become elongated in the direction of ice flow, appearing eventually to become extremely long grooves aligned with the flow. These grooves, which can run for hundreds of kilometres, are called mega-scale glacial lineations (MSGL), and give the landscape the appearance of having been combed. Figure 10.17 shows a systems of MSGL in Northern Canada.

[22]The word 'drumlin' is of Irish origin, generally thought to be a diminutive of the word *druim*, meaning a hill, and thus a drumlin is a 'small hill'.

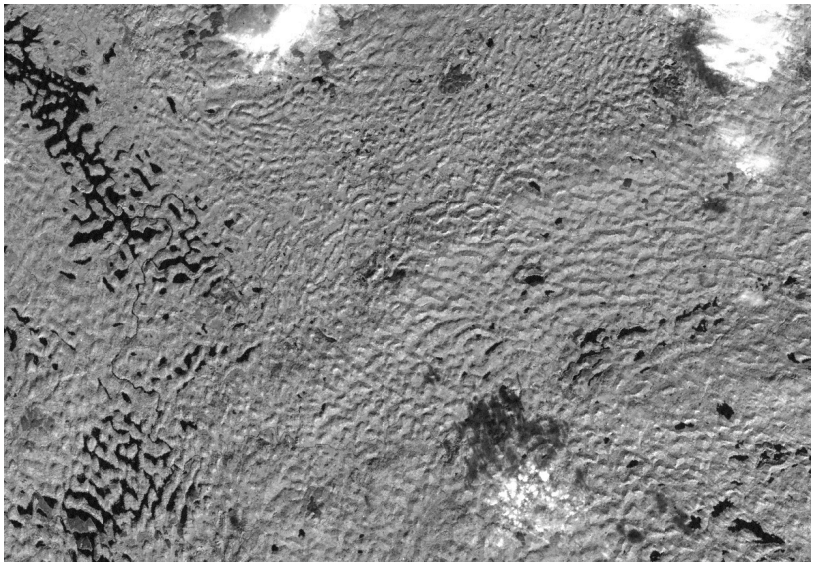

Figure 10.15: Drumlins in Northern Ireland. Satellite view.

Figure 10.16: Drumlins in the Ards Peninsula of Northern Ireland.

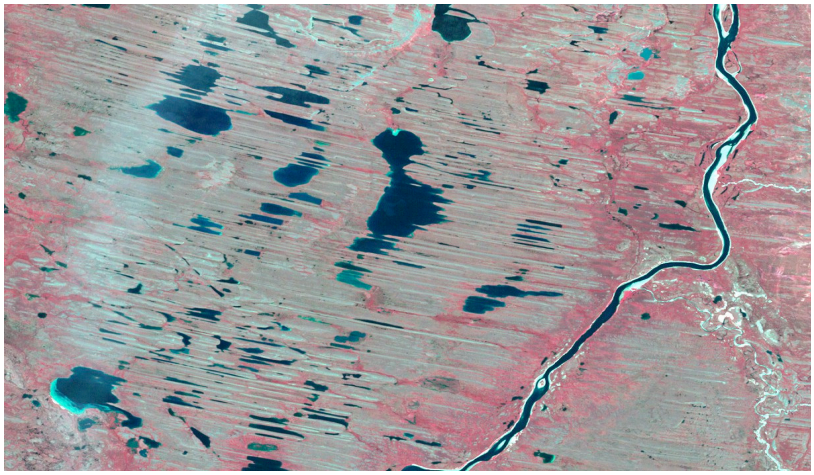

Figure 10.17: Satellite view of MSGL in Northern Canada. The lineations are about a hundred metres in width, and of the order of a hundred kilometres in length.

Eskers[23] are sinuous ridges of gravel and sand, of similar dimensions to drumlins, having elevations of tens of metres. They are associated with former drainage channels under the ice, most probably Röthlisberger channels, which have become infilled with subglacial sediment. Figure 10.18 shows a satellite view of an esker system in Northern Canada. The eskers are the red lineations, and their disordered and nonlinear arrangement suggests that they may have been formed at different times, as the ice flow changes direction.

10.5.1 Drumlins

We build a theory of drumlin formation by analogy with the theory of dune formation. An ice sheet flows as indicated in figure 10.19 over a deformable substrate at $z = s$, where s is the elevation of the bedrock. The ice at the base is at the melting point, and there is a local drainage system for the resulting meltwater. How we treat this drainage system is key. To begin with, we suppose that the drainage system organises itself as described earlier, independently of the evolution of the bed elevation.

The surface elevation of the ice sheet is $z = z_i$, relative to a level $z = 0$ located at the elevation of the local drainage system. We suppose the bed consists of a saturated till of porosity ϕ. If the pore water pressure at the interface $z = s$ is p_w^s and the overburden normal stress there is P^s, then the corresponding pore and overburden pressures below the surface are taken to be

$$p_w = p_w^s + \rho_w g(s - z), \quad P = P^s + [\rho_w \phi + \rho_s(1 - \phi)]g(s - z), \tag{10.337}$$

simply through hydrostatic and lithostatic balance: ρ_w and ρ_s are the densities of water and sediment, respectively. Within the till, the effective pressure is defined as

$$p_e = P - p_w, \tag{10.338}$$

[23]The term esker is also Irish, from *eiscir*, meaning a small ridge.

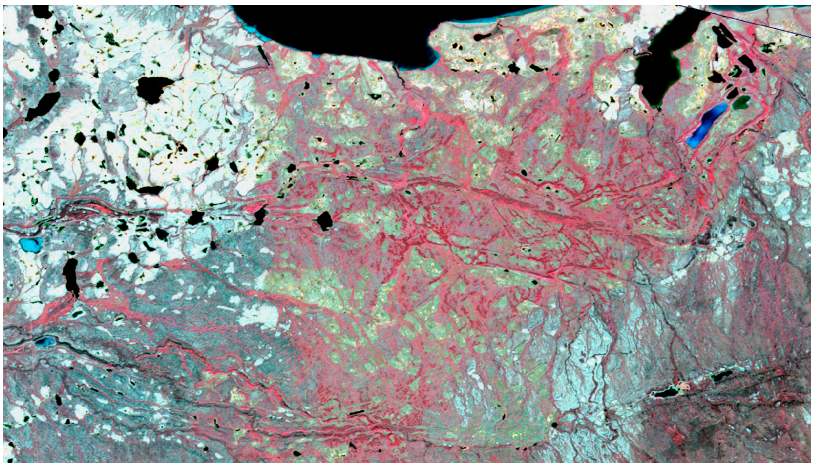

Figure 10.18: A system of eskers in Northern Canada. This false colur satellite image shows the eskers as the criss-crossed red linear features.

and thus

$$p_e = N + (1 - \phi)\Delta\rho_{sw} g(s - z), \tag{10.339}$$

where

$$\Delta\rho_{sw} = \rho_s - \rho_w, \tag{10.340}$$

and N is the effective pressure at the interface,

$$N = P^s - p_w^s. \tag{10.341}$$

The interfacial normal stress P^s is related to the stress in the ice by

$$P^s = -\sigma_{nn} = p_i^s - \tau_{nn}, \tag{10.342}$$

where σ_{nn} is the normal stress in the ice, τ_{nn} is the deviatoric normal stress in the ice, and p_i^s is the ice pressure at the bed. As is customary in ice sheet dynamics, we define the reduced pressure Π in the ice by

$$p_i = p_a + \rho_i g(z_i - z) + \Pi, \tag{10.343}$$

where p_a is atmospheric pressure, and we define the effective pressure in the drainage system as

$$N_c = p_a + \rho_i g z_i - p_c, \tag{10.344}$$

where p_c is the water pressure in the local drainage system, which we presume known. From these it follows that the effective pressure at the bed is given by

$$N = N_c + \Delta\rho_{wi} g s + \Pi - \tau_{nn}, \tag{10.345}$$

where

$$\Delta\rho_{wi} = \rho_w - \rho_i. \tag{10.346}$$

The drainage effective pressure N_c is presumed to be determined by the properties of the local hydraulic drainage system, as discussed in section 10.3.

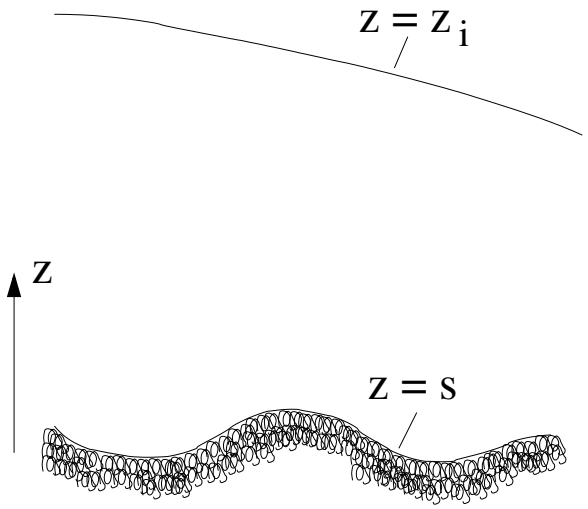

Figure 10.19: System geometry.

Bed evolution

We restrict our initial presentation of the model to two dimensions (x, z), for the sake of clarity. The generalisation to three dimensions is given subsequently (see also question 10.16). The evolution of the bed is given by the Exner equation

$$s_t + q_x = 0, \tag{10.347}$$

where q is the basal sediment flux. Ideally, q would be determined in the field or laboratory, but this is not very practicable. Alternatively, we might propose a sediment transport law based on a presumed rheology of the till. This also is problematic, since the determination of the rheology of granular materials is difficult and controversial. For the present purpose, we can largely avoid the issue, recognising only that there is sediment transport ($q \neq 0$), and that it is likely to depend on both the basal shear stress τ and the basal effective pressure N, thus

$$q = q(\tau, N). \tag{10.348}$$

Ice flow

For simplicity we suppose the flow of ice is Newtonian, with a constant viscosity η. In two dimensions, the equations for the velocity (u, w) can be written in the form

$$\begin{aligned} u_x + w_z &= 0, \\ 0 &= -\Pi_x - \rho_i g z_i' + \eta \nabla^2 u, \\ 0 &= -\Pi_z + \eta \nabla^2 w, \end{aligned} \tag{10.349}$$

where Π is the reduced pressure defined earlier, and $z_i' = \dfrac{\partial z_i}{\partial x}$.

Surface boundary conditions

The conditions which we apply at the surface are those of stress continuity and a kinematic condition, which take the form

$$\Pi - \tau_{nn} = 0, \quad \tau_{nt} = 0, \quad w = \frac{\partial z_i}{\partial t} + u\frac{\partial z_i}{\partial x} - a \quad \text{at} \quad z = z_i, \tag{10.350}$$

where τ_{nt} is the shear stress, a is the accumulation rate. We can anticipate that the horizontal length scale of interest will be that of drumlins, thus in the range 100–1000 m, and much less than the horizontal length scale appropriate to ice sheets. Therefore it seems reasonable to suppose that z_i will be almost constant, and the boundary conditions (10.350) can be approximately applied at a flat interface. Although the regional slope of the ice surface is negligible geometrically, it is necessary to retain it in the force balance equation (10.349).[24]

There is an alternative possibility for the upper boundary condition, which arises in the case that the parameter

$$\sigma = \frac{l}{d_i} \tag{10.351}$$

is small, where l is the horizontal drumlin length scale and d_i is the ice depth scale. In this case, the flow near the base is akin to a boundary layer flow, and the appropriate condition is a matching condition to the outer ice sheet flow, which sees the base as essentially flat with small scale wrinkles. Assuming this outer ice sheet flow is a shear flow which varies on a horizontal length scale $\gg d_i$, appropriate matching conditions are

$$\Pi \to 0, \quad \eta u_z \to \tau_b, \quad w \to 0 \quad \text{as} \quad z \to \infty. \tag{10.352}$$

The quantity τ_b is the basal shear stress determined by the outer flow, and is given by

$$\tau_b = -\rho_i g z_i z_i'. \tag{10.353}$$

It is not clear which of the limits for σ is the more appropriate. Four hundred metre drumlins under eight hundred metres of ice suggest $\sigma = O(1)$, but two hundred metre drumlins under two thousand metres of ice suggest $\sigma \ll 1$. Nor is it clear whether there might be any essential difference in the resulting stability analysis. Since the limit $\sigma \ll 1$ is the simpler, we focus henceforth on that case.

Basal boundary conditions

To write the basal boundary conditions, we need to construct the normal and shear stress, and the tangential velocity, using the unit normal and tangent vectors. (In three dimensions, there are two tangent vectors to be used, see question 10.16.)

[24] This is analogous to the Boussinesq approximation in convection: the surface slope is important in determining the driving stress, but negligible otherwise.

In two dimensions, the normal and shear deviatoric stresses are

$$\begin{aligned} -\tau_{nn} &= \frac{2\eta}{1+s_x^2}\left[(1-s_x^2)u_x + s_x(u_z+w_x)\right], \\ \tau &= \frac{\eta}{1+s_x^2}\left[(1-s_x^2)(u_z+w_x) - 4s_x u_x\right]. \end{aligned} \tag{10.354}$$

We suppose that there is a sliding velocity, which we denote by U, and as for sediment transport, we suppose that this depends on the interfacial shear stress[25] τ and interfacial effective pressure N. Accounting for the tangential velocity at the bed, the sliding law then takes the form

$$\frac{u + ws_x}{(1+s_x^2)^{1/2}} = U(\tau, N). \tag{10.355}$$

As for the sediment transport, we avoid specification of how sliding is achieved; it might be by deformation of the underlying till, or by slip at the ice-till interface. In either case we expect dependence of U on τ and N.

The final condition at the bed is the kinematic condition,

$$w = s_t + us_x; \tag{10.356}$$

we ignore interfacial melting, usually of the order of millimetres per year, and negligible in this context.

Between them, the equations (10.345), (10.348), (10.354), (10.355) and (10.356) need to provide a total of two interfacial boundary conditions for the ice flow; the Exner equation (10.347) provides the evolution equation for s. We can take the two interfacial conditions to be the velocity conditions (10.355) and (10.356), which are given in terms of τ, N and s. Then (10.345) and $(10.354)_1$ determine N, (10.347) and (10.348) determine s, and $(10.354)_2$ determines τ. The model is therefore complete.

A reduced model

We begin by non-dimensionalising the model. There are a number of length scales present in the equations. We define the quantities

$$z_i \sim d_i, \quad d_D = \frac{N_c}{\Delta\rho_{iw}g}, \quad d_T = \frac{N_c}{\Delta\rho_{sw}g(1-\phi)}. \tag{10.357}$$

These length scales are the ice depth scale d_I, the drumlin depth scale d_D, and the till deformation depth scale d_T. To explain the significance of these scales, we resume our earlier discussion of till deformation.

[25] Some confusion is liable to occur between the values of shear stress and other quantities at the ice-till interface, and the values of these quantities far from the interface, because it is normal to refer to the far field values as 'basal', since on the ice sheet scale, they are at the base of the large scale ice flow. We will endeavour to avoid this confusion by referring to 'far field' and 'interfacial' values (despite having defined the basal shear stress in (10.353)!).

Subglacial till is a granular material, consisting of rough angular fragments in a matrix of finer grained material, the whole being water saturated when it is being deformed. In common with all granular materials, we expect that when subjected to a shear stress, it will not deform until the shear stress exceeds a critical value, called the yield stress. The reason for this is simple, insofar as we expect two solid surfaces not to permit sliding until the static coefficient of friction is exceeded. More specifically, if the normal stress between two clasts is p_e, and the shear stress is τ, then slip will occur if

$$\tau > \mu p_e, \tag{10.358}$$

where μ is the coefficient of friction. More generally, the Mohr-Coulomb yield stress τ_c in a granular material is

$$\tau_c = c + \mu p_e, \tag{10.359}$$

where c is the cohesion, often ignored as being small for subglacial till. The coefficient μ is of $O(1)$, and is related to the angle of friction ϕ_f by $\mu = \tan \phi_f$.

If we now consult (10.339) and (10.345), two observations can be made. Till deformation will cease at effective pressures larger than τ/μ. Typical basal shear stresses are likely to be in the range 0.1–1 bar, so that till will only deform at all if p_e is of this order. In particular, till deformation can only occur at values of $N_c \lesssim 1$ bar. Such low values of the effective stress have been measured under the Ross ice streams, and may be associated with a distributed, canal type of drainage. Assuming, then, that $\tau \sim N_c$, we see from (10.339) that till deformation is only viable to a depth of order d_T, as defined in (10.357). Below this depth, the effective pressure is too large to promote till deformation. This observation allows us to suggest a typical value of till transport.

The second observation is drawn from (10.345). If we anticipate that drumlins grow as a consequence of instability of a flat bed, then the effective pressure increases with drumlin elevation. When the drumlins attain an elevation of order d_D given by (10.357), the summit effective pressure will be large enough to slow down the till and thus also deformation, which presumably stunts further growth. This depth scale thus provides an estimate for the eventual height of drumlins. Choosing $N_c = 0.4$ bars gives a depth scale of 50 m, although numerical solutions generally give smaller values.

We use these ideas in choosing scales for the variables. It is first convenient to define a stream function for the flow via

$$\psi_z = u, \quad -\psi_x = w. \tag{10.360}$$

We take the basic shear flow without bed perturbations to be

$$\psi = u_0 z + \frac{\tau_b}{2\eta} z^2, \tag{10.361}$$

where the mean velocity $\bar{u}(t)$ is introduced as the developing bedforms alter the average sliding velocity. Specifically, we scale the model by choosing

$$z_i = d_i h, \quad x, z \sim l, \quad p_e, N, \Pi, \tau_{nn}, \tau \sim N_c, \quad s \sim d_D,$$

$$\psi = u_0 \bar{u} z + \frac{\tau_b}{2\eta} z^2 + u_0 d_D \Psi, \quad U \sim u_0, \quad q \sim u_0 d_T, \quad t \sim \frac{d_D l}{d_T u_0}, \tag{10.362}$$

and we scale the depth of the till by writing

$$s - z = d_T \zeta. \tag{10.363}$$

Thus the dimensionless effective pressure in the till is

$$p_e = N + \zeta, \tag{10.364}$$

and the yield criterion (10.358) becomes

$$\zeta < \frac{\tau}{\mu} - N. \tag{10.365}$$

The value of u_0 is determined by the magnitude of the sliding velocity, and the horizontal length scale is defined by balancing the stress and strain rates, thus

$$l = \left(\frac{\eta u_0 d_D}{N_c} \right)^{1/2} = \left(\frac{\eta u_0}{\Delta \rho_{iw} g} \right)^{1/2}. \tag{10.366}$$

If we choose $u_0 = 100$ m y^{-1} and $\eta = 6$ bar year ($\approx 2 \times 10^{13}$ Pa s), then $l = 271$ m. Other typical values, with $\rho_s = 2.5 \times 10^3$ kg m^{-3} and $n = 0.4$, are $d_T = 4.6$ m, and the time scale is 29 y.[26]

With this choice of scaling, the dimensionless model for the ice flow is

$$\begin{aligned} 0 &= -\Pi_x + \nabla^2 \Psi_z + \sigma\theta, \\ 0 &= -\Pi_z - \nabla^2 \Psi_x, \end{aligned} \tag{10.367}$$

with far field boundary conditions (appropriate for small σ)

$$\Pi \to 0, \quad \Psi \to 0 \quad \text{as} \quad z \to \infty. \tag{10.368}$$

The basal conditions take the form

$$\begin{aligned} -\tau_{nn} &= \frac{2\left[(1-\nu^2 s_x^2)\Psi_{zx} + \nu s_x(\theta + \Psi_{zz} - \Psi_{xx})\right]}{1+\nu^2 s_x^2}, \\ \tau &= \frac{(1-\nu^2 s_x^2)(\theta + \Psi_{zz} - \Psi_{xx}) - 4\nu s_x \Psi_{zx}}{1+\nu^2 s_x^2}, \\ \frac{\bar{u} + \nu\theta z + \nu\Psi_z - \nu^2 \Psi_x s_x}{(1+\nu^2 s_x^2)^{1/2}} &= U(\tau, N), \\ -\Psi_x &= \alpha s_t + \left[\bar{u} + \nu\theta z + \nu\Psi_z\right] s_x, \\ N &= 1 + s + \Pi - \tau_{nn}, \\ s_t + q_x &= 0, \end{aligned} \tag{10.369}$$

[26] This time scale is rather long, given recent observations of bedforms growing in a matter of years. As we shall see below, the instability does in fact occur on a much shorter time scale (and also on a shorter length scale).

and these are all applied at $z = \nu s$.

The dimensionless parameters σ, θ, ν and α are defined by

$$\sigma = \frac{l}{d_i}, \quad \theta = \frac{\tau_b}{N_c}, \quad \nu = \frac{d_D}{l}, \quad \alpha = \frac{d_T}{d_D}. \tag{10.370}$$

Supposing $l = 300$ m, $d_i = 1500$ m, thus $\tau_b = 0.15$ bar with an assumed ice surface slope of 10^{-3}, $d_D = 50$ m, $N_c = 0.4$ bar, $d_T = 5$ m, typical values are

$$\sigma \sim 0.2, \quad \theta \sim 0.38, \quad \nu \sim 0.16, \quad \alpha \sim 0.1. \tag{10.371}$$

We now simplify the model by considering the aspect ratio $\nu \ll 1$. Putting $\nu = 0$ (and putting $\sigma = 0$ in the momentum equations), the reduced model is then

$$\begin{aligned} 0 &= -\Pi_x + \nabla^2 \Psi_z, \\ 0 &= -\Pi_z - \nabla^2 \Psi_x, \end{aligned} \tag{10.372}$$

with matching condition (10.368), and interfacial conditions applied at $z = 0$:

$$\begin{aligned} -\tau_{nn} &= 2\Psi_{zx}, \\ \tau &= \theta + \Psi_{zz} - \Psi_{xx}, \\ \bar{u} &= U(\tau, N), \\ -\Psi_x &= \alpha s_t + \bar{u} s_x, \\ N &= 1 + s + \Pi - \tau_{nn}, \\ s_t + q_x &= 0. \end{aligned} \tag{10.373}$$

The stability of the uniform solution of this reduced model is studied in the following subsection.

It is straightforward to carry through this procedure in three dimensions (see also question 10.16), and here we simply state the result. The position coordinates are now (x, y, z), with y being the transverse horizontal coordinate, and the corresponding velocity vector is $(u, v, w) = \mathbf{u}$. The reduced dimensionless model is

$$\begin{aligned} \boldsymbol{\nabla} \Pi &= \nabla^2 \mathbf{u}, \\ \boldsymbol{\nabla} . \mathbf{u} &= 0, \end{aligned} \tag{10.374}$$

subject to

$$\Pi \to 0, \quad u_z \to \theta, \quad v, \, w \to 0 \quad \text{as} \quad z \to \infty, \tag{10.375}$$

and

$$\begin{aligned}
\tau_{nn} &= 2w_z, \\
\tau_1 &= \theta + u_z + w_x, \\
\tau_2 &= v_z + w_y, \\
\tau &= \left[\tau_1^2 + \tau_2^2\right]^{1/2}, \\
\bar{u} &= \frac{U(\tau, N)\tau_1}{\tau}, \\
0 &= \frac{U(\tau, N)\tau_2}{\tau}, \\
w &= \alpha s_t + \bar{u} s_x, \\
N &= 1 + s + \Pi - \tau_{nn}, \\
s_t + \boldsymbol{\nabla}.\,\mathbf{q} &= 0,
\end{aligned} \tag{10.376}$$

all applied at $z = 0$. One might suppose that, since also α is quite small, it too could be neglected. As our linear stability analysis will show, this is not possible, since it provides a stabilising term at high wave number.

Ice flow solution

Reverting to the two-dimensional problem, the ice flow problem is linear, and can be solved conveniently using the Fourier transform

$$\hat{f}(k) = \int_{-\infty}^{\infty} f(x) e^{ikx}\, dx; \tag{10.377}$$

omitting details, we then find that

$$N = 1 + s - 2\mathcal{H}\left\{\alpha s_{xt} + \bar{u} s_{xx}\right\}, \tag{10.378}$$

where the Hilbert transform is

$$\mathcal{H}(g) = \frac{1}{\pi} \int_{-\infty}^{\infty} \frac{g(t)\, dt}{t - x}. \tag{10.379}$$

The interfacial shear stress $\tau \approx \tau_1$ can be inverted to the form

$$\tau = f(\bar{u}, N), \tag{10.380}$$

while a horizontal average of this yields the condition

$$\theta = \overline{f(\bar{u}, N)}, \tag{10.381}$$

which serves to specify the average dimensionless sliding velocity $\bar{u}$.

The sediment flux q was taken to depend on τ and N. It is the product of a dimensionless deformable till thickness A and a mean velocity V, which we suppose

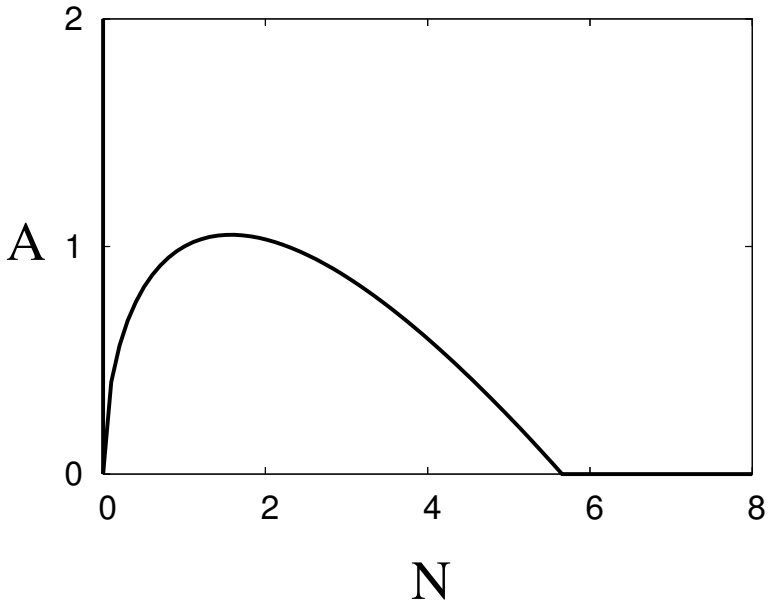

Figure 10.20: The function $A(N)$ given by (10.382), where $f(\bar{u}, N) = \theta \bar{u}^a N^b$. The parameters used are $b = 0.6$, $\mu = 0.4$, $\theta = 0.8$, $\bar{u} = 1$.

is constrained by the ice velocity $\bar{u}$. The deformable depth is constrained by (10.365), which suggests that we choose

$$A = A(N) = \left[\frac{f(\bar{u}, N)}{\mu} - N \right]_+ \tag{10.382}$$

($[x]_+ = \max(x, 0)$). Since we suppose $V \sim \bar{u}$, which itself depends on N, we may as well take $V = 1$ and thus $q = A$. Our model for bed elevation is thus completed by solving the Exner equation

$$\frac{\partial s}{\partial t} + \frac{\partial A(N)}{\partial x} = 0, \tag{10.383}$$

together with the normal stress condition (10.378). Note that this is a nonlinear model for the bed elevation. A typical form of the sediment flux function $q = A$ is shown in figure 10.20.

Linear stability

We now consider the linear stability of the reduced, two-dimensional model (10.378) and (10.383). The basic uniform state is (assuming the sliding law $\tau = \theta \bar{u}^a N^b$)

$$N = 1, \quad s = 0. \tag{10.384}$$

For simplicity we suppose $\bar{u} \equiv 1$, which is in any case valid in the linearised theory.

We linearise about this basic state by putting $N = 1 + P$, and linearising for small s and P. Denoting the transforms with an overhat, and using the facts that

$\widehat{f_x} = -ik\hat{f}$ and $\widehat{\mathcal{H}(g_x)} = -|k|\hat{g}$, we find that $\hat{s} \propto e^{\sigma t}$, with

$$\sigma = \frac{ikA'(1 - 2ik|k|)}{1 - 2ik|k|\alpha A'}, \tag{10.385}$$

where $A' = A'(1)$. With $\sigma = r + ikc$, this implies that the growth rate is

$$r = \frac{2k^2|k|A'(1 - \alpha A')}{1 + 4\alpha^2 A'^2 k^4}, \tag{10.386}$$

and the wave speed is

$$c = \frac{A'(1 + 4\alpha A' k^4)}{1 + 4\alpha^2 A'^2 k^4}. \tag{10.387}$$

Bearing in mind that α is relatively small, we see from (10.386) that the flat bed is unstable if $A' > 0$, or equivalently if $q' > 0$. Since $q = q(\tau, N)$ and $\tau = f(u, N)$, we can interpret this instability criterion as follows. If we draw the two families of curves $\tau = f(u, N)$ with constant u, and $q = q(\tau, N)$ with constant q in the (N, τ) plane, then the criterion $q' > 0$ is equivalent (assuming $q_\tau > 0$) to

$$\left.\frac{d\tau}{dN}\right|_u > \left.\frac{d\tau}{dN}\right|_q. \tag{10.388}$$

This criterion is easily satisfied for reasonable choices of sediment flux and sliding law. If we use the sliding law $\tau = \theta u^a N^b$, then the instability criterion is

$$\theta > \frac{\mu}{b}. \tag{10.389}$$

Providing the base of the ice is at the melting point, (10.389) shows that drumlins will form for large enough basal shear stress, or for low enough channel effective pressure. If we suppose that b is close to one, corresponding to a 'plastic' till, then the instability criterion is that $\tau_b \gtrsim \mu N_c$, which is simply the criterion that the till should deform. Roughly speaking, we can expect drumlinisation wherever till deforms.

The wave speed c is positive, and the growth rate has a maximum at a wavenumber

$$k = k_{\max} = \frac{3^{1/4}}{(2\alpha A')^{1/2}}. \tag{10.390}$$

If we take $\alpha = 0.1$ and $A' = \frac{1}{3}$, then $\dfrac{2\pi}{k_{\max}} \approx 1.23$, corresponding to a dimensional wavelength of 334 m. The corresponding growth time scale is

$$t_{\max} = \frac{1}{r} \approx \frac{1 + 4\alpha^2 A'^2 k_{\max}^2}{2k_{\max}^3 A'} \approx 0.038, \tag{10.391}$$

corresponding to a dimensional growth time of thirteen months. It is a hallmark of the instability that it is rapid.

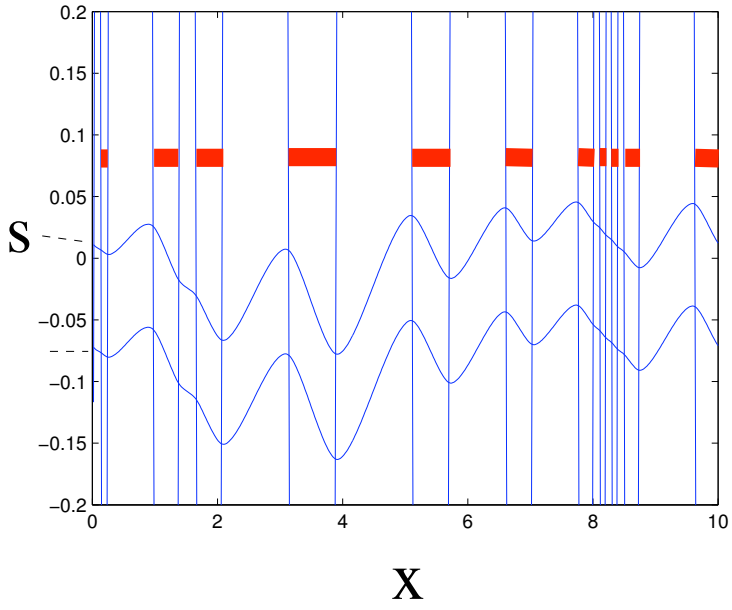

Figure 10.21: Finite amplitude till surface obtained from solving (10.393) with a suitable approximation for $A(N)$ resembling figure 10.20. The two surfaces are the ice base and the base of the deformable till layer (which is actually $s - \alpha A$). The red bands indicate the cavities, where $N = 0$.

Nonlinear results

The main difficulty in computing finite amplitude solutions of the model (10.378) with (10.383) is that as the instability develops, N decreases until it inevitably reaches zero; physically, cavities form in the lee of obstacles. If s continues to denote the base of the ice flow, then while (10.378) still applies, the Exner equation 10.383 must be replaced by the cavitation condition

$$N = 0. \tag{10.392}$$

This makes the model difficult to solve numerically. One way round this is to continue to solve (10.383), but to extend the definition of A so that it is any positive value when $N = 0$. As in fact indicated in figure 10.20, this makes A a piecewise smooth *graph*. The combined model is thus

$$\begin{aligned} N &= 1 + s - 2\mathcal{H}\left\{\alpha s_{xt} + \bar{u} s_{xx}\right\}, \\ \frac{\partial s}{\partial t} + \frac{\partial a}{\partial x} &= 0, \end{aligned} \tag{10.393}$$

with

$$\begin{cases} a = A(N), & N > 0, \\ a > 0, & N = 0. \end{cases} \tag{10.394}$$

Figure 10.22: An esker which formed during retreat of the Stagnation Glacier, Bylot Island, Nunavut, Canada in 1992. The bouldery ridge in the background is the inner face of the substantial lateral moraine surrounding the rapidly retreating glacier. The landform is actually composed mostly of glacial ice preserved by the insulating cover of about a metre of bouldery esker gravel. Photograph by Christian Zdanowicz, available at `www.inrs.illinois.edu/shilts`.

In practice, we approximate the graph of A by a smooth non-monotonic function. Despite this, the model is difficult to solve numerically. This is because as the oscillations grow, a transition takes place when the maximum of A is reached. When this happens, there is a rapid transition to a state in which N is piecewise constant, being positive on the upstream face of the bedforms, and (approximately) zero on the downstream cavities. At this transition, a spectral method (used because of the nice properties of the Hilbert transform in Hilbert space) generates transient high frequency components which can cause numerical breakdown. Figure 10.21 shows the result of one such calculation, in which the positions of the cavities are indicated in red. In this model, the drumlins reach a stationary state. In more detailed models, they form finite amplitude travelling waves, as discussed in the notes.

10.5.2 Eskers

Eskers are long, sinuous ridges of sand and gravel which, like drumlins, are associated with the existence of former ice sheets. They are thought to form through the deposition of sediments in sub-glacial or ice-walled pro-glacial channels, and form anastomosing patterns such as that in figure 10.18. On the ground, they look as shown in figure 10.22, although eskers which form under ice sheets are generally larger, having elevations in the range 10–50 m, and widths of 50–500 m. And they

are often shrouded in trees, and only properly visible from the air. In length, they can sometimes be traced for hundreds of kilometres, although often they are segmented. Indeed, eskers are often 'beaded', either consisting of independent beads, or having oscillations in elevation along their length.

Because they consist of sorted sands and gravels, they are associated with channelised water flow, but the detailed way in which they form is not properly known. Generally, they are associated with retreating ice, and are thought to form at the margin of the ice sheet. The sediment might be deposited within the sub-glacial channel. Alternatively, deposits might occur pro-glacially in a stream walled by dead ice; or, if the ice terminates in a pro-glacial lake, a sub-aqueous fan may occur. In all these cases, one imagines the esker being built regressively as the ice retreats; however, little is directly known of the process, and it is not inconceivable that eskers could form wholly below the ice sheet.

Models for the construction of eskers do not yet exist, but a clue to their formulation lies in our earlier discussion of different drainage theories. In our discussion of canals (section 10.3.3), we posited a drainage style in which a sediment-floored canal lay beneath an essentially flat roof. The astute reader will have been concerned as to why the ice roof should be flat, as no grounds were given for this supposition. Suppose the elevation of the ice roof above the local ice/till interface is h_i, and the depth of the stream base below it is h_s. Then the Röthlisberger channel corresponds to the assumption $h_i > 0$, $h_s = 0$, while the canal corresponds to the assumption $h_i = 0$, $h_s > 0$; an intermediate case has both being positive.

What is missing in our model is any reason for either assumption, but we can in principle supply a reason by positing a model in which both h_i and h_s are variables. We do this below, but now we can also realise that there is no reason why we cannot also have the cases $h_i > 0$, $h_s < 0$ and $h_i < 0$, $h_s > 0$; in the former case, sediment is deposited while the channel flow is maintained above it: this presumably corresponds to esker formation. In the latter case, the ice squeezes down while the stream evacuates the sediment; this corresponds to the formation of tunnel valleys.[27] Thus, at least in principle, a single model could predict all these features.

To see the structure of such a model, we generalise the discussion in section 10.3.3 to allow for separate ice roof elevation h_i and sediment floor depth h_s. In its simplest form, the model is written

$$\begin{aligned} \frac{\partial (w h_i)}{\partial t} &= \frac{\dot{m}_i}{\rho_i} - \frac{w^2}{\eta_i}(N + \Delta\rho_{wi} g h_i), \\ \frac{\partial (w h_s)}{\partial t} &= \frac{\dot{m}_s}{\rho_s} - \frac{w^2}{\eta_s}(N + \Delta\rho_{sw} g h_s); \end{aligned} \tag{10.395}$$

these represent the kinematic equations for the ice/water interface and the till/water interface, respectively, and involve a melting rate $\dot{m}_i$, erosion rate $\dot{m}_s$, and ice and

[27] Tunnel valleys are large (hundreds of metres deep, kilometres wide) braided systems of former drainage channels (presumably), often infilled with sediment. They are found in Northern Germany and Denmark, for example.

till viscosities η_i and η_s.[28] The particular closure relations in (10.395) are those for a wide channel, and for geometric simplicity we suppose the wetted perimeter $l = 2w$, where w is the channel width. From (10.238), (10.239), (10.240) and (10.242), we have

$$\dot{m}_i = C_i Q, \tag{10.396}$$

where

$$C_i = \frac{\rho_i g S_i}{2L}. \tag{10.397}$$

The erosion rate of a subglacial stream is a more complex matter. For a stream with banks, we might suppose erosion of the sides by bank collapse is proportional to the stream power. However, if the till squeezes up into the channel, there are no 'banks', and the erosion rate should presumably decrease to zero, unless we imagine a stream of varying cross section, thus with erosion in the shallows, and the principal downstream sediment transport in the deeper flow. For such a case, it is plausible to provide an analogous description for erosion rate,

$$\dot{m}_s = C_s Q, \tag{10.398}$$

where

$$C_s = \frac{\rho_i g S_i}{2L_E}, \tag{10.399}$$

and L_E is a term representing latent work of erosion. Finally, the extra gravitational terms in the closure rates arise through the contribution of the respective bed elevations to the driving hydraulic closure stress.

If we take the Chézy friction law $\tau = f\rho_w u^2$, then $u = \sqrt{Ch}$, where

$$C = \frac{\rho_i g S_i}{2f\rho_w}, \tag{10.400}$$

and the water flux is

$$Q = C^{1/2} w h^{3/2}, \tag{10.401}$$

where h is the total depth,

$$h = h_i + h_s. \tag{10.402}$$

If we suppose that sediment flux Q_s is described by a Meyer-Peter and Müller relation, then we have (cf. (6.14), or (5.5) and (5.6)),

$$Q_s = K' w (h - h_c)^{3/2}, \tag{10.403}$$

where

$$K' = \frac{\rho_i K S_i}{\Delta\rho_{sw}} \left(\frac{\rho_i g S_i}{8\rho_w}\right)^{1/2}, \quad h_c = \frac{2\tau_c^* \Delta\rho_{sw} D_s}{\rho_i S_i}, \tag{10.404}$$

with $\tau_c^* \approx 0.05$, $K = 8$. The units of Q_s are $\mathrm{m}^3\ \mathrm{s}^{-1}$.

[28] More exactly, they are parameters proportional to the viscosities with some suitable geometry-dependent coefficients.

In Röthlisberger channel theory, mass conservation of water determines the water volume flux Q as a function of distance downstream, and we might suppose that the equation of sediment conservation would likewise determine the sediment volume flux Q_s, both of them being increasing functions of distance downstream. This being so, the three equations in (10.395) and (10.402) serve to determine the three quantities N, h_i and h_s, with the channel width w and depth h being determined by (10.401) and (10.403). Unique values of $h > h_c$ and w exist provided

$$\frac{Q_s}{Q} < \frac{K'}{\sqrt{C}}, \tag{10.405}$$

and we suppose this to be true.

Steady solutions for h_i and N are then

$$h_i = \frac{(A_i - A_s)h^3}{\Delta\rho_{si}Q} + \frac{\Delta\rho_{sw}}{\Delta\rho_{si}}h, \tag{10.406}$$

where

$$A_i = \frac{\eta_i C C_i}{\rho_i g}, \quad A_s = \frac{\eta_s C C_s}{\rho_s g}, \tag{10.407}$$

and

$$N = \frac{g\Delta\rho_{wi}\Delta\rho_{sw}}{\Delta\rho_{si}}\left[\frac{h^2}{\beta^2 Q} - 1\right]h, \tag{10.408}$$

where

$$\beta = \left(\frac{\Delta\rho_{wi}\Delta\rho_{sw}}{\Delta\rho_{sw}A_i + \Delta\rho_{wi}A_s}\right)^{1/2}. \tag{10.409}$$

It is useful to write (10.406) in the form

$$h_i = \frac{B(1-\chi)h^3}{Q} + rh, \tag{10.410}$$

where

$$B = \frac{\rho_i g S_i^2 \eta_i}{4f\rho_w\Delta\rho_{si}L}, \quad \chi = \frac{A_s}{A_i} = \frac{\rho_i L\eta_s}{\rho_s L_E \eta_i}, \quad r = \frac{\Delta\rho_{sw}}{\Delta\rho_{si}}. \tag{10.411}$$

In figure 10.23 we plot representative graphs of h_i versus h for values $A_i > A_s$ ($\chi < 1$) and $A_i < A_s$ ($\chi > 1$). The physically accessible space where $h > 0$ is divided into three regions. When $0 < h_i < h$, channels exist, with both the ice and the sediment being excavated. There are two particular cases: $h_i = h$ corresponds to a Röthlisberger channel, while $h_i = 0$ corresponds to a canal. If $h_i > h$, then $h_s < 0$: the sediment infiltrates the channel, causing an esker to form. If $h_i < 0$, the ice collapses, forming a tunnel valley.

As sediment flux and water discharge increase downstream, h (determined by $\left(1 - \frac{h_c}{h}\right)^3 = \frac{CQ_s^2}{K'^2Q^2}$) may increase or decrease; plausibly it remains constant (if Q_s/Q is constant). However, as Q increases, the upper and lower curves become steeper, so that in this simple theory, eskers or tunnel valleys are promoted at larger

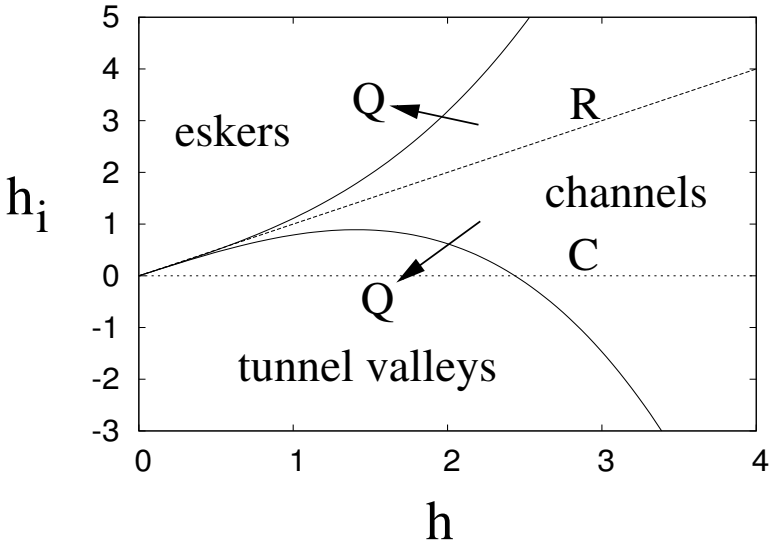

Figure 10.23: Ice roof elevation in metres as a function of channel depth in metres, based on (10.411), using values $B = 0.8$ m s^{-1}, $r = 0.95$, and values of $\chi = \dfrac{A_s}{A_i} = 0.8$ (upper curve) and $\chi = \dfrac{A_s}{A_i} = 1.2$ (lower curve). Channels exist for small volume and sediment fluxes, but eskers or tunnel valleys develop at larger fluxes, depending on the stiffness of the till. The lines $h_i = h$ (marked R) and $h_i = 0$ (marked C) indicate Röthlisberger channels and canals, respectively.

water fluxes, and which of them occurs depends sensitively on the stiffness of the till via the definition of χ. Stiff till (high χ) promotes tunnel valley formation, while soft till (high χ) promotes esker formation. Note that, from (10.408), N increases with h, and is only positive for $h > \beta\sqrt{Q}$. We associate the lower limit with the onset of channelised flow, supposing that for lower h, a distributed film flow exists, much as discussed earlier.

The present discussion promotes a pedagogical point, which is that it may be possible to provide an understanding of eskers and tunnel valleys, as well as Röthlisberger channels or canal, all on the basis of a self-consistent description of drainage mechanics. However, our rudimentary discussion falls a fair way short of genuine prediction. Most obviously, the ice viscosity depends on N, as does the till rheology (strongly, if it is essentially plastic), and so the critical parameter χ will depend on N and thus also h. In addition, variation with space and time is likely to be important. Furthermore, it is not immediately obvious whether the drainage characteristics of the different types of channel or canal are consistent with our earlier discussion of them.

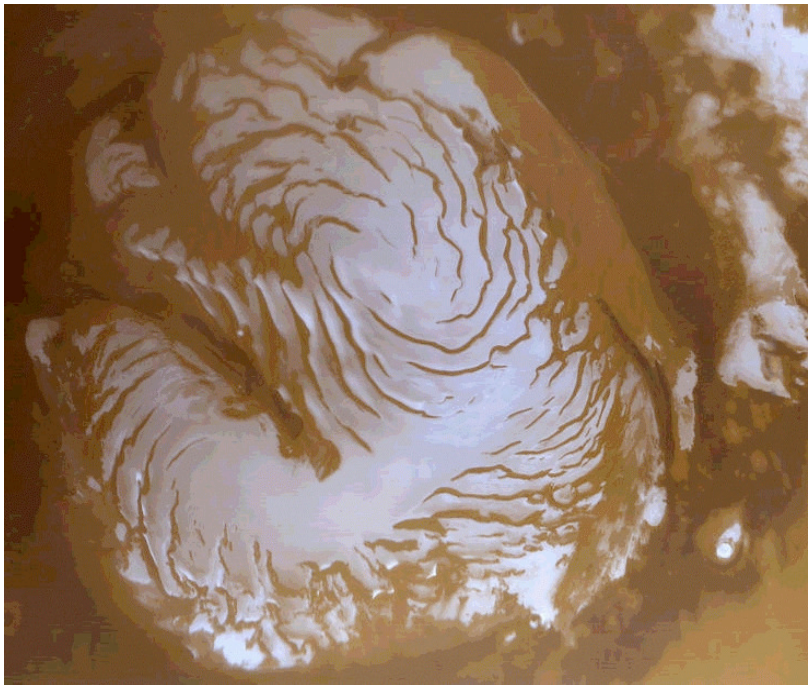

Figure 10.24: Mars orbital camera (MOC) image of the North Polar Ice Cap of Mars.

10.6 Glaciology on Mars

We are used to the existence of glaciers and ice sheets on Earth, but ice also exists elsewhere in the solar system, and is the source of interesting and elusive phenomena. As an example, we consider the polar ice caps of Mars. These apparently consist largely of water ice, and that at the north pole is the larger, being comparable in size to the Greenland ice sheet. Both ice caps are covered in their respective winters by an annual layer of CO_2 frost, which sublimates in the summer, leaving the residual ice caps.

We will focus our attention on the northern ice cap, shown in figure 10.24, which is some 3 kilometres in depth, and 1000 km in horizontal extent. As can be seen in the picture, this ice cap is quite unlike the large ice sheets on Earth. The surface is irregular. In particular, there is a large canyon which looks as if it has been gouged from the ice surface, towards the left of the picture. This is the *Chasma Borealis*. The other pronounced feature of the ice cap consists of the stripes on the surface. These stripes are arranged in a spiral, rotating anti-clockwise, and they consist of concentrations of dust, associated with a series of troughs in the ice. Figure 10.25 shows the troughs, carved into a cross section of the ice cap.

The spiral waves suggest a formation mechanism similar to that of the Fitzhugh-Nagumo equations, which form a reaction-diffusion system of activator-inhibitor type. When the kinetics of the reaction terms are oscillatorily unstable, the addition of diffusion causes the oscillations to propagate as travelling waves. The presence of 'impurities' can cause these waves to propagate as spiral waves (cf. question 1.20).

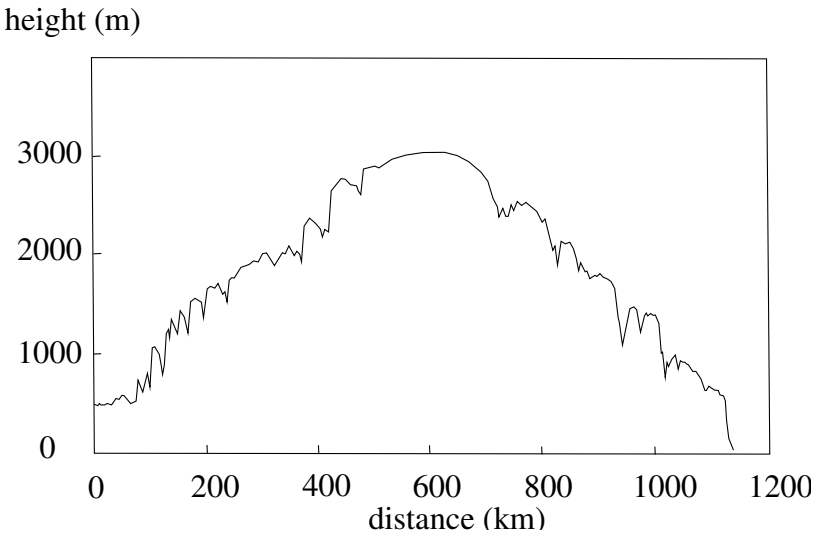

Figure 10.25: A cross section of the North Polar Ice Cap, showing the scarps and canyons. Redrawn from Ivanov and Muhleman (2000). The height is relative to a plane 5 km below the mean geoid. The North Pole is near the summit.

We thus set out seeking a model whose time-dependent behaviour is oscillatory. This can most easily be obtained by identifying a positive feedback in the system. The mechanism we will use is that of dust-albedo feedback. Dust on the surface causes a reduced albedo, and thus a greater absorption of solar radiation. In turn this leads to greater sublimation of the ice, and thus increasing residual dust concentration.

Fundamental quantities in the model are thus the albedo a, the dust fraction of ice at the surface, ϕ, and the mass rate of sublimation m_i. The rate of sublimation (or condensation) is given by

$$m_i = K(p_s - p), \tag{10.412}$$

where the rate coefficient K depends on wind speed and temperature, p is atmospheric water vapour pressure, and p_s is the saturation vapour pressures, given in terms of absolute temperature T by

$$p_s = p_s^{\mathrm{ref}} \exp\left[B\left\{1 - \frac{T_{\mathrm{ref}}}{T}\right\}\right], \tag{10.413}$$

where $p_s = p_s^{\mathrm{ref}}$ at $T = T_{\mathrm{ref}}$; for water vapour, we may take $T_{\mathrm{ref}} = 273$ K at $p_s^{\mathrm{ref}} = 6$ mbar (= 600 Pa), the *triple point*, and the parameter B is given by

$$B = \frac{M_w L}{R T_{\mathrm{ref}}}, \tag{10.414}$$

where M_w is the molecular weight of water, and R is the gas constant.

Albedo and sublimation rate are related by the radiative energy balance law

$$I(1-a) = \frac{\sigma T^4}{\Gamma} + m_i L, \tag{10.415}$$

where I is received solar insolation, Γ is a greenhouse factor which may depend on atmospheric dust and water vapour concentrations, and L is latent heat; the albedo will depend on the amount of dust in the ice.

Let us denote the ice surface accumulation rate of dust as m_s, with units of mass per unit area per unit time. Then the rate of decrease of ice surface elevation due both to sublimation/condensation and dust accrual is

$$s = \frac{m_i}{\rho_i} - \frac{m_s}{\rho_s}. \tag{10.416}$$

The basic equation describing the ice cap elevation h is then the dimensional equivalent of (10.45), which can be written in the form

$$\frac{\partial h}{\partial t} = -s + \frac{\partial}{\partial x}\left(D_i \frac{\partial h}{\partial x}\right), \tag{10.417}$$

where the effective diffusion coefficient is given by

$$D_i = \frac{2A(\rho g)^n}{n+2}|h_x|^{n-1}h^{n+2}, \tag{10.418}$$

A being the Glen flow rate coefficient for ice, assumed constant. In our discussion we will assume that D_i is constant: a simple estimate of its appropriate size is $D_i \sim u_i l_i$, where u_i is a typical ice velocity, and l_i is the ice cap radius.[29]

We introduce the atmospheric water vapour concentration ρ and the atmospheric dust concentration c (both measured as mass per unit volume), noting that we may expect the greenhouse factor $\Gamma = \Gamma(\rho, c)$. The water vapour pressure is then given by the perfect gas law

$$p = \frac{\rho R T}{M_w}, \tag{10.419}$$

where R is the gas constant and M_w is the molecular weight of water. The subsidiary variables m_i, p_s, T and p are defined by (10.412), (10.413), (10.415) and (10.419). A further two relations are then necessary to determine ρ and c. These arise from the concepts of sediment transport as expounded in chapter 5.

First, we propose two equations which describe conservation of mass of dust and water vapour in the near surface boundary layer. We will assume that a polar katabatic wind will flow downslope, transporting water vapour and dust in a thin near surface current. This current will entrain dust and water vapour from the troposphere above. If the current is of depth H, then suitable conservation laws for the vertically averaged vapour and dust concentrations ρ and c in the katabatic layer are

$$\begin{aligned} \frac{\partial (Hc)}{\partial t} + \frac{\partial (qc)}{\partial x} &= E_c + \rho_s v_E - v_s c + \frac{\partial}{\partial x}\left(D_c H \frac{\partial c}{\partial x}\right), \\ \frac{\partial (H\rho)}{\partial t} + \frac{\partial (q\rho)}{\partial x} &= E_\rho + m_i + \frac{\partial}{\partial x}\left(D_\rho H \frac{\partial \rho}{\partial x}\right), \end{aligned} \tag{10.420}$$

[29] A consequence of the assumption of constant D_i will be that a finite gradient of h at the margin will imply non-zero ice flux there. This is unrealistic, and in particular, the existence of a steady state ice cap requires that the net balance be zero, i. e., $\int_0^{l_i} s\,dx = 0$.

where q is the katabatic wind flux, E_c and E_ρ are the entrainment rates of dust and vapour from the overlying troposphere, and D_c and D_ρ are turbulent horizontal diffusivities in the katabatic layer. Just as in chapter 5, the term $\rho_s v_E$ represents erosion of dust from the surface, and the term $v_s c$ represents deposition of dust at the surface via settling; v_s is the settling velocity, and v_E is an erosional velocity.

The velocities v_s and v_E need to be specified, as do the amounts of frozen and unfrozen dust at the surface, and the ice dust accrual rate m_s. A reasonably general assumption about the surface is that there may be a thin surface layer of unfrozen dust which mantles the ice. If the 'depth' of this layer is F,[30] then conservation of unfrozen dust takes the form

$$\rho_s \frac{\partial F}{\partial t} = -\rho_s v_E + v_s c - m_s. \tag{10.421}$$

This layer is quite analogous to the bedload layer described in section 6.3 (and F is analogous to $(1-\phi)a$ in (6.7)).

In addition, we suppose that the ice at the surface (below the unfrozen layer) contains a volume fraction ϕ of dust. If $F \neq 0$, we can expect in general that the albedo is given by $a = a(\phi, F)$. It then remains to constitute ϕ and m_s. Quite generally, we find that for both sublimation and condensation

$$m_s = -\rho_s \phi s, \tag{10.422}$$

and thus from (10.416)

$$m_i = \rho_i (1-\phi) s. \tag{10.423}$$

If $s > 0$,

$$\begin{aligned} \phi &= \phi(x, \tau), \\ \int_\tau^t s(t')\, dt' &= 0 \quad \text{for} \quad s > 0. \end{aligned} \tag{10.424}$$

This simply states that if sublimation is occurring, the surface ice dust fraction is equal to its value at the last time the surface was exposed. Actually, (10.424) is an oversimplification, as it ignores the horizontal transport of the buried previous ice surface by ice flow. If $s < 0$, we suppose

$$\phi = \phi_s, \quad s < 0, \tag{10.425}$$

where ϕ_s is the dust volume fraction of the unfrozen dust layer. This assumes that $F > 0$.

If $F \equiv 0$ over a time interval, then m_s is still defined by (10.422), (10.421) is irrelevant, and the ice surface dust fraction is determined by a balance between volume of ice accretion and volume of dust deposited, thus

$$\phi = \frac{c v_s - \rho_s v_E}{c v_s - \rho_s v_E - r_{si} m_i}, \quad F \equiv 0, \tag{10.426}$$

[30] More precisely, F is the volume of unfrozen dust per unit surface area.

so long as ϕ is positive, where

$$r_{si} = \frac{\rho_s}{\rho_i}. \tag{10.427}$$

The discussion above assumes implicitly that condensation of ice occurs directly at the surface. A different possibility is that condensation occurs as snowfall. If the snow crystals are pure, then there is no difference in the model. However, we might also suppose that ice crystals nucleate on dust particles, so that dust accumulation in the ice is partly due to this. If in fact there is no deposition of unfrozen dust (thus $F = 0$), then when $s < 0$ (it is snowing), the surface ice dust fraction will be that of the snow particles. A simple partitioning by volume fraction of dust within snow then suggests

$$\phi = \frac{c}{c + r_{si}\rho}, \quad s < 0 \quad \text{(snowfall)}. \tag{10.428}$$

10.6.1 Non-dimensionalisation

We now proceed to make this model non-dimensional. We mostly denote appropriate scales with a subscript zero, and in particular we scale the variables as

$$\begin{gathered} m \sim m_0, \quad p, p_s \sim p_0, \quad T \sim T_0, \quad I \sim I_0, \\ s \sim s_0, \quad h \sim h_0, \quad t \sim t_0, \quad x \sim l_i, \quad \rho \sim \rho_0, \\ c \sim c_0, \quad q \sim q_0, \quad F \sim F_0, \end{gathered} \tag{10.429}$$

and we write

$$\frac{1-a}{1-a_0} = \alpha. \quad K = \frac{K'\kappa}{T}, \tag{10.430}$$

and suppose K' is constant, such that $\kappa = 1$ when there is no surface dust layer, $F = 0$: in general, we may expect κ to be a rapidly decreasing function of F; a_0 is the albedo of clean Martian ice. Balances of terms in the equations are effected by writing

$$\begin{gathered} T_0 = \left(\frac{I_0(1-a_0)}{\sigma}\right)^{1/4}, \quad p_0 = p_s^{\text{ref}} \exp\left[B\left\{1 - \frac{T_{\text{ref}}}{T_0}\right\}\right], \\ m_0 = \frac{K'p_0}{T_0}, \quad s_0 = \frac{m_0}{\rho_i}, \quad t_0 = \frac{l_i^2}{D_i}, \\ h_0 = s_0 t_0, \quad \rho_0 = \frac{M_w p_0}{RT_0}; \end{gathered} \tag{10.431}$$

in addition, the choice of q_0 is found from a prescription for the katabatic wind (see below), while F_0 is the depth of an unfrozen dust layer over which κ decreases significantly. Of the twelve scales in (10.429), (10.431) provides definition of seven; in addition, q_0 and F_0 are determined as described above, while we suppose also that I_0 is known from the received solar radiation. This leaves us two scales (l_i and c_0) to be determined, and this will be done by prescription of two of the dimensionless parameters which emerge in the model. We also write

$$v_E = v_0 V_E, \tag{10.432}$$

and suppose v_0 is known.

The dimensionless version of the model can then be written in the form

$$\begin{aligned} h_t &= -s + h_{xx}, \\ \mu c_t + (qc)_x &= R_c + \nu(\lambda V_E - c) + D c_{xx}, \\ \mu \rho_t + (q\rho)_x &= R_\rho + \gamma(1-\phi)s + D\rho_{xx}, \\ \delta F_t &= \sigma(c - \lambda V_E) + \phi s, \end{aligned} \tag{10.433}$$

where

$$\begin{aligned} s &= \frac{\kappa}{1-\phi}\left[\frac{1}{T}\exp\left\{\beta\left(1-\frac{1}{T}\right)\right\} - \rho\right], \\ T &= \Gamma\left[I\alpha - \varepsilon(1-\phi)s\right], \end{aligned} \tag{10.434}$$

and the parameters are defined by

$$\begin{gathered} \mu = \frac{H l_i}{q_0 t_0}, \quad D = \frac{D_c H}{q_0 l_i} = \frac{D_\rho H}{q_0 l_i}, \\ \delta = \frac{F_0}{h_0}, \quad R_c = \frac{l_i E_c}{q_0 c_0}, \quad R_\rho = \frac{l_i E_\rho}{q_0 \rho_0}, \\ \beta = \frac{M_w L}{R T_0}, \quad \varepsilon = \frac{K' p_0 L}{\sigma T_0^5}, \quad \lambda = \frac{\rho_s v_0}{v_s c_0}, \\ \sigma = \frac{v_s c_0}{\rho_s s_0}, \quad \nu = \frac{v_s l_i}{q_0}, \quad \gamma = \frac{\rho_i s_0 l_i}{q_0 \rho_0}. \end{gathered} \tag{10.435}$$

The issue now arises, how to choose the scales l_i and c_0. To do this, we need some understanding of how the model works, and for that, we need some idea of the size of the parameters.

We take values $I_0 = 130$ W m^{-2}, $a_0 = 0.3$, so that, with $\sigma = 5.67 \times 10^{-8}$ W m^{-2} K^{-4}, we find $T_0 = 200$ K. We use values $M_w = 18 \times 10^{-3}$ kg mole^{-1}, $L = 2.8 \times 10^6$ J kg^{-1}, $R = 8.3$ J mole^{-1} K^{-1}, $T_{\rm ref} = 273$ K, $p_s^{\rm ref} = 600$ Pa, from which we find $p_s^0 \approx 0.18$ Pa, and thus $\rho_0 = 2 \times 10^{-5}$ kg m^{-3}. We take $K' = 2.2 \times 10^{-5}$ m^{-1} s K, whence we find $m_0 \approx 2 \times 10^{-8}$ kg m^{-2} s^{-1}, and with $\rho_i \sim 0.9 \times 10^3$ kg m^{-3}, $s_0 \approx 2.2 \times 10^{-11}$ m s^{-1}.

We suppose that a katabatic wind of magnitude $u_w = 10$ m s^{-1} exists in a layer of depth $H = 100$ m, so that we take $q_0 = 10^3$ m^2 s^{-1}. To estimate D_i, we use (10.418) with $n = 3$ to motivate the choice $D_i \approx \bar{D} h_0^7$, where $\bar{D} = 0.4A(\rho_i g)^3/l_i^2$, and we use the observed value $l_i = 500$ km, and $A = 3 \times 10^{-27}$ Pa^{-3} s^{-1}, based on a basal ice temperature of 220 K, itself based on a surface ice temperature of 200 K and an areothermal heat flux of 20 mW m^{-2}. Using the definitions of the depth scale, time scale and diffusion coefficient, this leads to

$$h_0 = \left(\frac{s_0 l_i^2}{\bar{D}}\right)^{1/8} \approx 3{,}600 \text{ m}, \tag{10.436}$$

and then $t_0 \approx 1.6 \times 10^{14}$ s ≈ 5 Ma and $D_i = 1.6 \times 10^{-3}$ m^2 s^{-1} (corresponding to an ice velocity of some 0.1 m y^{-1}). We suppose that the depth scale over which a surface dust layer occludes the ice reflectivity is $F_0 = 1$ cm, and we take the turbulent diffusivity of the katabatic layer to be $D_c = D_\rho = 0.1 u_w H = 0.1 q_0$.

With all these values, we find

$$\mu \approx 0.3 \times 10^{-9}, \quad D \approx 2 \times 10^{-5}, \quad \delta \approx 0.3 \times 10^{-5},$$
$$\beta \approx 30.4, \quad \varepsilon \approx 0.6 \times 10^{-3}, \quad \gamma \approx 0.5. \tag{10.437}$$

The values of σ, λ and ν depend on what we assume about erosion and settlement of dust. We suppose that suspended dust grains have a diameter of the order of 1–2 microns. Then the Stokes settling velocity (5.8) is

$$v_s = \frac{\Delta\rho g D_s^2}{18\eta} \approx 10^{-4} \text{ m s}^{-1}, \tag{10.438}$$

assuming $\Delta\rho = 2 \times 10^3$ kg m^{-3}, $g = 3.7$ m s^{-2}, and the atmospheric viscosity is $\eta = 10^{-5}$ Pa s; we also suppose (see (5.7) and the line after (5.9)) that $v_0 \approx 10^{-2} v_s$. If we define $A = \dfrac{c_0}{\rho_s}$, then we have

$$\sigma \approx 0.5 \times 10^7 A, \quad \nu \approx 0.05, \quad \lambda \approx \frac{10^{-2}}{A}. \tag{10.439}$$

The sizes (and signs) of the entrainment parameters R_c and R_ρ depend on what we assume about the entrainment rates E_c and E_ρ. There is little to guide us in this, except for the expectation that the numerators of R_c and R_ρ represent the total entrained dust and vapour, while the denominators represent the magnitude of the downslope fluxes; we thus expect numerators and denominators to be comparable, and this suggests that in practice $R_c, R_\rho \lesssim O(1)$.

The issue of how we choose the precise values of l_i and c_0 now arises. The fact that numerically the parameter $\gamma = O(1)$ is strongly suggestive of the idea that we choose l_i by *requiring* that $\gamma = O(1)$, and without loss of generality we may define $\gamma = 1$. The choice of c_0 depends on how we imagine the dust behaves at the ice surface. One possibility is that the dust-albedo feedback is engineered through occasional atmospheric dust storms, which affects the temperature through the dependence of Γ and α on c. In this view, $F \equiv 0$; the settlement velocity is so small that no accretion can occur, and dust is incorporated in the surface via snowfall, wherein ice accretes on dust nuclei. We then choose c_0 by requiring that

$$\nu = \sigma, \tag{10.440}$$

which is equivalent (with $\gamma = 1$) to choosing

$$c_0 = r_{si} \rho_0, \tag{10.441}$$

where r_{si} is given by (10.427). It then follows from (10.428) that, dimensionlessly,

$$\phi = \frac{c}{c + \rho}, \quad s < 0, \tag{10.442}$$

and in fact we will assume that (10.442) applies also for $s > 0$.

The equations for c and ρ now take the form

$$\begin{aligned} \mu c_t + (qc)_x &= R_c + \phi s + D c_{xx}, \\ \mu \rho_t + (q\rho)_x &= R_\rho + (1-\phi)s + D\rho_{xx}, \end{aligned} \tag{10.443}$$

and can be combined if we suppose that μ, R_c, R_ρ and D are all small, and that q is constant. With the definition of ϕ in (10.442), we then have

$$\frac{dc}{d\rho} = \frac{\phi}{1-\phi} = \frac{c}{\rho}, \tag{10.444}$$

whence $c \propto \rho$, and thus ϕ is constant. With this assumption, we can eliminate ρ from the definition of s, and the equation for c takes the form

$$\mu c_t + (qc)_x = R_c + \phi s(T, c) + D c_{xx}, \tag{10.445}$$

where s can be expressed as

$$s = \frac{1}{(1-\phi)T} \exp\left\{\beta\left(1 - \frac{1}{T}\right)\right\} - \frac{c}{\phi}. \tag{10.446}$$

Because ε is small, we can take

$$T \approx I\Gamma\alpha. \tag{10.447}$$

The dimensionless incident radiation depends weakly on slope, and can be taken to be

$$I = I_0(c)(1 - mh_x), \tag{10.448}$$

where $m \approx 0.02$. The incident radiation may also depend on dustiness through the cooling effect associated with increased reflectivity in a dusty atmosphere, hence the decreasing function $I_0(c)$. In general, the scaled co-albedo α will be an increasing function of both ϕ and F; here we take it to be constant, $\alpha = 1$. The feedback in this version of the model thus operates through the dependence of the greenhouse factor Γ on c: Γ is an increasing function of c. Because β in (10.446) is large, s is very sensitive to c.

The 'derivation' of (10.445) is suggestive rather than rigorous, but will serve as the basis of a model for trough formation. Whether the conclusions we draw will extend to the full system, and indeed, whether the concept of dust suspension and snowfall is correct at all: these are questions which await further study.

10.6.2 Multiple steady states.

The reduced model which we now consider is that for h and c described by $(10.433)_1$ and (10.445), with s and T defined by (10.446), (10.447) and (10.448). It is clear from the definition of s in (10.446) that if T increases with c, then s can be non-monotonic. In general, s may have three zeroes as a function of c, and if we allow for the cooling

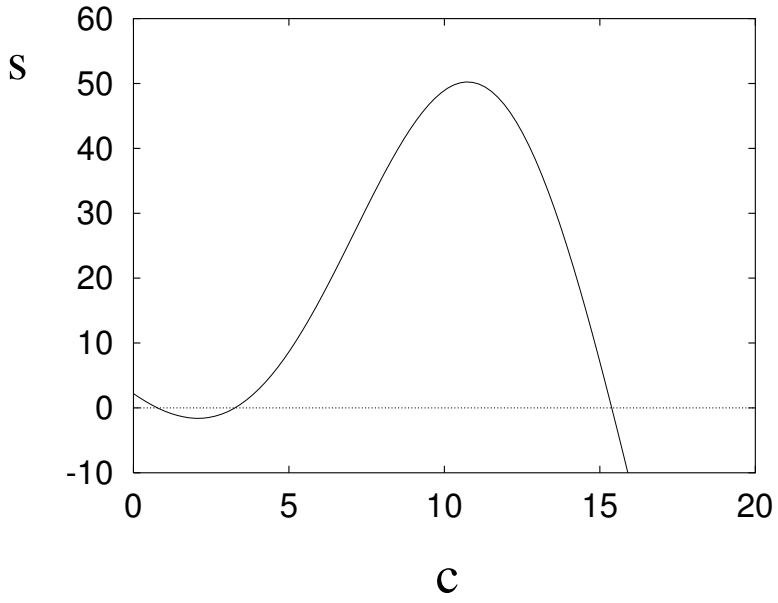

Figure 10.26: The sublimation function s defined by (10.446), where we take $T = (1-\sigma c)(1-mh_x)(1+gc)$, and use values $m = 0.02$, $-h_x = 1$, $g = 0.05$, $\beta = 30$, $\sigma = 0.023$, $\phi = 0.2$.

effect of a dusty atmosphere at high dust concentrations, the highest zero can be quite modest, as indicated in figure 10.26.

The non-monotonicity of s allows the possibility of multiple steady states. The simplest way to see this is to consider (10.445) with q constant, and to ignore the very small terms in μ and D (we will reconsider their importance subsequently). With q constant, a summit condition for c must be prescribed at $x = 0$. If $s(c)$ has three zeroes as shown in figure 10.26, denoted c_1, c_2 and c_3, then for sufficiently small R_c, c will tend towards either the largest or smallest zero of $R_c + \phi s$. For both values, the value of $s = -R_c/\phi$ is the same and the steady profile for h is a parabola,

$$h = \frac{R_c}{2\phi}(1 - x^2), \tag{10.449}$$

assuming boundary conditions

$$h_x = 0 \quad \text{at} \quad x = 0, \quad h = 0 \quad \text{at} \quad x = 1. \tag{10.450}$$

The multiplicity above depends on the choice of summit dust concentration, and this is somewhat artificial, as there is no physical reason to prescribe c at the summit. In reality, the downslope katabatic wind must be zero at the summit, so that in general q will depend on the slope $-h_x$. The simplest assumption is to take

$$q = -h_x, \tag{10.451}$$

and in this case, the equation for c is degenerate. Satisfaction of (10.445) (with $\mu = D = 0$) at $x = 0$ requires c to satisfy

$$(\phi + c)s(c) = -R_c. \tag{10.452}$$

Again, there can be three different values, and each of these leads to a genuinely different solution for h and c. In particular, if we denote a zero of (10.452) as c^*, then the steady state solution for h corresponding to $c = c^*$ is

$$h = \frac{R_c}{2(\phi + c^*)}(1 - x^2); \tag{10.453}$$

in particular, when c^* is large, the ice cap is essentially removed.

The discussion above assumes s independent of slope, i. e., $m = 0$. Non-zero values of m modify the discussion, but only quantitatively.

10.6.3 Trough formation

The presence of multiple steady states suggests the possibility of hysteretic transitions between the lowest and highest values of c. We expect the middle steady state to be unstable. Although the steady state solutions depend on x, and in particular, $c = c(x)$ if $m \neq 0$, we will continue to refer to the steady states in terms of the (possibly three) solutions of (10.452) as c_i^*, $i = 1, 2, 3$, bearing in mind that the space-dependent solutions for c are simply the continuation to $m \neq 0$ of the constant solutions.

Suppose now that incident radiation I increases so that c_1^* and c_2^* coalesce and disappear; essentially the graph of s in figure 10.26 is pulled upwards. A pre-existing ice cap with $c = c_1^*$ will undergo a transition to $c = c_3^*$: the ice cap will disappear. How does this happen? The slope dependence of T and thus s means that coalescence of the roots occurs first, locally, where the slope $-h_x$ is greatest, at the margin of the ice cap. As I increases further, the point on the ice cap where coalescence occurs moves progressively back towards the summit.

In order to describe the transition, we consider the system

$$\begin{aligned} h_t &= -s + h_{xx}, \\ \mu c_t - (h_x c)_x &= R_c + \phi s + D c_{xx}, \end{aligned} \tag{10.454}$$

and to mimic the dependence of s on c and $-h_x$, we choose

$$s = f(c) + \Delta I - m h_x, \tag{10.455}$$

with

$$f(c) = A(c - c_1)(c - c_2)\left(1 - \frac{c}{c_3}\right), \tag{10.456}$$

where we expect $c_1,\ c_2 \sim O(1)$, $c_3 \gg 1$, $A \gtrsim 1$. We define

$$c = c_3 C, \quad f = A c_3^2 g, \quad s = A c_3^2 S, \quad t = \frac{\mu}{A c_3}\tau,$$

$$x = x_B(\tau) + \sqrt{\frac{D}{Ac_3}}\xi, \quad h = h_0(x) + \lambda H, \tag{10.457}$$

where

$$\lambda = \mu\sqrt{AD}c_3^{3/2}, \tag{10.458}$$

so that

$$g = \left(C - \frac{c_1}{c_3}\right)\left(C - \frac{c_2}{c_3}\right)(1-C) \approx C^2(1-C), \tag{10.459}$$

$$S = g(C) + \frac{\Delta I}{Ac_3^2} - \frac{mh_0'}{Ac_3^2} - \mu m H_\xi, \tag{10.460}$$

and if we define

$$\dot{x}_B = -\frac{h_0'}{Ac_3}, \tag{10.461}$$

then H and C satisfy

$$\begin{aligned} \sqrt{c_3 DA}H_\tau + h_0' H_\xi &= -S + \frac{h_0''}{Ac_3^2} + \mu\sqrt{\frac{Ac_3}{D}}H_{\xi\xi}, \\ C_\tau &= \phi S + \frac{R_c}{Ac_3^2} + \frac{h_0'' C}{Ac_3} + C_{\xi\xi} + \Lambda\left(H_\xi C\right)_\xi, \end{aligned} \tag{10.462}$$

where

$$\Lambda = \frac{\lambda}{D} = \frac{\mu c_3^{3/2}\sqrt{A}}{\sqrt{D}}. \tag{10.463}$$

Suppose firstly that $\Lambda \ll 1$. In that case, C satisfies

$$C_\tau \approx \phi g(C) + C_{\xi\xi}. \tag{10.464}$$

For small C, $g \approx C^2$, and and an initial blow-up begins to occur, in which C tends to infinity at finite time at one position. However, when $C \sim O(1)$, $g \approx C^2(1-C)$, and C saturates at $C = 1$ and a pair of travelling waves propagate outwards from the initial blow-up position.

The consequent perturbation to the depth is computed from $(10.462)_1$. If we assume $\sqrt{c_3 DA} \ll 1$, $\mu\sqrt{\frac{c_3 A}{D}} \ll 1$, then H is approximately given by

$$H \approx \frac{1}{h_0'}\int_\xi^\infty S\, d\xi, \tag{10.465}$$

and this describes the front of the trough.[31] As $\xi \to -\infty$, the depth of the trough is

$$\Delta H = \frac{1}{|h_0'|}\int_{-\infty}^\infty S\, d\xi. \tag{10.466}$$

[31] We have applied the boundary condition that $H \to 0$ as $\xi \to \infty$, rather than $H \to 0$ as $\xi \to -\infty$; why?

This is not a uniformly valid description of H, because we require $H \to 0$ as $\xi \to -\infty$. Behind the blow-up region for C, the diffusion term and time derivative of H become significant. Essentially, the trough drawdown diffuses backwards. We can recover this region by defining

$$\xi = \mu\sqrt{\frac{c_3 A}{D}}X, \quad \tau = \mu c_3 A T, \tag{10.467}$$

and then

$$H_T - |h_0'|H_X = H_{XX} + \frac{\mu\sqrt{c_3 A}}{\sqrt{D}}\left(-S + \frac{h_0''}{A c_3^2}\right), \tag{10.468}$$

with $H = 0$ on $T = 0,\ X < 0$ and as $X \to -\infty$, and $H = -\Delta H$ at $X = 0$. At large times, the solution of this is essentially

$$H \approx -\tfrac{1}{2}\Delta H \operatorname{erfc}\left(-\frac{X + |h_0'|T}{2\sqrt{T}}\right), \tag{10.469}$$

and one can show that this diffusive wave travels backwards relative to x_B at the same rate that x_B travels forwards.

The consequence of all this is that local blow-up of c causes a trough to form and deepen as the region of saturated dust spreads. The trough thus formed will have an essentially stationary rear face of length $O(\mu)$, and a shallower front face of length $O\left(\mu\sqrt{\frac{c_3}{D}}\right)$ (and these slopes become less severe with time).

If we take $\mu = 10^{-10}$, $D = 10^{-6}$, $c_3 = 10^4$, $A = 1$, then $\Lambda = 0.1$; uncertainty in parameter values means that in practice values of $\Lambda = O(1)$ are plausible. In this case, we cannot neglect the extra term in $(10.462)_2$. However, note that the diffusive coefficient $\mu\sqrt{\frac{Ac_3}{D}} = \frac{\Lambda}{c_3}$ in $(10.462)_1$ remains small. If in addition $\sqrt{c_3 DA} \ll 1$, then it is still the case that $h_0' H_\xi \approx -g(C)$, so that the blow-up equation (10.464) is simply modified to

$$C_\tau - \frac{\Lambda}{|h_0'|}\{Cg(C)\}_\xi \approx \phi g(C) + C_{\xi\xi}, \tag{10.470}$$

and the same blow-up and formation of travelling waves occurs, modifed only by the advective drift upstream.

If in addition $\sqrt{c_3 DA} \sim O(1)$, then the time derivative term in $(10.462)_1$ comes into play. By inspection, it seems that blow-up will still occur, and that there will be travelling wave solutions also in this case (see question 10.19).

10.6.4 Multiple troughs

Our discussion shows that troughs can form through local blow-up of the dust concentration profile. In order to describe the Martian polar caps, we need this blow-up to occur at many different places along the surface. The simplest way in which this can occur is that as the insolation increment ΔI increases to the point where the

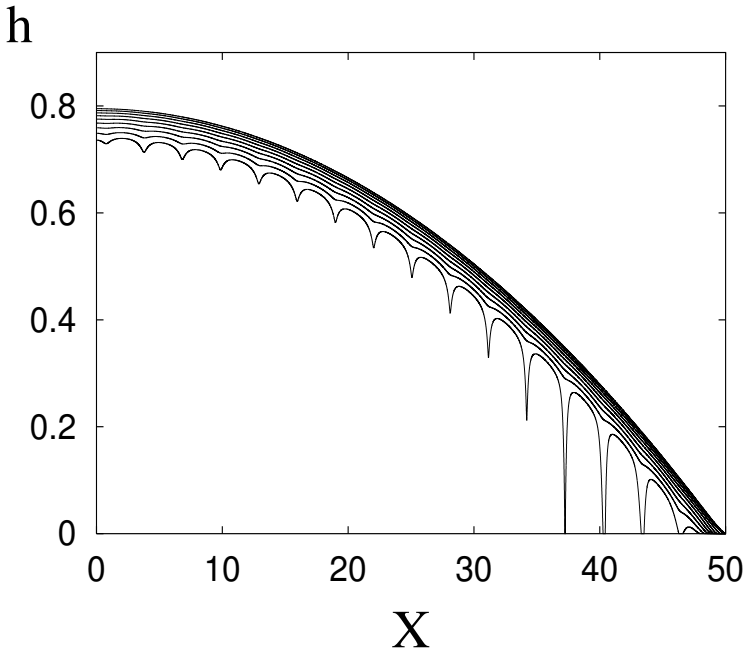

Figure 10.27: A simulation of the equations (10.454), (10.455) and (10.456). The space variable has been rescaled as $x = X/L$ (largely for historical reasons, so that the trough spacing in X will be $O(1)$), and the equations are then solved in the same form, but using rescaled variables $T = L^2 t$, $S = s/L^2$, and with modified parameters $\bar{R} = R_c/L^2$, $\bar{I} = \Delta I/L^2$, $\bar{A} = A/L^2$, $\bar{m} = m/L$. The parameter values used to obtain the sequence of profiles of h above (plotted at time intervals in T of 0.2 up to a maximum of 2.6) are then $L = 50$, $\bar{m} = 0.14$, $\bar{R} = 0.001$, $\mu = 0.1$, $D = 0.002$, $\bar{I} = 0.24 + 0.02T$, $c_3 = 90$, $\bar{A} = 1$, $\phi = 0.2$, time step $\Delta T = 0.005$ and space step $\Delta X = 0.002$. The initial profile for h is $h_0 = 0.8\left(1 - \dfrac{X^2}{L^2}\right)$, and the initial concentration profile for c is $c_0 = 1.5 - 0.005X + 0.02\sin\left(\dfrac{2\pi X}{3}\right)$.

steady states c_1 and c_2 coalesce, the resulting instability occurs at a non-zero wave number.

A straightforward local instability analysis of (10.454) and (10.455) suggests that normal modes proportional to $\exp(ikx + \sigma t)$ have slow solutions (corresponding to diffusive ice surface relaxation) $\mathrm{Re}\,\sigma \sim -k^2$, and rapid growth solutions $\mathrm{Re}\,\sigma \sim \dfrac{\phi f'}{\mu}$, assuming μ and D are small. A next approximation is then (if the steady dust concentratrion is c_0)

$$\mathrm{Re}\,\sigma \approx \phi f' + \left(\frac{\mu c_0}{\phi} - D\right) k^2 + \ldots, \tag{10.471}$$

so that we can expect growth of troughs if D is sufficiently small.[32]

[32]But not if $\mu < D$, as we have suggested.

Figure 10.27 shows a simulation in which troughs grow from an initial state in which a small superimposed sinusoidal variation of dust concentration is applied. This figure is suggestive of the idea that the model has the ability to reproduce features which resemble the Martian troughs, but it is by no means clear that the simple theory suggested here is correct. Further discussion follows in the notes. In the model, trough formation occurs as the initial stages of collapse of the polar ice cap. Numerical outputs vary widely with parameter choices. In particular, it is common to find initial blow-up near the margin, leading to a large trough reminiscent of the *Chasma Borealis*.

10.7 Notes and references

The best source for general information about glaciers and ice sheets is the book by Paterson (1994). This famous book was first published in 1968, upgraded to a second edition in 1981 (but in typescript), then to an apparently terminal third edition (and in LaTeX) in 1994, and now miraculously to a fourth edition (Cuffey and Paterson 2010). Other books with a similar aim are those by Hooke (2005) and Van der Veen (1999). Books which are more concerned with observations in the field and geomorphic processes include those by Benn and Evans (1998) and Bennett and Glasser (2010), while the books by Lliboutry (1987) and Hutter (1983) are much more abstract. Lliboutry's (1964, 1965) earlier voluminous work gives useful descriptions of early work in the subject, particularly in the nineteenth century, but was unfortunately never translated from the French. There is a good deal of historical and geographical material, but the theoretical parts are inevitably dated.

From its origins as a hobby for geographers and climbers, glaciology has come to occupy centre stage in the modern preoccupation with climate, and there are many popular books detailing some of the more recent discoveries. Amongst these are the books by Imbrie and Imbrie (1979), Alley (2002) and Walker (2003): the first two by scientists, the third by a journalist, all of them entertaining.

Scaling

Apart from some of the work at the end of the nineteenth century, detailed by Lliboutry (1965), the application of theoretical mechanics to problems in glaciology really begins after the second world war with the work of Nye, Weertman and Lliboutry. Egged on by the vituperative Lliboutry, the decades after the war saw enormous advances in the theoretical understanding of glacier flow. Applied mathematical principles come late to the scene, so that even something as simple as non-dimensionalisation does not happen till the mid-seventies. Possibly the first paper to do this in a formal way was that by Grigoryan *et al.* (1976), a paper which is not often cited because of its impenetrability, occluding the matter as it does with a heavy shroud of curvilinear coordinates. The basic lubrication approximation which describes glacier and ice sheet flow was introduced as the 'shallow ice approximation' in my thesis (Fowler 1977) and in print by Fowler and Larson (1978), and this

phrase is still widely used. Fowler and Larson dealt explicitly with valley glaciers, but the same small aspect ratio approximation can be used for ice sheets (Morland and Johnson 1980, Hutter 1983, Morland 1984, Hutter *et al.* 1986 and Fowler 1992a, of whom we follow the latter) and ice shelves (Morland and Shoemaker 1982), although in practice similar approximations had been introduced earlier (Nye 1959, Weertman 1957b).

Waves on glaciers

Both surface and seasonal waves were well known in the nineteenth century. An early discussion of surface waves is by Finsterwalder (1907), while Deeley and Parr (1914) provide a discussion of seasonal waves. Between the wars, glaciology enters its barren period, and the emergence from this is perhaps seeded by Gerald Seligman's foundation of the Glaciological Society (first British, later International) in 1936, but it is only after the war that some of the earlier investigations are revived. Lliboutry, in particular, was a great advocate of the expertise of the early glaciological researchers.

The modern theory of surface wave motion received its impulse from John Nye's stay at CalTech, where a youthful Gerry Whitham had recently developed the theory of kinematic waves (Lighthill and Whitham 1955a,b). This theory was adapted by Nye (1960, 1963) to the study of linear waves on glaciers; a nonlinear analysis is given by Fowler and Larson (1980b). A parallel development was reported by Weertman (1958). Nye's theory, based on perturbations of a parallel-sided slab, yields the unphysical singularity at the snout which was mentioned in section 10.4.1.

Apart from the early work by Deeley and Parr (1914), there has been relatively little interest in seasonal waves. The main exception to this is the paper by Hodge (1974). Hewitt and Fowler (2008) provide a mathematical model which can produce certain of the observed features.

Wave ogives are lucidly discussed by Waddington (1986).

The head and the tail

As mentioned earlier, wave theory for glaciers is confounded by both the head of the glacier and its snout. To my knowledge, no one has paid any attention to the modelling issue with the upstream boundary condition, as discussed here in question 10.11. The resolution of the description of the *bergschrund*[33] is likely to involve steepening bed slopes, and longitudinal stresses which reach the fracture strength of ice (around 2 bars).

The snout of a glacier is a good deal more accessible. Even so, little attention has been paid to that either. Nye and Lliboutry had a little engagement[34] about this in the 1950s (Lliboutry 1956, Nye 1957, Lliboutry 1958b, Nye 1958), and chapter 6

[33]The crevasse which marks the head of the glacier, where the ice separates from the stagnant apron of snow and ice above it.

[34]Or perhaps a spat; Nye's opening sentence in his 1958 note is the wonderful comment: "In so far as Professor Lliboutry is trying to make the theory of glacier flow more realistic one can only wish him well and hope that he is on the right track."

of my thesis (Fowler 1977) uses the method of strained coordinates to calculate the finite slope at the front. This involves inclusion of the longitudinal stresses, in much the same way as in question 10.11. If these are ignored, then the solution of the isothermal equation has infinite snout slope if it is stationary or advancing, much as for (10.117); see also question 10.12.

Boulton and Hindmarsh's (1987) seven data points of basal shear stress, effective pressure and till strain rate were presumably gleaned from observations near the glacier snout. The original data was never published, so that one can only guess how the values of shear stress were computed. In the absence of a local analysis of behaviour near the snout, such values are tantamount to guesswork.

Surges

Surging glaciers are located in various places round the world, including Alaska and Svalbard. Famously, there are no surging glaciers in the European Alps, but it is thought that there used to be at least one, Vernagtferner, in the Austrian Alps, which last surged in about 1900.[35] Early paintings, documented by Nicolussi (1990) indicate surges occurring in about 1600 and 1680, to judge from the jagged surface of the glacier in the images, and further surges occurred in 1772, 1844, and the small, perhaps final one in 1898. Apart from the last of these, the ice advanced to block the outlet stream from Hintereisferner, causing an ice-dammed lake to form, which burst through the ice, sometimes more than once, sending a flood wave down the valley to the village of Vent.

The surge on Variegated Glacier is discussed by Kamb *et al.* (1985), and theoretical descriptions are given by Kamb (1987) and Fowler (1987a). The present discussion is based on this latter paper, the mathematical details of which are worked out in Fowler (1989). Observations of Trapridge Glacier are described by Clarke *et al.* (1984) and Frappé-Sénéclauze and Clarke (2007). The issue of the Journal of Geophysical Research in which Fowler's (1987a) article appears is a collection of articles on fast glacier flow, including both ice streams, surging glaciers, and tidewater glaciers.

Streams, shelves, sheets

The dynamics of ice streams are reviewed by Bentley (1987), see also Engelhardt *et al.* (1990), while the theory of Hudson Strait mega-surges is due to MacAyeal (1993). Heinrich events are discussed by Bond *et al.* (1992), while the discussion here is based on a paper by Fowler and Johnson (1995). The recent acceleration of Jakobshavn Isbrae in West Greenland is described by Holland *et al.* (2008).

The discussion of approximate temperature profiles follows that in Fowler (1992a); the profiles shown in figure 10.7 are reminiscent of those shown in Paterson's (1994) book, and are also similar to the computed profiles of Dahl-Jensen (1989). The concept of thermally induced instability was enunciated by Robin (1955) and taken up by Clarke et al. (1977) and Yuen and Schubert (1979), but more or less scotched by

[35] See `http://www.lrz.de/~a2901ad/webserver/webdata/vernagt/vernagt_E.html`.

Fowler and Larson (1980a), at least in the context of two-dimensional flows; see also Fowler *et al.* (2009). However, Hindmarsh (2009) has shown that thermally induced instabilities do occur in three dimensions, and are capable of forming ice stream-like features.

The basic approximation for the analysis of ice shelves was done by Weertman (1957b). A general scaling analysis is given by Morland and Shoemaker (1982). Typical values of sub-ice shelf melt rates are given by Holland *et al.* (2003), for example.

The mechanics of ice streams are thoroughly described by Van der Veen (1999). The shear stress on the Siple coast ice streams, particularly the Whillans ice stream, is small, of order 0.1–0.2 bars, but Kamb's (1991) laboratory tests indicated that the yield stress for the basal marine sediments is an order of magnitude smaller. If one supposes that the rheology of till is such that the yield stress cannot be exceeded without allowing rapid acceleration, then the presence of stable ice streams indicates that the driving stress is taken up elsewhere, most likely by lateral shear, and this is consistent with transverse velocity profiles, as shown by Van der Veen (figure 12.10), and as discussed in section 10.3.4.

The use of longitudinal stresses in producing the membrane stress approximation is due to MacAyeal (1989). The version we present here is similar to that presented by Blatter (1995), and perhaps more in the style of Schoof and Hindmarsh (2010). Bueler and Brown (2009) present a related model, although they partition the ice velocity in an arbitrary way between shearing and sliding.

The mechanism whereby ice streams form is less clear, although some kind of spatial instability is the likely cause. As alluded to above, Hindmarsh (2009) showed, following earlier work by Payne and Dongelmans (1997), that thermal instability was a possible cause; Sayag and Tziperman (2008), following Fowler and Johnson (1996), suggested that a water-mediated feedback could also provide a mechanism.

Grounding line

The possible collapse of the West Antarctic Ice Sheet was discussed by Hughes (1973), and Weertman (1974) gave the first theoretical discussion of grounding line stability. Subsequent authors who discuss the issue include Thomas (1979) and Hindmarsh (1993); the latter advocated a concept of neutral equilibrium for grounding line position.

The issue of the extra condition which describes the position of the grounding line is a thorny one, which is as yet not completely resolved. At a formal level, the most detailed studies are those of Wilchinsky (Chugunov and Wilchinsky 1996, Wilchinsky and Chugunov 2000, 2001), but these papers are severely impenetrable, even to initiates. Wilchinsky (2007, 2009) adds further comments to his earlier analysis. Chugunov and Wilchinsky (1996) consider the transition zone in a similar manner to that presented here. They assume Newtonian flow and a steady state, and claim to deduce the grounding line position. Two key assumptions are apparent in their reasoning. The first is the arbitrary assumption that the horizontal length scale for the ice shelf is comparable to that for the ice sheet. This allows them to deduce that

(with present notation) $H_G = \beta(\varepsilon/\delta)^{1/3}$ for some $O(1)$ coefficient β (not the same β as in 10.2.7); the origin of this (correct) scale is, however, mysterious. The deduction of a numerical value of $\beta \approx 1.5$ from a numerical calculation appears to involve (in the appendix to the paper) the assumption that the bed $B(X)$ (in present notation) is smooth, i. e., $B'(0) = 0$. This assumption appears to be arbitrary, though reasonable. Wilchinsky and Chugunov (2000) extend this analysis to the junction between a rapidly moving ice stream, where shear is less important, and an ice shelf. They now state that the grounding line position is determined by the requirement of continuity of the lower ice surface at the grounding line, but they do not carry through the calculation. The scaling analysis involved is rather different than for the shear-dominated sheet/shelf transition. Finally, Wilchinsky and Chugunov (2001) extend the scaling of the 1996 paper to the nonlinear rheology of Glen's law. The flow is still steady, and it is stated that the condition $B(0+) = 0$ determines the grounding line position, and that the flux at the grounding line is, in present notation,

$$q_G = \left(\frac{\beta\varepsilon}{\delta}\right)^n H_G^{n+2}; \tag{10.472}$$

this can be compared with (10.162). Numerical evaluation of β is again only done for the Newtonian case $n = 1$, under the additional assumptions of $B_X = B_{XX} = 0$ at $X = 0+$. Like its predecessors, this paper is hard to fathom.

More recently, the transition problem has been studied numerically by Nowicki and Wingham (2008), and it is here that the rôle of contact conditions has been emphasised. They studied the transition problem described in section 10.2.7, assuming $\dot{x}_G = 0$, and for a range of incoming mass fluxes—essentially a range of values of Λ. They also allowed sliding, so that on the grounded base $X < 0$, the sliding velocity is

$$U = kT_3, \tag{10.473}$$

which replaces the second condition in (10.153). In general, solutions are obtained for any value of Λ, but in general the (scaled) normal effective stress $B + \Pi + T_1$ on the grounded ice is singular at $X = 0$, tending to either ∞ or $-\infty$ as $X \to 0-$. In addition, one finds $B_X(0) > 0$ if $B+\Pi+T_1 \to -\infty$, and $B_X(0) < 0$ if $B+\Pi+T_1 \to \infty$. Consequently, none of these solutions are admissible. For each $k > 0$ there is precisely one value of Λ for which the contact conditions (10.175) and (10.176) are satisfied, and for this value also $B_X(0) = 0$, which can also be deduced from (10.166), which implies that

$$B + \Pi + T_1 = -\frac{2T_1 B_X^2}{1 - B_X^2} \tag{10.474}$$

on $Z = B$, $X > 0$.

These results have not yet been extended to the non-stationary case $\dot{x}_G \neq 0$, or to the no slip case $k = 0$. The difficulty in the latter case appears to be associated with the greater numerical difficulty encountered in dealing with the more severe singularity which will occur in that case (cf. Barcilon and MacAyeal 1993). Durand *et al.* (2009) have used the same contact conditions in a full numerical ice sheet model in which $\dot{x}_G \neq 0$, with encouraging results.

The limit $k \to \infty$ in (10.473) corresponds to the case of sliding dominated flow as in an ice stream, and this limit has been studied directly by Schoof (2007b,c) using a version of the membrane stress approximation. In order to complete his theory, he also needs an extra condition, which is taken to be that T_1 is continuous. It is not entirely obvious that this would be a consequence of the contact conditions in a suitably rescaled version of the finite k theory, although it seems likely. Schoof (2007c) is able to show directly that the Weertman slope-induced instability does indeed apply, and we have followed his presentation here.

Sliding

The theory of basal sliding over hard beds stems from Weertman (1957a) and Lliboutry (1968). Weertman presented the basic concept of the regelative lubricating film, and described in order of magnitude fashion how to obtain a sliding law. Lliboutry presents more elaborate calculations, and importantly introduces the importance of basal water. Two reviews of progress by the end of the seventies are by Lliboutry (1979) and Weertman (1979). The linear theory is primarily due to Nye (1969, 1970) and Kamb (1970). Morland (1976a,b) introduced complex variable methods, while the material presented here is based largely on Fowler (1986, 1987b). The first of these uses complex variable methods to study cavitation over simple periodic beds, and the second uses a heuristic, Lliboutry-style method to suggest a generalised Weertman model for sliding over non-periodic beds. An up to date theoretical discussion of sub-glacial cavitation is given by Schoof (2005), who also provides significant theoretical advances in the study of sliding over non-periodic beds, indicating in particular that Fowler's (1987) theory is flawed, though repairable. His essential conclusion is that Iken's (1981) concept of a maximum friction (shear stress divided by normal effective stress) is valid, even for non-periodic beds, with the maximum value of the friction being set by the amplitude and slope of the largest bumps.

Weertman's original model is as follows. Consider a bed consisting of an array of (cubical) obstacles of dimension a a distance l apart, and suppose the ice flow exerts an (average) shear stress τ at the bed. The drag on each obstacle is therefore τl^2, and thus the pressure increase upstream of an obstacle is (approximately) $\tau l^2/2a^2$, while the decrease downstream is $-\tau l^2/2a^2$. The pressure difference causes a temperature difference (due to the Clapeyron effect) of

$$\delta T \approx C\tau l^2/a^2 \tag{10.475}$$

where C is the slope of the Clapeyron curve, $-dT_m/dp = C \approx 0.0074$ K bar^{-1}; T_m is the melting temperature. Let u_R be the regelative ice velocity: then $u_R a^2$ is the regelative water flux. The latent heat required to melt this is $\rho_i L u_R a^2$, where ρ_i is ice density and L is latent heat. The heat transfer is effected through the obstacle, at a rate $(k\delta T/a)a^2 = k\delta T a$, where k is the thermal conductivity of the bedrock. Equating these suggests that

$$u_R = \left(\frac{kC}{\rho_i L a}\right)\frac{\tau}{\nu^2}, \tag{10.476}$$

where the aspect ratio $\nu = a/l$ is a measure of the roughness of the bedrock. Regelation is thus effective at *small* wavelengths.

On the other hand, let u_V be the velocity due to viscous shearing past the obstacle, with no shear stress at the bed. The differential stress generated is $\approx \tau/\nu^2$, and for a nonlinear (Glen's) flow law $\dot{\varepsilon} = A\tau^n$, the resulting strain rate is $\approx 2A(\tau/\nu^2)^n$, with $n \approx 3$. Hence we infer

$$u_V \approx 2aA(\tau/\nu^2)^n. \tag{10.477}$$

It can be argued[36] that the stresses should be added, thus

$$\tau = \nu^2[R_r au + R_v(u/a)^{1/n}], \tag{10.478}$$

where R_r and R_v are material roughness coefficients, given approximately by

$$R_r \approx \frac{\rho_i L}{kC}, \quad R_v \approx \left(\frac{1}{2A}\right)^{1/n}. \tag{10.479}$$

We see that motion past small obstacles occurs mainly by regelation, while motion past larger obstacles occurs largely by viscous deformation. There is a *controlling obstacle size* at which the stresses are comparable, and if we take a as this value, we obtain the Weertman sliding law

$$\tau \approx \nu^2 R u^{\frac{2}{n+1}}, \tag{10.480}$$

where

$$R = \left(\frac{\rho_i L}{2kCA}\right)^{1/(n+1)}. \tag{10.481}$$

Subtemperate sliding

Sometimes modellers who implement sliding laws in their ice sheet computations assume that the sliding law $u = U(\tau)$ applies when the basal temperature $T = T_m$, and that $u = 0$ for $T < T_m$. This assumption is incorrect (Fowler and Larson 1980a), and it is more appropriate to allow sliding to increase continuously over a small range of temperature below the melting point, to reflect the fact that creation of a water film will occur in a patchy fashion as the melting point is approached (Hindmarsh and Le Meur 2001, Pattyn *et al.* 2004).

If one assumes a discontinuous sliding law, then if basal stress is continuous, one would have an inadmissible discontinuity of velocity: this was the downfall of the EISMINT ice shelf numerical modelling experiments in the 1990s. If the velocity is to be continuous, then stresses must be discontinuous and in fact singular (Hutter and Olunloyo 1980). It has indeed been suggested that such stress concentrations may have a bearing on thrust faults in glaciers (e. g., Kleman and Hättestrand 1999), but the theoretical basis for supposing they exist is dubious.

We can derive a sliding law in a Weertman-like way for basal temperatures below T_m as follows. Again we suppose that bumps of size a are spaced a distance l apart.

[36] Weertman added the velocities instead.

Now we suppose that the basal temperature is at a temperature $T_b < T_m$, and we define the undercooling to be

$$\Delta T = T_m - T_b. \tag{10.482}$$

It is no longer appropriate to conceive of the water film covering the bed between the bumps, and so there is an additional component to the stress due to stick-slip friction. We will ignore this here, and suppose that as before the resistance comes primarily from the film-assisted flow over the bumps. Because the ice is below the pressure melting point, there is an additional conductive heat flow away from the bumps given approximately by $\dfrac{k\Delta T}{l}$, and therefore (10.476) is replaced, using (10.479), by

$$R_r a u_R = \frac{\tau}{\nu^2} - \frac{\nu \Delta T}{C}, \tag{10.483}$$

and (10.478) is replaced by

$$\tau = \nu^2 \left[R_r a u + R_v \left(\frac{u}{a} \right)^{1/n} + \frac{\nu \Delta T}{C} \right], \tag{10.484}$$

which shows that for fixed τ, u decreases to zero continuously as ΔT increases to a temperature $\Delta T_{\max}$ given by

$$\Delta T_{\max} = \frac{C\tau}{\nu^3}. \tag{10.485}$$

For $\tau = 0.1$ bar and $\nu = 0.1$, this is $\approx 1^\circ$ K.

The rheology of till

Although glacial geologists were aware of the widespread occurrence of subglacial drift, or subglacial till, the early theoretical studies of sliding focussed on sliding over hard beds. An abrupt shift in this view occurred on the publication of the benchmark paper by Boulton and Hindmarsh (1987), which focussed attention on the basal motion of ice due to deformation of the subglacial till. In particular, Boulton and Hindmarsh described possible viscous-type rheologies for till based on reported measurements on a subglacial till below an Icelandic glacier. Unfortunately, the original data from which the shear stresses were inferred are unavailable, and thus the experimental basis for the viscous rheology is uncertain. When laboratory measurements of subglacial till properties are made, it has been largely found that till behaves as a plastic material, having a yield stress which when reached allows indefinite strain (Kamb 1991, Hooke *et al.* 1997, Iverson *et al.* 1997, Tulaczyk *et al.* 2000, Rathbun *et al.* 2008, Altuhafi *et al.* 2009). This is to be expected, since till is a granular material. Ignoring cohesion, we would then have a prescription for basal shear stress in the form

$$\tau = \mu N, \tag{10.486}$$

where μ is a suitable coefficient of friction and N is effective pressure. Lliboutry suggested such a sliding law in his 1968 paper.

However, the story is more complicated than this. The rheology of a plastic material comprises the prescription of a yield stress surface (for example, the Von Mises yield stress surface $\tau_{ij}\tau_{ij} = 2\tau_c^2$) together with a flow law. The simplest such flow law allows a strain rate proportional to stress, so that the actual rheology would be that of a viscous material, where the effective viscosity is determined by the necessity to remain on the yield surface. In addition, purely geometrical considerations suggest that, in order to shear a granular material at all, a normal stress must be induced in order that the grains can move round each other. The generation of normal stresses by shear flows is a property of viscoelastic materials, and suggests that the issue of till rheology is not a simple one. The consequent dilation of the till in shear induces a reduction of pore pressure, and consequent hardening (Moore and Iverson 2002). In addition, deformation of granular materials often occurs through the formation of shear bands (Li and Richmond 1997, François *et al.* 2002), whose presence complicates the determination of an effective till rheology. Fowler (2003) discusses some of these issues further.

Drainage

Water is abundant under glaciers and ice sheets, and it seems usually to be the case that subglacial water cannot be evacuated through the bed, so that a subglacial hydraulic system must exist. The classical theory of drainage through channels incised upwards into the ice is due to Röthlisberger (1972), while the time-dependent development of this theory for jökulhlaups is due to Nye (1976). The ice-incised channels are called Röthlisberger, or simply R, channels, but channels cut down into underlying bedrock have been observed, and are termed Nye channels, following Nye (1973). Weertman (1972) preferred a distributed water film, although Walder (1982) showed that such a film is unstable (indeed, it is this instability which is responsible for the formation of R channels in the first place). However, the concept of a patchy film is more tenable (Alley 1989), particularly if allied to the concept that the ice-till interface can itself evolve; more on this below.

Linked cavities were first implicitly described by Lliboutry (1968), and were observed in deglaciated beds by Walder and Hallet (1979). Kamb *et al.* (1985) and Walder (1986) developed theoretical descriptions for the consequent hydraulic régime. While linked cavities are generally (though not necessarily, see below) associated with flow over hard beds, a similar sort of system of distributed canals was invoked by Walder and Fowler (1994) to describe channelled flow over soft till beds. For field measurements of subglacial hydrological systems, see Hodge (1974), Hubbard *et al.* (1995), Nienow *et al.* (1998) and Fudge *et al.* (2008). A recent review of subglacial processes of current interest is by Clarke (2005).

Drumlins

The word 'drumlin' apparently derives from the Irish, and means 'small hill'. The word appears to have first been published in the paper by Bryce (1833)[37], and is in common scientific usage by the time of Kinahan and Close (1872), although the study of such bedforms was also described much earlier by Hall (1815), who was concerned with crag-and-tail features in Scotland (perhaps the best known being the Royal Mile in Edinburgh, a ridge of drift which lies in the lee of the volcanic outcrop of Edinburgh Castle). There are two interesting things about Hall's paper. First, it appears before Agassiz's glacial theory (as does Bryce's), and thus ascribes crag-and-tail features to the biblical flood. Hall and Bryce had no knowledge of ice ages. The second interesting thing is that a modern edition of Hall's biblical theory has reappeared in the flood hypothesis of John Shaw (e. g., Shaw 1983, Shaw *et al.* 1989). Shaw's ideas are largely derided, but are vigorously supported by a number of scientists.

So we need to explain Shaw's hypothesis and its reception rather carefully (see also the discussion in section 11.8). Essentially, his idea is that massive subglacial meltwater floods cause the formation of drumlins, and the apparent motivation for this idea is that only the turbulent flow of water can erode such bedforms: ice is too slow. This conceit is evidently misguided, but its application requires him to produce massive subglacial floods below ice sheets. The twist in the story (see chapter 11) is that such floods now seem likely to have occurred, but the basic difficulty with the Shaw theory remains: he needs floods to be everywhere, of incomprehensible volume, and to produce bedforms which do not actually look fluvial: a tall order.

In my view, one can be fairly circumspect about the matter. Shaw's theory, in any of its forms, is not in fact a theory: it does not provide a mechanistic process to produce the observations. A suitable point of discussion is his 1983 paper. Inspired by his mentor's monumental book masquerading as a paper (Allen 1971), Shaw provides a very persuasive analogy between between some erosional marks, such as the cave scallops described by Allen, and the resulting inverted casts under ice sheets, which

[37]The paper is not so easy to find. The reference in Drozdowski (1986) which most likely follows that of Menzies (1984) is marginally incorrect (it is the Journal of the Geological Society of Dublin, not of the Royal Geological Society of Dublin, and this makes a difference, since the journal subsequently changed its name to the Journal of the Royal Geological Society of Ireland). Copies of the original journal can be found in the National Library of Ireland (Kildare St., Dublin, call number IR5541g1), as well as in the library of the Royal Dublin Society in Ballsbridge. Bryce did not coin the word; he says the following: "*The gravel hills, on the other hand, have an elongated form, are generally steepest towards one side, and rise in every other direction by much more gentle acclivities. This peculiar form is so striking that the peasantry have appropriated an expressive name to such ridges . . . the names* Drum *and* Drumlin (*Dorsum*) *have been applied to such hills . . . .*" Why the Latin word *Dorsum* (meaning back, but also ridge) is included in parenthesis is not clear. Bryce's paper largely concerns the constituents of the till which constitute the drumlins of northern Ireland, from which he infers that motion was largely from the north west. He also provides what may be the first description of ribbed moraine, and deduces in effect that Belfast Lough, Lough Neagh and Lough Foyle were formed during the ice ages. Earlier uses cited in the Oxford English Dictionary are by Innes (1732) and Sinclair (1791–1799; particularly volume IX, pp. 131, 262–263 and volume XIX, pp. 342–344, 369), but it seems that the *dryms* of Innes on the shores of Lough Foyle in Ireland are in fact fossil dunes, while the *drums* of Sinclair near Blairgowrie in Perthshire, Scotland, are interfluves of former meltwater channels.

result as drumlins. Nothing wrong with the idea. But it is not a theory. To be a theory, it needs, for example, a predictive wavelength for scallops. Scallop formation is an interesting problem (Blumberg and Curl 1974), but is basically unsolved. One can thus criticise Shaw's ideas either on the basis that their fundamental environment is invented (massive floods), or on the basis that nothing is actually predicted. But at the same time, we have to be aware as scientists, that we must try to avoid dogmatic reaction associated with paucity of imagination, because we know that this has littered our scientific history. Consider, for example, the receptions accorded to Wegener (chapter 8) and Bretz (chapter 11).

The development of the theory of drumlins over the nineteenth and twentieth centuries is in a similar parlous state. Although the literature describes the debate between the 'erosional' and 'depositional' theories, there is really no theory that deserves the name until Hindmarsh's landmark paper (Hindmarsh 1998), which is the first time that the word 'instability' makes an appearance, and in which an instability theory is proposed. Hindmarsh showed numerically that instability could occur, and essentially the same theory was solved analytically by Fowler (2000). The theory is developed further by Schoof (2007a), who revisits the same stability theory and extends it in various ways. He does, however, draw a cloud over proceedings: 'Hindmarsh and Fowler's theory does not reproduce a number of known features of drumlins'; and in his conclusions, he draws attention to certain apparent problems with the theory: the problems of three-dimensionality, the issue of stratified drumlin cores, the problem of amplitude. Gloomily, he thinks there is a 'tenuous link between the model and the origin of drumlins'. His gloom is misplaced. There is no other tenable theory in existence, and there is nothing as yet which rules it out. While the problem is certainly hard, it is likely that a clear theoretical framework will emerge over the next decade or two. In his recent book, Pelletier (2008) follows Schoof's view, and proposes a model based, bizarrely, on a compaction model for magma transport, with little connection to the physical processes involved, although he is able to produce interesting looking patterns—much like his theory of the spiral canyons on the Martian north polar ice cap (see below).

Eskers

The Irish eskers were perhaps first described scientifically by Close (1867), and later by Flint (1930). General descriptions are given by Embleton and King (1968) and Sugden and John (1976). More up to date discussions are those by Shreve (1985) and Warren and Ashley (1994). Clark and Walder (1994) noted that in the Laurentide ice sheet, the former central part, the Canadian Shield, is essentially wiped clean of sediment, which has piled up in the outer parts of the former ice sheet. And eskers are found in the Shield but not beyond it. Clark and Walder inferred the obvious conclusion, that Röthlisberger channels (hence the eskers) are the drainage pattern on the (hard) Shield, while their absence on the sediment-covered margins indicates a canal-type drainage. We will come back to this observation in chapter 11.

In our discussion of the various drainage systems which exist beneath a glacier, we have always been thinking of an isolated set of channels, or linked cavities, or canals,

which somehow exist independently of the overlying ice and underlying sediments or bedrock. Finally, as we contemplate the construction of drumlins and eskers, we may come to realise that this separatist view is misguided. In our simple theory of drumlin formation, we imagine a drainage system which moves water through the landscape without interacting with it. But this is unrealistic: the development of ridges will pond water and alter drainage paths. What we need to do is to allow the drainage system to interact with the bedforms.

We might then ask ourselves, what actually is the difference between a lee-side cavity and a subglacial stream? And the answer, at least from the point of a sensible model, is none. A fully integrated model for ice, water and sediment (or rock) allows for parts of the bed where effective pressure $N > 0$ and the ice is attached, i. e., the water layer thickness $h = 0$, and parts of the bed where the ice flow is separated ($h > 0$), and where $N = 0$. In this view a cavity is the same as a stream, the precise geometrical distinction between them being simply one of degree. A model of this type has recently appeared (Fowler 2010), although its numerical solution has yet to be attempted.

Glaciology on Mars

The theory of dust–albedo feedback used in the description of the possible mechanism for the formation of the spiral troughs on the Martian polar ice caps was advanced by Howard (1978), although mathematical efforts to establish a theory had to await the models of Pelletier (2004) and Ng and Zuber (2003, 2006). Pelletier's model is essentially equivalent to the Fitzhugh-Nagumo equations, which are known to produce spiral waves, but appears to have been constructed with a view to obtaining the waves he sought. While the resulting numerical solutions which he found are suggestive, there is no coherent physical basis for the model. Ng and Zuber's model is more clearly based on Howard's idea, and uses Ivanov and Muhleman's (2000) description of radiative transport as its basis. Our description is largely based on Ng and Zuber's work, although we diverge in our development of the model and its conclusion: see Zammett and Fowler (2010).

Exercises

10.1 The downstream velocity u over the cross section S of a glacier is given by

$$\boldsymbol{\nabla}.[\eta\{A, |\boldsymbol{\nabla}u|\}\boldsymbol{\nabla}u] = -1 \quad \text{in} \quad S,$$

where the viscosity is given by

$$\eta = A^{-1/n}|\boldsymbol{\nabla}u|^{-(n-1)/n}.$$

Assuming the rate factor $A = 1$ and a semi-circular profile for the ice cross section S. Give suitable boundary conditions for the flow, and hence derive the solution. Deduce the ice flux Q as a function of the cross sectional area of the flow.

10.2 Use lubrication theory to derive an approximate model for two-dimensional flow of a valley glacier, assuming Glen's flow law with a rate constant independent of temperature, and no sliding at the base. Non-dimensionalise the model, and show that for typical lengths of 10 km, accumulation rates of 1 m y^{-1}, and if the rate constant in Glen's law is 0.2 bar^{-3} y^{-1} (with the Glen exponent being $n = 3$), a typical glacier depth is 100 m. Show that the dimensionless model depends on the single dimensionless parameter $\mu = d \cot \alpha / l$, where d is the depth scale, l is the length scale, and α is the valley slope. What are typical values of μ?

Show that if $\mu \ll 1$, the model takes the form of a first order hyperbolic wave equation. Write down the solution for small perturbations to the steady state, and show that the perturbations grow unboundedly near the glacier snout. Why is this? Write an alternative linearisation which allows a bounded solution to be obtained.

More generally, an exact characteristic solution of the model allows shocks to form (and thus for the glacier snout to advance). Discuss the rôle of μ in shock formation.

10.3 A glacier is subject to an accumulation rate a whose amplitude varies sinusoidally in time about a mean (space dependent) value; specifically

$$a = a_0(x) + a_1 e^{i\omega t},$$

where a_1 is constant (the real part may be assumed). Use an appropriate linearised wave theory to determine the resultant form of the perturbed surface. What can you say about the effect of millennial scale climate changes? About annual balance changes?

How would you generalise your result to a general time dependent amplitude variation?

10.4 Write down the equations governing three-dimensional flow of an ice sheet, and show how they can be non-dimensionalised to obtain

$$H_t = \boldsymbol{\nabla}. \left[\left\{ \frac{|\boldsymbol{\nabla} s|^{n-1} H^{n+2}}{n+2} \boldsymbol{\nabla} s \right\} - H \mathbf{u}_b \right] + a,$$

assuming Glen's flow law and a temperature independent rate coefficient. Show that the dimensionless basal shear stress is $\boldsymbol{\tau} = -H \boldsymbol{\nabla} s$.

10.5 An ice sheet in steady state has profile $z = s(x, y)$ and horizontal velocity $\mathbf{u} = (u, v)$ independent of depth, with $\mathbf{u} = -K \boldsymbol{\nabla} s$, for some scalar K. Suppose that χ is a coordinate anti-clockwise along level s contours, and that U is a function such that $u = U\chi_y$, $v = -U\chi_x$, and which satisfies (in terms of independent coordinates s, χ)

$$\frac{\partial}{\partial s} \left(\frac{U}{|\mathbf{u}|} \right) = -\frac{1}{|\boldsymbol{\nabla} s|} \frac{\partial \theta}{\partial \chi},$$

where $\theta = \tan^{-1}\left(\frac{v}{u}\right)$.

If σ measures arc length on a level s contour $C(s)$, show that

$$\frac{U\,d\chi}{|\mathbf{u}|} = d\sigma$$

on C. Show also that $\oint_{C(s)} d\theta = 2\pi$. Show that distance ξ along a flow line satisfies $d\xi = -\dfrac{ds}{|\boldsymbol{\nabla} s|}$, and deduce that

$$\frac{\partial}{\partial \xi}\left(\frac{U}{|\mathbf{u}|}\right) = \frac{\partial \theta}{\partial \chi}.$$

Show that integration of this equation round a closed contour $C(s)$ appears to imply that $\dfrac{\partial L(s)}{\partial \xi} = 2\pi$, where $L(s) = \oint_C d\sigma$ is the circumferential length of C. This is incorrect: why?

Show that a correct inference is that

$$-\frac{dL}{ds} = \oint_C \frac{d\theta}{|\boldsymbol{\nabla} s|},$$

and show that this equation can be deduced on purely geometrical grounds.

The ice sheet profile satisfies the equation

$$\boldsymbol{\nabla}.(s\mathbf{u}) = a,$$

where we suppose $a(x, y) > 0$. By using s and χ as independent coordinates, show that

$$\frac{\partial (sU)}{\partial s} = -\frac{a}{J},$$

where $J = -\dfrac{\partial(s, \chi)}{\partial(x, y)}$ is the Jacobian of the transformation from (x, y) to $(-s, \chi)$. Explain why $J > 0$ away from the ice sheet summit, and deduce that sU is a monotone increasing function of ξ along a flow path.

10.6 Suppose that an ice sheet has the symmetric profile $s = 1 - r^2$, where r is the polar radius from the centre. The curvature of the level s contours is thus $\kappa = \dfrac{1}{r}$, and the distance along a steepest descent path is r. The temperature away from the bed is given by

$$T = f(zU),$$

where

$$U = u \exp\left[\int^r \kappa\, dr\right],$$

and $u(r)$ is the radial outwards plug flow velocity of the ice; the ice depth is related to the accumulation rate $a(r)$ by

$$\frac{1}{r}\frac{\partial}{\partial r}(rsu) = a.$$

Show that $rsu = B$, where $B = \displaystyle\int_0^r ra\,dr$, and thus that $U = \dfrac{B}{s}$, and deduce that

$$T = f\left(\frac{Bz}{s}\right).$$

For the particular case where $a = 1$ and the surface temperature is $T_s = -\Gamma s$, show that the interior temperature is given by

$$T = -\Gamma\left[1 - \frac{r^2 z}{s}\right].$$

(*This temperature decreases with increasing depth, a typical result of the advection of cold inland surface ice below warmer coastal ice. Such profiles are seen in measured temperature profiles, but with an inversion near the base where the geothermal heat flux causes the basal ice to become warmer.*)

10.7 The averaged (dimensional) horizontal force balance at the calving front of an ice shelf can be written in the form

$$\int_b^s \sigma_{11}\,dz = -\int_b^0 p_w\,dz - p_a s,$$

where p_w is the (hydrostatic) water pressure, p_a is atmospheric pressure, and $z = s$ and $z = b$ are the positions of the ice top surface and bottom surface relative to sea level at $z = 0$. Show that, when written in terms of the ice sheet scales, this condition takes the form

$$\frac{(1+\delta)b^2}{2} - \frac{(s-b)^2}{2} + \varepsilon^2\int_b^s(-p+\tau_1)\,dz = 0,$$

where $\delta = (\rho_w - \rho_i)/\rho_i$. Hence show that in terms of the ice shelf scales, the condition can be written in the form

$$b^2 - \delta s^2 + 2sb + 4\tau_1(\delta s - b) = 0,$$

assuming the approximate results $-p \approx \tau_1 = \tau_1(x,t)$. Taking $s \approx -b$, show that the vertically averaged deviatoric longitudinal stress at the calving front is

$$\bar{\tau}_1 = -\tfrac{1}{4}b,$$

and if this is taken as the boundary condition for the ice shelf stress τ_1, show that (by solving $(10.141)_2$)

$$\tau_1 = -\tfrac{1}{4}b$$

everywhere.

10.8 Suppose that

$$H_t = -q_x + a,$$
$$q = -D(H, H_x)H_x,$$

where a is constant, and the boundary conditions are

$$q = 0 \quad \text{at} \quad x = 0,$$
$$q = q_G(x_G), \quad H = H_G(x_G) \quad \text{at} \quad x = x_G.$$

If the steady state solution is denoted with a suffix or superscript zero, show, by writing $H = H_0(x) + \eta$, $q = q_0(x) + Q$, and $x_G = x_G^0 + \gamma$, that the linearised system for the perturbation can be written in the form

$$\eta_t = -Q_x,$$
$$Q = -\bar{p}\eta_x - \bar{q}\eta,$$
$$Q = 0 \quad \text{at} \quad x = 0.$$
$$Q = K\eta \quad \text{at} \quad x = x_G^0,$$

where

$$K = \frac{q_G'(x_G^0) - q_0'(x_G^0)}{H_G'(x_G^0) - H_0'(x_G^0)}, \quad \bar{p} = D_0 + D_{H'}H_0'', \quad \bar{q} = D_H H_0',$$

and

$$D_{H'} = \frac{\partial D}{\partial H_x}, \quad D_H = \frac{\partial D}{\partial H},$$

the derivatives being evaluated at the steady state. Note that

$$\bar{p} = -\frac{\partial q}{\partial H_x} > 0, \quad \bar{q} = -\frac{\partial q}{\partial H} < 0.$$

Show that solutions exist in the form $\eta = y(x)e^{\sigma t}$, and show that the equation for y can be written in Sturm-Liouville form

$$(py')' + (s - \sigma r)y = 0,$$

where primes denote differentiation with respect to x,

$$p = \bar{p}r, \quad r = \exp\left(\int_0^x \frac{\bar{q}\,dx}{\bar{p}}\right), \quad s = r\bar{q}'.$$

Deduce that there exists a denumerable, decreasing sequence of eigenvalues σ, and that for the maximum of these, σ_1, the corresponding eigenfunction y_1 is of one sign (say positive).

Show that

$$\sigma_1 \int_0^{x_G^0} y_1\,dx = -Ky_1(x_G^0),$$

and deduce that the steady state is unstable if and only if $K < 0$.

10.9 The drainage pressure in a subglacial channel is determined by the Röthlisberger equations

$$\rho_w g \sin\alpha_c = \frac{f_1 Q^2}{S^{8/3}},$$
$$mL = \rho_w g Q \sin\alpha_c,$$
$$\frac{m}{\rho_i} = KSN^n.$$

Explain the meaning of these equations, and use them to express the effective pressure N in terms of the water flux Q. Find a typical value of N, if $Q \sim 1$ m^3 s^{-1}, and $\sin\alpha_c \sim 0.1$, $f_1 = f\rho_w g$, $f = 0.05$ m$^{-2/3}$ s^2, $n = 3$, $L = 3.3 \times 10^5$ J kg^{-1} and $K = 0.1$ bar^{-3} y^{-1}.

Use a stability argument to explain why Röthlisberger channels can be expected to form an arterial network.

10.10 Drainage through a linked cavity system relates the effective pressure N_K to the water flux Q by the implicit relation

$$N_K e^{S(\Lambda)} = \delta N_R(Q),$$

where $S = S'\Lambda$, (S' constant), $\Lambda = \dfrac{u}{N_K^n}$, $\delta < 1$ and

$$N_R(Q) = \beta Q^{1/4n},$$

with $n = 3$. Explain why this drainage system should be stable if $N_K'(Q) < 0$. Show that

$$-\frac{N_K'}{N_K}(n\Lambda S' - 1) = \frac{N_R'}{N_R},$$

and deduce that linked cavity drainage is stable for $\Lambda > \Lambda_c \equiv \dfrac{1}{nS'}$.

10.11 A correction for the basal shear stress near the head of a glacier which allows for longitudinal stress is

$$\tau = H(1 - H_X) + \gamma \left(H|u_X|^{\frac{1}{n}-1} u_X \right)_X,$$

where u is the velocity (assumed to be a plug flow), X is distance from the head, and γ is small. Assume that near the head of the glacier, conservation of mass takes the form

$$Hu = X,$$

and the sliding law is of the Weertman type

$$\tau = u^r,$$

where $0 < r < 1$.

We wish to apply the boundary conditions

$$H = 0 \quad \text{at} \quad X = 0,$$

$$H \sim X^{\frac{r}{r+1}} \quad \text{as} \quad X \to \infty.$$

Consider first an outer approximation in which the term in γ is ignored. Show that there is a unique value of $H(0) = H_0 > 0$ such that the boundary condition at ∞ can be satisfied.

Now suppose $n = 1$. Show, by writing first $X = e^{\xi}$ and then $\xi = \gamma\Xi$, that there is a boundary layer, in which H changes from 0 at $X = 0$ to H_0 as X increases, and show that $H \sim X^{H_0^2/2\gamma}$ as $X \to 0$.

Carry through the analysis when $n \neq 1$, and show that in this case $H \sim X^{(H_0^2/2\gamma)^n}$ as $X \to 0$.

Do these solutions make physical sense?

10.12 The depth H of an isothermal glacier satisfies the equation

$$H_t + \frac{\partial}{\partial x}\left[(1 - \mu H_x)^n \frac{H^{n+2}}{n+2}\right] = a,$$

and $H = 0$ at the snout $x_s(t)$. Assuming that $a_s = a(x_s) < 0$ at $x = x_s$, show, by consideration of the local behaviour of H, that if the glacier is advancing, $\dot{x}_s = v_+ > 0$, then

$$H \sim A_+ (x_s - x)^{\frac{n}{n+1}},$$

and determine A_+ in terms of v_+. If the glacier is retreating, $\dot{x}_s = -v_- < 0$, show that

$$H \sim A_-(x_s - x),$$

and determine A_- in terms of v_-.

Finally show that in the steady state,

$$H \sim A_0 (x_s - x)^{1/2},$$

and determine A_0.

10.13 The relation between ice volume flux and depth for a surging glacier is found to be a multivalued function, consisting of two monotonically increasing parts, from $(0, 0)$ to (H_+, Q_+) and from (H_-, Q_-) to (∞, ∞) in (H, Q) space, where $H_+ > H_-$ and $Q_+ > Q_-$, with a branch which joins (H_-, Q_-) to (H_+, Q_+). Explain how such a flux law can be used to explain glacier surges if the balance function $s(x)$ satisfies $\max s > Q_+$, and give a rough estimate for the surge period.

What happens if $\max s < Q_-$? $\max s \in (Q_-, Q_+)$?

10.14 The depth h and velocity u of an ice sheet fan are given by the thermo-hydraulic sliding law

$$h = \frac{fu^r}{[G + Rhu - au^{1/2}]^m},$$

where $r = \frac{1}{3}$, $m = \frac{1}{9}$, $G = 0.06$ W m^{-2}, $R = 3 \times 10^{-7}$ W m^{-4} y, $a = 0.8 \times 10^{-2}$ W m$^{-5/2}$ y$^{1/2}$, and $f = 126$ W$^{1/9}$ m$^{4/9}$ y$^{1/3}$. Assuming $hu \sim Q_i \approx 5 \times 10^5$ m^2 y^{-1}, show how to non-dimensionalise the equation to the form

$$h = \frac{\phi u^r}{[\Gamma + hu - u^{1/2}]^m},$$

and give the definitions of the dimensionless parameters ϕ and Γ. Using the values above, show that $\Gamma \approx 0.4$, $\phi \approx 0.77$.

Define $v = u^{1/2}$, and show that

$$L \equiv \Gamma - v + hv^2 = \left(\frac{v}{v^*}\right)^{2r/m} \equiv R,$$

where

$$v^*(h) = \left(\frac{h}{\phi}\right)^{3/2}.$$

By considering the intersections of the graphs of L and R, show that multiple steady states are possible for sufficiently small h. Using the observation that $\dfrac{2r}{m} = 6$ is large, show explicitly that if $h \lesssim \dfrac{1}{4\Gamma}$, then there is a solution $v \approx v^*$ for $v^* < v_-$, $v \approx v_-$ for $v^* > v_-$, and if in addition $v^* > v_+$, there are a further two roots $v \approx v_+, v^*$, where $v_\pm$ are the two roots for v of $L = 0$. Show also that if $h \gtrsim \dfrac{1}{4\Gamma}$, then there is a unique solution $v \approx v^*$.

By consideration of the graphs of $v^*(h)$ and $v_\pm(h)$ (*hint: for the latter, first draw the graph of* $L = 0$ *for* h *as a function of* v), show that multiple solutions exist for sufficiently small ϕ, and by finding when the graph of v^* goes through the nose of the $v_\pm$ curve, show that multiple steady states exist in the approximate range

$$\phi < \phi_c = \frac{1}{2^{8/3}\Gamma^{5/3}},$$

and find the value of ϕ_c.

Show that if $\phi < \phi_c$ and $hu = q$ is prescribed, there is a unique solution, but that there is a range $q_- < q < q_+$ where such a solution is unstable (as it lies on the negatively sloping part of the u versus h curve). What do you think happens if q lies in this intermediate range?

10.15 The depth of a glacier satisfies the equation

$$H_t + \frac{\partial}{\partial x}\left[(1 - \mu H_x)^n \frac{H^{n+2}}{n+2}\right] = B'(x),$$

where $\mu \ll 1$. Suppose first that $\mu \ll 1$, so that the diffusion term can be neglected. Write down the characteristic solution for an arbitrary initial depth profile. What is the criterion on the initial profile which determines whether shocks will form?

Now suppose $B = \dfrac{1}{n+2}$ is constant, so that a uniform steady state is possible. Describe the evolution of a perturbation consisting of a uniform increase in depth between $x = 0$ and $x = 1$, and draw the characteristic diagram.

Shock structure. By allowing $\mu \neq 0$, the shock structure is described by the local rescaling $x = x_s(t) + \mu X$. Derive the resulting leading order equation for H, and find a first integral satisfying the boundary conditions $H \to H_\pm$ as $X \to \pm\infty$, where $H_- > H_+$ are the values behind and ahead of the shock. Deduce that the shock speed is

$$\dot{x}_s = \frac{[H^{n+2}]^+_-}{[H]^+_-},$$

and that $\phi = H/H_+$ satisfies the equation

$$\phi_\xi = -[g(\phi)^{1/n} - 1],$$

where $\xi = X/H_+$, $\phi \to r$ as $\xi \to -\infty$, $\phi \to 1$ as $\xi \to \infty$, and

$$g(\phi) = \frac{(r^{n+2} - 1)(\phi - 1) + (r - 1)}{(r - 1)\phi^{n+2}},$$

with $r = H_-/H_+ > 1$. Show that $g(1) = g(r) = 1$, and that $g(\phi) > 1$ for $1 < \phi < r$, and deduce that a monotonic shock structure solution joining H_- to H_+ does indeed exist.

Suppose that $\delta = \Delta H/H_+$ is small, where $\Delta H = H_- - H_+$. By putting $r = 1+\delta$ and $\phi = 1 + \delta\Phi$, show that

$$g = 1 + \frac{\delta^2(n+1)(n+2)}{2}\Phi(1 - \Phi) + \ldots,$$

and deduce that

$$\Phi_\Xi \approx -\Phi(1 - \Phi),$$

where

$$\Xi = \frac{\delta(n+1)(n+2)}{2n}\xi.$$

Deduce that the width of the shock structure is of dimensionless order

$$x - x_s \sim \frac{2n\mu H_+}{\delta(n+1)(n+2)},$$

or dimensionally

$$\frac{2n}{(n+1)(n+2)}\frac{d_+^2}{\Delta d\, \tan\alpha},$$

and that for a glacier of depth 100 m, slope ($\tan\alpha$) 0.1, with $n = 3$, a wave of height 10 m has a shock structure of width 3 km. (*This is the monoclinal flood wave for glaciers, analogous to that for rivers discussed in chapter 4.*)[38]

10.16 In deriving the reduced, three-dimensional model for drumlin formation, it is necessary to compute the three dimensional components of the stress tensor at the bed. Show that the normal, x-tangential and 'y-tangential' vectors at the bed $z = s(x, y, t)$ are

$$\mathbf{n} = \frac{(-s_x, -s_y, 1)}{(1 + |\boldsymbol{\nabla} s|^2)^{1/2}}, \quad \mathbf{t}_1 = \frac{(1, 0, s_x)}{(1 + s_x^2)^{1/2}}, \quad \mathbf{t}_2 = \mathbf{n}\times\mathbf{t}_1 = \frac{(-s_x s_y, 1 + s_x^2, s_y)}{(1 + |\boldsymbol{\nabla} s|^2)^{1/2}(1 + s_x^2)^{1/2}},$$

where $\boldsymbol{\nabla} s = (s_x, s_y)$, and hence show that

$$-\tau_{nn} = \frac{2\eta\left[u_x(1 - s_x^2) + v_y(1 - s_y^2) + s_x(u_z + w_x) + s_y(v_z + w_y) - s_x s_y(u_y + v_x)\right]}{1 + |\boldsymbol{\nabla} s|^2}.$$

Show also that the horizontal basal shear stress vector (τ_1, τ_2), where $\tau_i = \mathbf{n}.\boldsymbol{\tau}.\mathbf{t}_i$, has components

$$\tau_1 = \frac{\eta\left[(1 - s_x^2)(u_z + w_x) - 2s_x(u_x - w_z) - s_y(u_y + v_x) - s_x s_y(v_z + w_y)\right]}{(1 + |\boldsymbol{\nabla} s|^2)^{1/2}(1 + s_x^2)^{1/2}},$$

$$\tau_2 = \frac{\begin{array}{r}\eta\left[(1 + s_x^2 - s_y^2)(v_z + w_y) - 2s_y\{v_y(1 + s_x^2) - w_z - s_x^2 u_x\}\right.\\ \left. -s_x(u_y + v_x)(1 + s_x^2 - s_y^2) - 2s_x s_y(u_z + w_x)\right]\end{array}}{(1 + |\boldsymbol{\nabla} s|^2)(1 + s_x^2)^{1/2}}.$$

Show also that the two x-tangential and y-tangential components of the basal velocity are

$$u_1 = \frac{u + w s_x}{(1 + s_x^2)^{1/2}}, \quad u_2 = \frac{-u s_x s_y + v(1 + s_x^2) + w s_y}{(1 + |\boldsymbol{\nabla} s|^2)^{1/2}(1 + s_x^2)^{1/2}}.$$

Write down the appropriate equations for ice flow, and a suitable matching condition when $l \ll d_I$, where l is the horizontal drumlin length scale, and d_I is the ice sheet depth. By scaling the equations and assuming the aspect ratio $\nu \ll 1$, derive a reduced form of the model as in (10.374)–(10.376).

10.17 A model of two-dimensional ice flow over a deformable bed $z = \nu s$ is given by the equations

$$\Pi_x = \nabla^2 \psi_z,$$
$$\Pi_z = -\nabla^2 \psi_x,$$

with matching condition

$$\Pi \to 0, \quad \psi_{zz} \to \theta, \quad \psi_x \to 0 \quad \text{as} \quad z \to \infty,$$

[38]The observation that the smallness of surface slope diffusion is offset by the smallness of surface amplitude is made, for example, by Gudmundsson (2003) (see paragraph 16).

and at the base $z = \nu s$,

$$-\tau_{nn} = \frac{2\left[(1-\nu^2 s_x^2)\psi_{zx} + \nu s_x(\psi_{zz} - \psi_{xx})\right]}{1+\nu^2 s_x^2},$$

$$\tau = \frac{\left[(1-\nu^2 s_x^2)(\psi_{zz} - \psi_{xx}) - 4\nu s_x \psi_{zx}\right]}{1+\nu^2 s_x^2},$$

$$\frac{\psi_z - \nu\psi_x s_x}{(1+\nu^2 s_x^2)^{1/2}} = U(\tau, N),$$

$$-\psi_x = \alpha\nu s_t + \nu\psi_z s_x,$$

$$N = 1 + s + \Pi - \tau_{nn},$$

$$q = q(\tau, N),$$

$$s_t + q_x = 0.$$

Assuming a basic state $\psi = \bar{u}z + \frac{1}{2}\theta z^2$, $\Pi = s = 0$, show that by putting $\psi = \bar{u}z + \frac{1}{2}\theta z^2 + \Psi$ and linearising the model, Ψ, Π and s satisfy the system

$$\Pi_x = \nabla^2 \Psi_z,$$

$$\Pi_z = -\nabla^2 \Psi_x,$$

with

$$\Pi,\ \psi_{zz},\ \psi_x \to 0 \quad \text{as} \quad z \to \infty,$$

and

$$\hat{\tau} = \Psi_{zz} - \Psi_{xx},$$

$$\Psi_z = U_\tau \hat{\tau} + U_N \hat{N},$$

$$-\Psi_x = \alpha\nu s_t + \nu\bar{u} s_x,$$

$$\hat{N} = s + \Pi + 2(\Psi_{zx} + \nu\theta s_x),$$

$$s_t + q_\tau \hat{\tau}_x + q_N \hat{N}_x = 0$$

at $z = 0$, where $\hat{\tau}$ and $\hat{N}$ denote the perturbations to τ and N.
Show that the solution for Ψ is of the form

$$\Psi = (a + bz)\exp[-kz + ikx + \sigma t],$$

and hence show that

$$\sigma = r - ikc,$$

where the wave speed is

$$c = \frac{R[1 + 4\nu^2\alpha k^3 R(\theta + k\bar{u})]}{1 + 4\nu^2\alpha^2 k^4 R^2},$$

where

$$R = \frac{q_N + 2k(q_N U_\tau - U_N q_\tau)}{1 + 2kU_\tau},$$

and the growth rate is

$$r = \frac{2\nu k^2 R[\theta + k\bar{u} - \alpha R k]}{1 + 4\nu^2\alpha^2 k^4 R^2}.$$

Deduce that the uniform flow is unstable if $R > 0$.

10.18 The growth rate of the instability in question 10.17 is given by

$$r = \frac{2\nu k^2 R[\theta + k\bar{u} - \alpha R k]}{1 + 4\nu^2\alpha^2 k^4 R^2},$$

where k is the wave number,

$$R = \frac{q_N + 2k(q_N U_\tau - U_N q_\tau)}{1 + 2kU_\tau},$$

and α and ν are small. Show that the maximum value of r will occur when k is large, and in this case show that we can take

$$R \approx R_\infty = q_N - \frac{U_N q_\tau}{U_\tau},$$

and hence show that the maximum of r occurs when

$$k = k_{\max} \approx \left(\frac{3}{4\nu^2\alpha^2 R_\infty^2}\right)^{1/4},$$

where

$$r = r_{\max} \approx \frac{3^{3/4}\bar{u}}{2^{5/2}\alpha^{3/2}(\nu R_\infty)^{1/2}}.$$

The uniform bed is thus unstable if $R_\infty > 0$. Suppose now that

$$q = \left[\frac{\tau}{\mu} - N\right]_+ U(\phi),$$

where $\phi = \dfrac{\tau}{N}$, the notation $[x]_+$ denotes $\max(x, 0)$, and $U = 0$ for $\phi < \mu$. Show that $R_\infty > 0$ when $\phi > \mu$ for any such function $U(\phi)$.

10.19 The scaled surface perturbation H and the atmospheric dust concentration C of the Martian north polar ice cap are taken to satisfy the equations

$$\alpha H_\tau - v H_\xi = -g(C),$$

$$C_\tau = \phi g(C) + C_{\xi\xi} + \Lambda\left(H_\xi C\right)_\xi,$$

where $g(C) = C^2(1 - C)$, and the positive constants α, v, ϕ and Λ are $O(1)$.

If the boundary conditions are taken to be that

$$H, C \to 0 \quad \text{as} \quad \xi \to \infty, \quad C \to 1 \quad \text{as} \quad \xi \to -\infty,$$

show that travelling wave solutions with speed w exist if $w > w_0$, and find a (numerical) method to determine the value of w_0.